1949

Investigation of the physicochemical properties of Bi(III)-complexes formed with triaza and tetraaza ligands for the purpose of developing radiopharmaceuticals

PhD thesis

Dávid Horváth
Supervisors: Dr. Zsolt Baranyai
Dr. Gyula Tircsó

Investigation of the physicochemical properties of Bi(III)-complexes formed with triaza and tetraaza ligands for the purpose of developing radiopharmaceuticals

PhD thesis

Dávid Horváth

Supervisors: Dr. Zsolt Baranyai

Dr. Gyula Tircsó

Bracco Imaging S.p.a.

Via Caduti di Marcinelle, 13,

20134 Milano, Olaszország

Ezen értekezést a Debreceni Egyetem Természettudományi és Informatikai Doktori Tanács Kémia Doktori Iskola K2 programja keretében készítettem a Debreceni Egyetem természettudományi doktori (PhD) fokozatának elnyerése céljából.

Nyilatkozom arról, hogy a tézisekben leírt eredmények nem képezik más PhD disszertáció részét.

Debrecen, 2023 . . . .

a jelölt aláírása

Tanúsítom, hogy Horváth Dávid doktorjelölt 2018- 2022 között a fent megnevezett Doktori Iskola K2 programjának keretében irányításommal végezte munkáját. Az értekezésben foglalt eredményekhez a jelölt önálló alkotó tevékenységével meghatározóan hozzájárult. Nyilatkozom továbbá arról, hogy a tézisekben leírt eredmények nem képezik más PhD disszertáció részét.

Az értekezés elfogadását javasolom.

Debrecen, 2023 . . . .

a témavezető aláírása

Triaza és tetraaza ligandumok Bi(III)-komplexeinek fizikai-kémiai sajátosságai radiofarmakonok fejlesztése szempontjából

Értekezés a doktori (Ph.D.) fokozat megszerzése érdekében
a koordinációs kémia tudományágban

Írta: Horváth Dávid okleveles vegyész

Készült a Debreceni Egyetem Kémia doktori iskolája
(K/2 programja) keretében

Témavezetők: Dr. Baranyai Zsolt
Dr. Tircsó Gyula

Az értekezés bírálói:

Dr. ....

Dr. ....

A bírálóbizottság:

elnök: Dr. ....

tagok: Dr. ....

Dr. ....

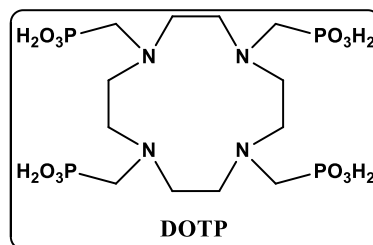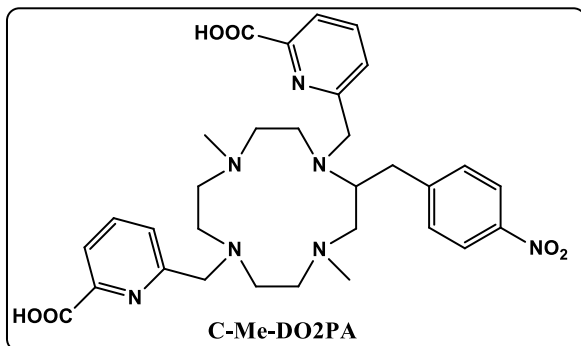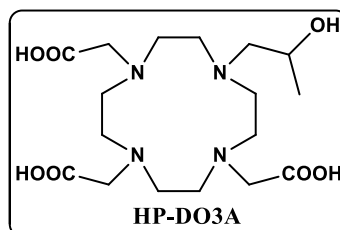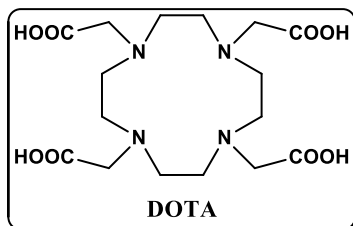Dr. ....

Dr. ....

Az értekezés védésének időpontja: 2024.

Table of contents

Structure of the ligands in the dissertation:

DOTA

HP-DO3A

C-Me-DO2PA

DOTP

PEPA

3p-C-DEPA

C-DTPA

p-NO$_2$-Bn-CHX-A''-DTPA

C-NE3TA

3p-C-NETA

H$_4$neunpa

1B4M-DTPA

HEDTA

NTA

n = 3,   AAZTA-C4-COOH

AAZTA

AAZTA-TATE
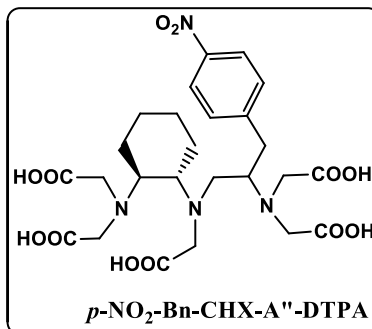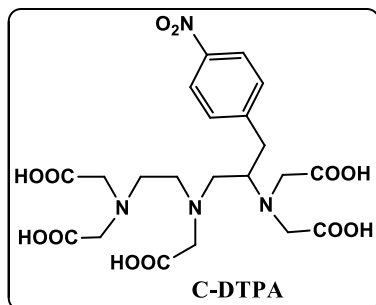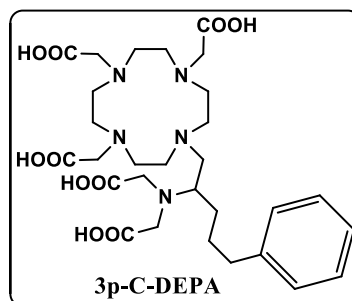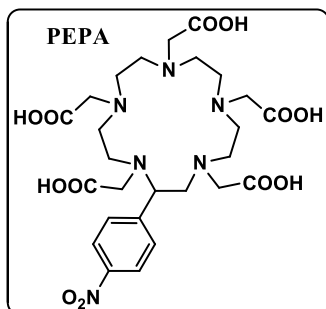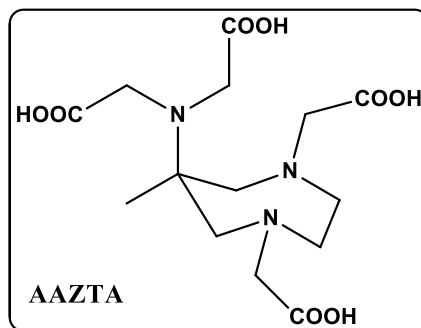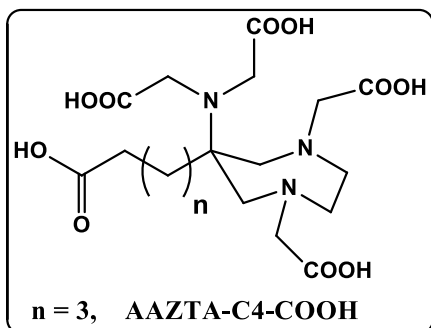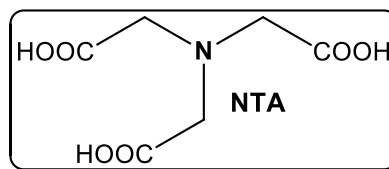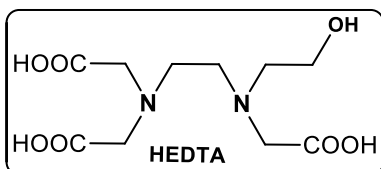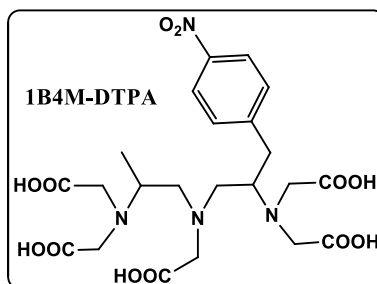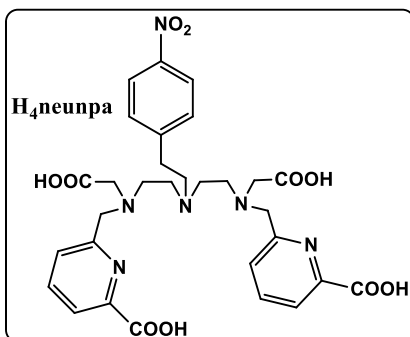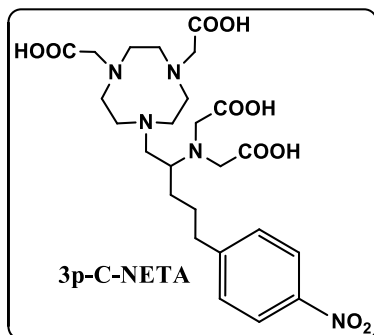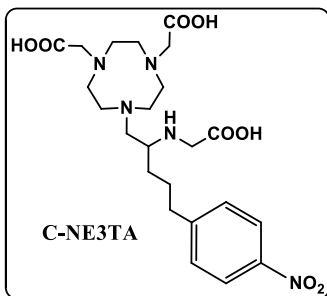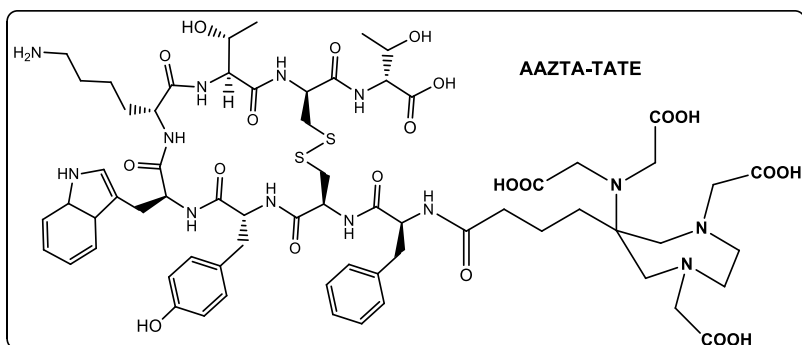
Name of the ligands:

H₄DOTA: Tetraazacyclododecane-1,4,7,10-tetraacetic acid

H₈DOTP: 1,4,7,10-Tetraazacyclododecane-1,4,7,10-tetra(methylene phosphonic acid)

H₃HP-DO3A: 10-(2-hydroxypropyl)-1,4,7,10-tetraazacyclododecane-1,4,7-triacetic acid

H₂C-Me-DO2PA: 6,6'-((4,10-dimethyl-2-(4-nitrobenzyl)-1,4,7,10-tetraazacyclododecane-1,7-diyl)bis(methylene))dipicolinic acid

H₅3p-C-DEPA: 2,2',2''-(10-(2-(bis(carboxymethyl)amino)-5-phenylpentyl)-1,4,7,10-tetraazacyclododecane-1,4,7-triyl)triacetic acid

H₅PEPA: 2,2',2'',2''',2''''-(2-(4-nitrophenyl)-1,4,7,10,13-pentaazacyclopentadecane-1,4,7,10,13-pentayl)pentaacetic acid

H₅DTPA: diethylene-triamine-*N,N,N',N''N''*-pentaacetic acid

H₃HEDTA: 2,2',2'',2'''-(Ethane-1,2-diyldinitrilo)tetraacetic acid

H₅C-DTPA: 2,2'-((2-((2-(bis(carboxymethyl)amino)-3-(4-nitrophenyl)propyl)(carboxymethyl)amino)ethyl)azanediyl)diacetic acid

H₅p-NO2-Bn-CHX-A''-DTPA: 2,2'-(((1S,2S)-2-((2-(bis(carboxymethyl)amino)-3-(4-nitrophenyl)propyl)(carboxymethyl)amino)cyclohexyl)azanediyl)diacetic acid

H₅1B4M-DTPA: 2,2'-((1-((2-(bis(carboxymethyl)amino)-3-(4-nitrophenyl)propyl)(carboxymethyl)amino)propan-2-yl)azanediyl)diacetic acid

H₄neunpa: 6,6'-(((((4-nitrophenethyl)azanediyl)bis(ethane-2,1-diyl))bis((carboxymethyl)azanediyl))bis(methylene))dipicolinic acid

H₃C-NE3TA: 2,2'-(7-(2-((carboxymethyl)amino)-5-(4-nitrophenyl)pentyl)-1,4,7-triazonane-1,4-diyl)diacetic acid

H4̱3p-C-NETA: 2,2'-((1-(4,7-bis(carboxymethyl)-1,4,7-triazonan-1-yl)-5-(4-nitrophenyl)pentan-2-yl)azanediyl)diacetic acid

H₄AAZTA: 6-amino-6-methylperhydro-1,4-diazepine -*N,N',N'',N''*-tetraacetic acid

H₄AAZTA-C4-COOH: 2,2'-((1,4-bis(carboxymethyl)-6-(3-carboxypropyl)-1,4-diazepan-6-yl)azanediyl)diacetic acid

AAZTA-TATE: AAZTA-[Tyr3]-Octreotate

H₃NTA: nitrilotriacetic acid

List of abbreviations

PET: Positron Emmision Tomography

SPECT: Single-Photon Emission Computed Tomography

MRI: Magnetic Resonance Imaging

CAs: Contrast Agents

TAT: Targeted Alpha Therapy

QRE: Quadrupolar Relaxation Enhancement

LET: Linear Energy Transfer

DNA: Deoxyribonucleic acid

FDA: Food and Drug Administration

PA: Picolinic acid

CZE: Capillary Zone Electrophoresis

DMSO: Dimethyl Sulfoxide

NMP: N-methyl-piperazine

MES: 2-(N-morpholino)ethanesulfonic acid

TLC: Thin Layer Chromatography

EXSY: Exchange Spectroscopy

COSY: Correlated Spectroscopy

HSQC: Heteronuclear Single Quantum Coherence

HMBC: Heteronuclear Multiple Bond Correlation

EOF: Electro osmotic flow

LOD: Limit of detection

RCP: Radiochemical purity

RCY: Radiochemical yield

TOPO: Trioctyl-phosphine oxide

I.   Introduction

Bismuth is the heaviest element in the Group of 15 in the periodic table with atomic number is 83 and relative mass of 209. Its first written mention dates from *Valentius Basilius* in 1450. The name of metallic element comes from the German *Wismut* word. *Wismut* means white metal. The name of the element was changed from *Wismut* to *bisemutum* by German scientist *Bauer* in XVI century[1].

Bismuth is commonly used in metal industry (e. g. Wood metal), metallurgical application and medicine. Bismuth has not known biological role in nature, nevertheless application of bismuth containing medicines dates back centuries.

Bismuth was used as treatment of different disorders or war wounds in medicine. Since 1901 Pepto-Bismol (bismuth subsalicylate, BSS) is used in the treatment of gastritis and dyspepsia. There are some other bismuth based medicines (e.g. De-Nol, colloidal bismuth subcitrate, CBS and Pylorid, ranitidine bismuth subcitrate, RBC), which are applied for the treatment of H. pylori and ulcers[2].

Nowadays the modern healthcare is not conceivable without usage of radioisotopes in medical diagnosis and therapy. Among the radioisotope-based imaging modalities the **P**ositron **E**mission **T**omography (**PET**) is the most sensitive molecular imaging technique. During the PET examinations there is a delivery of the compound labeled with a short-lived positron emitting (β^+) radionuclide, which is an active participant in various biochemical and biophysical processes. The positron (β^+) emitted by the radionuclide of the labeled molecule annihilates upon

encountering with an electron followed by the generation of two γ-photons (released at 180° relative to each other). The signal requires the simultaneous detection of both γ-photons by the ring shaped detectors (γ-cameras), which indicates the distribution and the accumulation of the radioisotope in the cross-sectional planes. By recording the two-dimensional image of several cross-section planes, three-dimensional PET image of the whole body can be created by the suitable image software. The most commonly used isotopes are ^{11}C (methionine), ^{13}N (ammonia), ^{15}O (butyl alcohol) and ^{18}F (fluorodeoxyglucose)[3]. Another imaging technique with the application of γ-photon emitting radioisotpes is **S**ingle-**P**hoton **E**mission **C**omputed **T**omography (SPECT). Isotopes suitable for SPECT experiments should emit γ-photon with an energy greater than 70 keV in order to obtain detectable radiation outside the body. By considering this criteria isotopes suitable for SPECT applications are ^{99m}Tc (γ , $t_{1/2}$ = 6.0 hour), ^{111}In (γ , $t_{1/2}$ = 2.8 days) ^{201}Tl (γ , $t_{1/2}$ = 73.5 hour)[4]. Bismuth and its isotopes have been proposed for the application in computed tomography (^{209}Bi)[5], single-photon emission computed tomography (^{213}Bi)[6] and multimodal imaging purposes (the quadruple ^{209}Bi isotope may serve a relaxation enhancing agent in magnetic resonance imaging (MRI) and photoacoustic imaging) [7]·[8]. On the other hand bismuth has two important α-emitter isotopes ^{212}Bi and ^{213}Bi which have been proposed for **T**argeted **A**lpha **T**herapy (**TAT**) [9]·[10]. Recently there is a growing interest for TAT application of ^{212}Bi (β$^-$: 64 %; α: 36%, $t_{1/2}$=60.6 min) and ^{213}Bi (β$^-$: 98 %; α: 2 %, $t_{1/2}$=45.6 min) due to the availability of both isotopes through commercial benchtop generators (^{212}Pb/^{212}Bi and ^{225}Ac/^{213}Bi). Moreover, ^{212}Pb can also serve as an *in vivo* generator of ^{212}Bi in TAT application (^{212}Pb: β$^-$, $t_{1/2}$=10.6 h). The *in vivo*

2

application of [212/213]Bi isotopes requires thermodynamically stable and kinetically inert complexes at physiological conditions (being stable in competitive biological media where several endogenous ligands and metal ions are present). These requirements are generally fulfilled by the the tetraaza macrocyclic DOTA ligand, the triaza open-chain DTPA ligands and their derivatives. However, the physico-chemical properties of Bi(III) complexes have attracted only moderate interest, which is probably related to the difficulties arising during the studies of the Bi(III) complexes in solution owing to its strong tendency to hydrolyze (Bi^{3+}(aq) ion is present only in strongly acidic solutions, and some $[Bi(OH)]^{2+}$ is formed even in 1.0 M $HClO_4$ solution)[11].

In our work, we aimed to explore the equilibrium, formation, and dissociation kinetic properties of some Bi(III) complexes proposed for diagnostic and therapeutic applications.

The core aims of this work are summarized below:

- Characterization of equilibrium, formation and dissociation kinetic properties of $[Bi(DOTA)]^-$ and $[Bi(DOTP)]^{5-}$ complexes.

- Study of structural feature of $[Bi(DOTP)]^{5-}$ complex in solution

- Optimization of the radiolabeling procedure of H_4DOTA with [213]Bi(III) isotope.

- Exploring the thermodynamic and kinetic properties of $[Bi(AAZTA)]^-$, $[Bi(AAZTA-C4-COO^-)]^{2-}$ and $[Bi(AAZTA-C4-TATE)]^-$ complexes.

- Investigation of the structural properties of $[Bi(AAZTA)]^-$ and $[Bi(AAZTA-C4-COO^-)]^{2-}$ complexes in solution and in solid state.

- Radiolabeling of AAZTA-C4-TATE with [205/206]Bi

- *Ex vivo* and *in vivo* biodistribution studies of the [$^{205/206}$Bi][Bi(AAZTA-C4-TATE)]$^-$ conjugate in animal models.

II. Literature overview

II.1. Chemistry of bismuth

Bismuth is a rare element in the Earth's crust (0.008 ppm). It is accumulated in oxide and sulphide ores mostly. Few bismuth-based minerals exist only (e.g. bismite Bi_2O_3, bismuthinite Bi_2S_3 and bismuthin $(BiO)_2CO_3$. In elemental state bismuth can also be found in the nature. However, this form of bismuth is very rare. It is commonly obtained as by-product of the zinc, lead and copper mining[1]. The occurrence of bismuth similar to gold and platinum[12]. Bismuth is monoisotopic element (natural abundance of ^{209}Bi is 100%). Bismuth is radioactive with extremely long half-life ($t_{1/2}= 9 \times 10^{19}$ years) which is even longer than the age of the universe. The colour of bismuth in elemental form is grey or white, and it is a brittle metal under normal conditions. The surface of the element is generally covered by an oxide layer caused by air oxidation, giving it a nice multicoloured sheen. It has low melting and boiling point (mp: 271°C bp: 1564°C) and high density (9.78 g/cm^3). It is one of the three elements (along with Ga and Ge) for which an increase of its volume is observed during the solidification of its melt [1]. It is unique among metals because it has the lowest thermal conductivity, the highest *Hall* effect and it is the most diamagnetic element[13]. The common oxidation state of bismuth is +3 (Bi(III)) and +5 (Bi(V)) due to $6s^26p^3$ electronic configuration of the valence shell. According to the inert-pair effect[14] the most common oxidation state of bismuth is +3.

Only few inorganic salts are known with bismuth in +5 oxidation state (e.g. BiF_5 and $NaBiO_3$ which are strong oxidizing agents). Bi reacts with halogens (X_2) by froming BiX_3 and BiX_5 if X=F, and burns in air (O_2) to produce Bi_2O_3. It also reacts with sulphuric acid, nitric acid and concentrated hydrochloric acid giving the related bismuth(III) salts. According to the Persons's hard-soft acid and base theory, Bi(III) is a borderline or „soft" metal ion. It has a very strong tendency to hydrolyse in aqueous solution.

$$x\,Bi^{3+} + yH_2O \rightleftharpoons \left[Bi_x(OH)_y\right]^{y-3} + y\,H^+ \qquad II.1.1$$
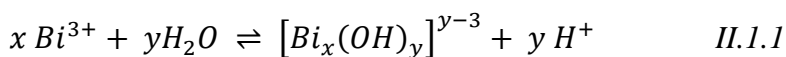
$$\beta_{xy} = \frac{[Bi_x(OH)_y]}{[Bi^{3+}]^x[OH^-]^y}$$

where $\log\beta_{11}$=-1.1; $\log\beta_{12}$=-4.0; $\log\beta_{13}$=-8.9; $\log\beta_{14}$=-21.8, $\log\beta_{6,12}$=0.33[15].

The coordination number of the trivalent Bi(III) ion spans from 3 to 10. Structure of Bi(III) compounds varies from pyramidal (CN: 3), through octahedral (CN: 6, $[Bi_6O_4OH)_4]^{6+}$), bicapped trigonal prism (CN: 8, [Bi(HEDTA)]·2H_2O) and square antiprism ($[Bi(NTA)_2]^{3-}$, [Bi(DOTA)])[16], [17] to tricapped trigonal prism (CN: 9, $[Bi(H_2O)_9]^{+3}$) [18]. The $[Bi(H_2O)_9]^{3+}$ exists only in very acidic solution. This is why, $[Bi(OH)_2]^+$ known to form even in very acidic solutions (even in 1M $HClO_4$) due to its strong tendency to hydrolize[11]. The structure of $[Bi(H_2O)_9]^{3+}$ cation is tricapped trigonal prismatic where the bismuth is coordinated by nine water molecules with 2.448 - 2.577Å Bi-O distances. In the hydrolysis of Bi(III) ion monomeric $[BiO^+]$ and polymeric cations such as $[Bi_6O_4(OH)_4]^{+4}$ are formed all the time before the precipitation of $Bi(OH)_3$[19]. The structure of the $[Bi_6O_4(OH)_4]^{+4}$ cation has been investigated by X-ray diffraction studies[20]. The obtained crystal

structure shows that the six Bi(III) ions are placed at the apices of an octahedron in non-bonding distances and the octahedron is face-capped by OH^- and O^{2-} with the formation of Bi-O-Bi bridges[21].

The strong interaction with heavier halides indicates the „softness" of Bi(III) ion. Bi(III) forms BiX_3 trihalides with all halogen anions ($X=F^-$, Cl^-, Br^- and I^-) except for F^- which can produce BiF_5 pentahalide. All the trihalides have trigonal pyramidal structure in vapour phase. Preparation of the halides is possible by direct reaction of the elements at high temperature.

All of the BiX_3 trihalides hydrolyze in water by producig BiOX species [22].

$$BiX_3 + H_2O \rightleftharpoons BiOX + 2\,HX \qquad\qquad II.1.2$$
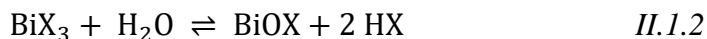
The resulting BiOX is insoluble in water, but the high concentration of HX results in the reformation of the water soluble BiX_3 according to Eq. (II.1.2). The trihalides form donor-acceptor complexes with ethers *e.g. fac*-[$BiCl_3(THF)_3$], halides *e.g.* [BiI_6]$^{3-}$ because these ligands are Lewis acids [22]. When the trihalides react with halide anions polynuclear halide anionic complex species of different structures are formed. The most polynuclear halide anionic complexes are binuclear (e.g. [Bi_2X_8]$^{2-}$, [Bi_2X_9]$^{3-}$, [Bi_2X_{10}]$^{4-}$ and [Bi_2X_{11}]$^{5-}$). The [Bi_2X_8]$^{2-}$ anion has square pyramidal structure, this is the rarest coordination type among the Bi(III) complexes. The structure of the other Bi_2X_x complexes is composed by octahedral units (e.g. two {BiX_6} moiety share a common face with three binding X ligands in [Bi_2X_9]$^{3-}$). Besides these, there are several polynuclear halide anionic complex with tri-, tetra-, penta-, hexa-, hepta- and octanuclear species (e.g. [Bi_3I_{12}]$^{2-}$, [Bi_4Cl_{18}]$^{6-}$, [Bi_5I_{19}]$^{4-}$, [Bi_6I_{22}]$^{4-}$, [Bi_7I_{24}]$^{3-}$ and [Bi_8I_{28}]$^{4-}$) [23].

Bismuth in its +5 oxidation state is a very strong oxidizing agent in aqueous solution. The potential of Bi(V)/Bi(III) redox couple is $E°=2.03V$, which is able to liberate Cl_2 from hydrochloric acid. Moerover, Bi(V) can oxidize Mn(II) to MnO_4^- in acidic solution used in the qualitative analytical chemistry to detect Mn(II) ion.

Only a few Bi(V) containing species are known (e.g. BiF_5, $[BiF_6]^-$ and Bi_2O_5). The most common Bi(V) salt is the $NaBiO_3$ (sodium bismuthate). It is an orange solid possessing poor solubility in water. It is made by heating Na_2O_2 and Bi_2O_3 mixture or melt NaOH and Bi_2O_3 suspension oxidized by bromine[22]. In organic and analytical chemistry $NaBiO_3$ is frequently used as oxidizing agent and to quantify manganese. One of its specific applications belongs to the oxidative cleavage of α-hydroxy ketones[24]. $Zn(BiO_3)_2$ is another bismuthate salt, which is used for the oxidation of alcohols to ketones, thiols to disulphides and thioethers to sulfoxides[25].

II.2. Medical applications of bismuth

The first medical application of bismuth compounds was made by Louis Odier for a treatment of dyspepsia in 1786. Bismuth compounds are widely used for the treatment of different microbial infection such as wound infections, syphilis, quartan malaria and colitis[26] but the most important medical applications of bismuth compounds are linked to the treatment of gastrointestinal disorders and ulcers. The medical use of these drugs is related to the inhibition of the *Helicobacter pylori* (slow-growing, micro-aerophilic, spiral shaped, gram-negative bacterium) which can prevent ulcers from healing[26]–[28]. Approximately about half of the world's population is infected with *Helicobacter pylori.* However, the

majority of infected people (< 80%) do not develop any associated diseases[29].

The bismuth subsalicylate ($BiOC_7H_5O_3$, *BSS*, *Pepto–Bismol*) is preferred for the rapid treatment of heartburn, upset stomach, indigestion, diarrhoea and nausea. Another type of bismuth containing drugs are based on Bi(III)-citrate complexes such as ranitidine bismuth citrate (*RBC*, *Tritec* and *Pylorid*, *GSK*, $C_{19}H_{27}N_4O_{10}SBi$), and colloidal bismuth subcitrate (*CBS*, De–Nol; Gist Brocades and Yamanouchi, $K_3(NH_4)_2[Bi_6O_3(OH)_5(C_6H_5O_7)_4]$) which is used around the globe to treat different type of gastrointestinal diseases, caused by the *Helicobacter pylori* infection[30, o. 34], [31, o. 77], [32, o. 50].

There is a growing interest in other Bi(III)-containing antibacterial/antifungal agents. Thiosemicarbazones have anti-parasitic, anti-bacterial and anti-cancer properties. Lessa and co-workers described some of Bi(III)-thiosemicarbazones ([Bi(2Ac4Ph)(dmso)Cl_2] H_2Ac4Ph= 1-(pyridine-2-yl)ethenone-4-phenyltiosemicarbazone)) and -bis (thiosemicarbazone)) complexes as a potential anti-bacterial agents[33]. The antibacterial activity of these complexes were better than those of the free ligands against the Gram-positive bacteria such as *Enterococcus faecalis*, *Staphylococcus aureus* and *Staphylococcus epidermidis* [2]. The anti-fungal activity of Bi(III)-hydrazone complex [Bi(HAcPh)Cl_2], HAcPh: 2,6-diacetylpiridine bis(benzoylhydrazone)) is better than that of the Sb(III) analogue or that of the well-known anti-fungal agent fluconazole[34]. Turel and co-workers developed the Bi(III)-based ciprofloxacin derivatives, which is a second generation fluoroquinolone antibiotics against antimicrobial resistant bacteria[35], [36].

Bi(III) complexes play also an important role as contrast agents in several imaging modalities. $[Bi(DTPA)]^{2-}$ was recently proposed as a computed tomography contrast agent with improved efficiency and reduced toxicity as compared to classical iodinated agents[7]. Recently, Bi(III) complexes have also been proposed as quadrupolar relaxation enhancement agent (QRE) in Magentic Resonance Imaging (MRI) due to the high quadrupolar moment of Bi(III) ion. Quadrupolar nuclei can also shorten the bulk solvent T_1 relaxation time and the given relaxation phenomena was utilized recently while proposing a new class of MRI contrast agents (CAs) [37], [38]. QRE takes place by the couple of the quadrupole moments of the nucleus and the nucleus with I=1/2 spin (for instance ^{1}H) via a dipole–dipole interaction. The loss of ^{1}H magnetisation takes place by time independent dipole–dipole coupling between the ^{1}H spins and the quadrupolar nucleus while time dependent fluctuating dipole–dipole interactions generate the QRE. In the literature ^{14}N- and ^{209}Bi(III)-based systems were proposed for QRE applications[39].

II.3. Alpha Radiotherapy

Medical application of radioisotopes for therapy has a very long history. The discovery of alpha emitting ^{226}Ra isotope by Pierre and Marie Salomea Skłodowska–Curie in 1898 was rapidly followed by the application of ^{226}Ra in the therapy of skin lesions in 1901. Alpha decay is a type of radioactive decay in which an atomic nucleus emits an alpha particle and thereby transforms or 'decays' into a different atomic nucleus, with a mass number that is reduced by four and an atomic number that is reduced by two. Alpha radiation occurs when the nucleus of an atom becomes unstable (the ratio of neutrons to protons is too low) and alpha particles are emitted to restore balance. Alpha decay occurs in elements with high atomic

numbers, such as uranium, radium, and thorium. In alpha decay, a positively charged particle, identical to the nucleus of ^{4}He, is emitted spontaneously. This particle, also known as an alpha particle, consists of two protons and two neutrons.

Since an alpha particle is more massive than other forms of radioactive decay, it can be stopped by a sheet of paper and cannot penetrate the human skin. A 4 MeV alpha particle can only travel about 2.54 cm through the air. Indeed, alpha radiation has the lowest penetrating power compared to other types of radiation. Alpha particles are highly ionising (high energy) because of their double positive charge, large mass (compared to a beta particle) and therefore they are relatively slow. In contrary, beta particles are much smaller than alpha particles and, that is why they have much less ionizing power (less ability to damage tissue), but owing to their small size their penetration power is greater.

The different physical properties of α vs. β particles offer various options for personalized medicine and endoradiotherapy. Both α and β radiations can be employed for targeted radiotherapy, though the first one is not commercial yet. The primary benefit of targeted alpha particle therapy is the ability to deliver radiation in a highly localized manner. Typical alpha particles have a range of only a few cell diameters (50-90 μm). Thus, if delivery to cancerous cells is achieved, there is lower risk of healthy cells being affected by the radiation "crossfire". The linear energy transfer (LET) of alpha particles, approximately 25-230 keV/μm, is about 100 to 1000 times greater than the average LET of beta particles[40]. The higher LET of alpha particles results in a greater potential for biologic damage as compared to beta particles. DNA double strand breaks are considered the major clinically relevant lesions caused by alpha particle

radiation[41]. The double strand breaks created by alpha particle radiation have been found to be highly complex, more resistant to normal repair, and thus more genotoxic than double strand breaks caused by other modalities. However, the downside of this lethality is a higher toxicity, if the emitters are not precisely localised inside the tumours. This can be caused by off-target localisation of the targeted radiopharmaceutical, or by radiation from daughter radionuclides released by the recoil energy. These phenomena need to be minimised by proper selection and optimization of the target/probe pair and by careful selection of a radionuclides with suitable radiochemical properties. In fact, upon α-emission, recoil energy imparted to the daughter (~100 keV) is about 1000 times higher than the binding energy of any chemical bond, resulting in the daughter's release.

Among the alpha emitter isotopes only six (^{227}Th, ^{225}Ac, ^{223}Ra, $^{212/213}$Bi, ^{211}At, ^{149}Tb) have been considered for clinical applications up to now [30]. Main radiochemical properties of the alpha emitter radioisotopes (half-life, decay scheme, energy, recoil energy and daughter isotopes) proposed for clinical applications are shown in II.3.1 Table[42].

II.3.1. **Table.** Radiochemical properties of the alpha-emitters proposed for TAT

Isotopes	Half-lives	Main emissions	Energy (MeV)	Energy recoil (keV)	Daughters
^{227}Th	18.7 d	α	6	–	^{223}Ra
^{225}Ac	10.0 d	α	5.8	–	^{221}Fr
^{223}Ra	11.4 d	α	5.7	108.4	^{219}Rn
^{213}Bi	45.6 m	α	6	132	^{213}Po
		β$^-$	0.444		^{209}Tl
		γ	0.440		^{209}Pb

^{212}Bi	60.6 m	α	6.1	–	^{212}Po
		β$^-$	–		^{208}Tl
^{211}At	7.2 h	α	5.9	116	^{207}Bi
		EC			^{211}Po

Among the alpha emitter isotopes native ^{223}Ra cation is the only one, which is approved by FDA [^{223}Ra]RaCl$_2$ (Xofigo®, Bayer) for the treatment of symptomatic bone metastases from castration-resistant prostate cancer[43]. On the other hand, the weak γ-emission from ^{223}Ra (1.1%) allows a quick dosimetric evaluation of the absorbed dose. Nowadays ^{225}Ac, $^{212/213}$Bi and ^{211}At alpha emitters are under intense scrutiny for the development of targeted alpha therapeutics[44].

II.4. Production of the bismuth isotopes

Bismuth has 41 isotopes from A=184-224. ^{209}Bi isotope can be considered as stable (it has very long half-life $t_{\frac{1}{2}} = 1.9 \times 10^{19}$ years) while the remaining 40 isotopes are unstable and suffer radioactive decay. The unstable isotopes of Bi have different decay mode (e.g. γ, β$^+$, β$^-$ and α). The α emitter isotopes $^{212/213}$Bi are the most important in the clinical application. In the decay chain of ^{229}Th, ^{213}Bi is formed as a daughter radionuclide of ^{215}Ac (Figure II.4.1), it has a short half-life ($t_{\frac{1}{2}} = 45.6$ min) and emits high-energy (8 MeV) α particles. The range of the α particles is 50-80µm in tissue. Worldwide there are three places where ^{229}Th is produced: Directorate for Nuclear Safety and Security of the JRC of the European Commission in Karlsruhe, Germany[31], Oak Ridge National Laboratory (ORNL) USA[45], and the Institute of Physics and Power Engineering (IPPE) in Obninsk, Russia.
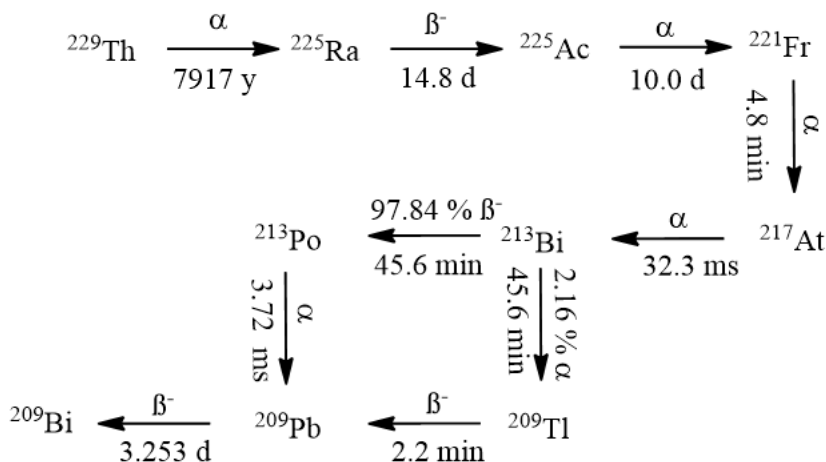
Figure II.4.1. Decay chain of ^{229}Th

Since 1990s, the main production of ^{225}Ac takes place by the radiochemical extraction. Amount of the ^{225}Ac produced by radiochemical extraction is approximately 55-65 GBq[31]. ^{213}Bi is generally produced with ^{225}Ac/^{213}Bi generators. Many types of generators were designed worldwide[32] and these generators are well known and explored. In the frequently used generators, ^{225}Ac is bound to the cation exchange resin, which is eluted from time to time using diluted acids (e.g. 0.1 M solution of HCl or 0.1 M HCl/0.1 M NaI mixture etc.) in order to obtain ^{213}Bi isotope.

In the automated PNNL generator (commercialized by Pacific Northwest National Laboratory), ^{225}Ac is fixed on AG MP 50 cation exchange resin and the ^{213}Bi is eluted by 0.1 M HCl solution. Further purification of the elute from ^{225}Ac is performed by anion exchange resin which is able to absorbe ^{213}Bi isotope in the form of $[^{213}\text{Bi}][\text{BiX}_x]^{(x-3)-}$ complexes. The resin gets washed with 0.5M HCl solution to remove the traces of ^{225}Ac, which

is followed by the elution of [213]Bi with sodium-acetate (NaOAc) buffer solution (4M) (pH 4.0-5.5).

Generator produced by MSKCC (Memorial Sloan-Kettering Cancer Center) based on its setup is very similar to that of PNNL. The acidic solution of [225]Ac is loaded to the analytical-grade macroporous cation-exchange resin (AGMP-50). The small plug of acid-washed glass wool is applied on top of the [225]Ac-loaded resin followed by 25 mg of clean resin[30]. The [213]Bi isotope is eluated with mixture of 0.1M NaI and 0.1M HCl in $[^{213}Bi][BiI_x]^{3-x}$ (where x is 4,5 and 6) form. The given form can be used directly during the radiolabeling experiments. Owing to the transient equilibrium these generators can be milked every three hours[46]. The generators that have high activity (up to 4 GBq [225]Ac) and are developed at JRC Karlsruhe yields [213]Bi elution exceeding 80% and with low breakthrough of [225]Ac (less than 0.2 ppm) [46]. Due to the relatively long half-life of the [225]Ac, these generators can be used for 3-4 weeks in a clinical practice. Moreover, the long half-life of [225]Ac allows for the shipment of the generator to places of application at long distance.

At the present time the global supply of the [225]Ac obtained from [229]Th is still inadequate for widespread consumption of the [225]Ac and [213]Bi-labeled compounds in the radiotherapy. As a result, alternative methods for a production of [225]Ac have been investigated by considering the irradiation of [226]Ra targets with gamma-rays, deuterons and protons, the spallation of [232]Th or natural U targets with highly energetic protons[47].

The [212]Bi ($t_{1/2}$=60.6 min) is formed from [224]Ra ($t_{1/2}$=3.6 days) in the decay chain of [228]Th ($t_{1/2}$=1.9 years)[48] (Figure II.4.2). [228]Th is available by [228]Ra from [232]Th or from [232]U. Due to the difficulties of natural [228]Ra separation form [232]Th it must be processed on the scale of thousands of kilo

in order to obtain sufficient quantities. ^{228}Th also can be produced from consecutive neutron capture and β^- decay of ^{226}Ra[49].
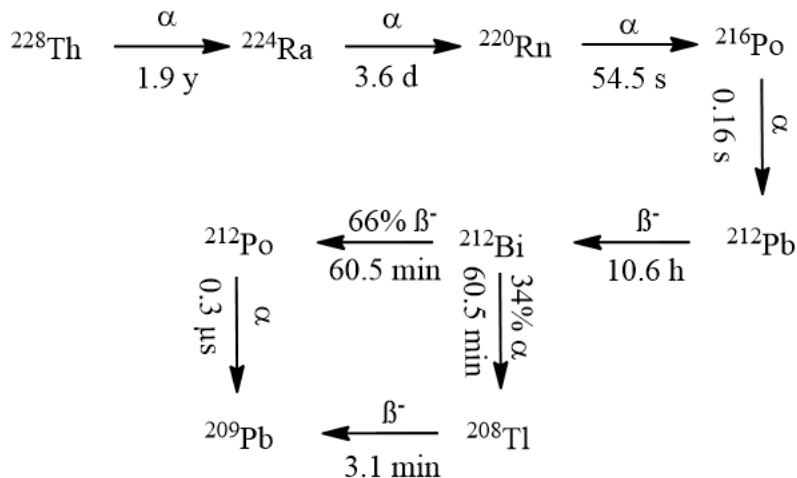

Figure II.4.2. Decay chain of ^{228}Th

During the production of ^{212}Bi isotope the ^{228}Th dissolved in 8 N HNO$_3$ solution passing through an anion-exchange resin, which retains Th(IV), while the ^{224}Ra^{2+} and its daughter elements are coeluted. In the preparation of the generator the ^{224}Ra isotope is loaded to the cation-exchange resin and ^{212}Bi can be eluted with the use of 0.5-2.0 M HCl or HI solution. By the application of less acidic eluent, the elution of ^{212}Pb can be minimized, nevertheless both radionuclides are frequently coeluted and labeled in transient equilibrium[50]–[52].

Westrøm et al. prepared a ^{228}Th/^{224}Ra generator based on thorium. In this case, ^{228}Th was loaded on a DIPEX (Eichrom) actinide resin. The dauther element ^{224}Ra could be eluated regularly from the generator by using 1 M hydrochloric acid[53].

Another very interesting way for the production of ^{212}Bi takes place by its separation from the gaseous or aqueous ^{220}Rn. Radon is easily

removed because it is solubility (460 ml/dm^3 at 0°C). However, these methods have not been further explored due to the limited availability of ^{228}Th [27], [54]–[56]. The ^{208}Tl (daughter element of ^{212}Bi), emits high-energy (2.6 MeV) gamma photons which require the shielding of the medical staff. It may limit the clinical applicability of ^{212}Bi, whereas ^{213}Bi is a preferred radioisotope and it has a high potential for TAT applications [27].

II.5. Selected $^{212/213}$Bi(III) chelators

Radiometals play an important role in the diagnoses of physiological processes *in vivo* by imaging techniques, but they also contribute to the treatment of diseases. Only in very few cases, the radiometals are applied as cations: ^{82}Rb and ^{201}Tl used for myocardial imaging, ^{89}Sr and ^{223}Ra are applied for the treatment of bone metastases. Thus, the use of metal ion-based radioisotopes implies the use of their corresponding complexes formed with sutable ligands. Most of the trivalent, but also some divalent and tetravalent radiometals utilize amino-polycarboxylate and polyphosphonate ligands to coordinate the metal cation. The radiometal complexes must be characterized by several requirements for therapeutic applications such as: high thermodynamic stability, kinetic inertness, fast formation, slow dissociation, availability, low cost and easy conjugation to the targeting vectors (through bifunctional ligands). By considering the thermodynamic stability and kinetic inertness of the resulting complexes acyclic DTPA and macrocyclic DOTA, NOTA and their derivatives have been proposed for the chelation of $^{212/213}$Bi isotopes.

DTPA forms a very stable complex with Bi(III) ion (log$K_{Bi(DTPA)}$=33.9 – 35.2). However, the early *in vivo* studies revealed the low inertness of

$[^{212/213}Bi][Bi(DTPA)]^{2-}$, which resulted in the accumulation of the released (free) $^{212/213}Bi$ isotope in kidneys. Therefore, $[^{212/213}Bi][Bi(CHX-A''-DTPA)]^{2-}$ has been proposed for targeted applications due to its similar stability ($\log K_{Bi(CHX-A''-DTPA)}$=34.9 – 35.6) and condsiderably enhanced inertness[57]. Crystal structure of $[Bi(CHX-A''-DTPA)]^{2-}$ revealed the coordination of Bi(III) ion by three N and five carboxylate $-O^{-}$ donor atoms in square antiprismatic coordination geometry. The similar Bi − O (2.4−2.5 Å) and Bi − N bond lengths (2.5−2.6 Å) are in line with the softer character of the Bi(III) ion as compared to the bonding preferences of harder metal ions such as Y(III) and Lu(III). The rigid cyclohexyl moiety embedded in the backbone of CHX-A''-DTPA chelator resulted in a slower ^{213}Bi labeling compared to DTPA[58]. *In vivo* studies of the ^{206}Bi labeled DTPA, 1B4M-DTPA and CHX-A''-DTPA confirmed the significantly lower kidney uptake evidenced for $[^{206}Bi][Bi(1B4M-DTPA)]^{2-}$ and $[^{206}Bi][Bi(CHX-A''-DTPA)]^{2-}$ complexes, which can be explained by their improved kinetic inertness due to the increase in the rigidity of the ligands. Despite of the kidney uptake, $[^{213}Bi][Bi(CHX-A''-DTPA)]^{2-}$ is commonly used for targeted application due to the widespread availability of CHX-A''-DTPA [59], [60].

NEUNPA ligand is a DTPA analogue bearing two picolinic acid (PA) pendant arms attached to the terminal N atoms. The stability constant of the Bi(III) complex ($\log K_{BiL}$ = 28.8) is lower than that of DTPA and DOTA complexes. However, the conditional stability of the $[Bi(NEUNPA)]^{-}$ is similar to that of $[Bi(DOTA)]^{-}$ [57]

DOTA can be regarded as "gold standard" chelator of $^{212/213}Bi$ isotopes. Several studies reveal the stability of $[^{213}Bi]Bi(DOTA)$-bioconjugates for at least two hours *in vivo* and *in vitro* experiments [51][52]. Based on the X-

ray diffraction studies of [Bi(DOTA)]⁻ the Bi(III) ion is wrapped around by four ring-N and four carboxylate-O donor atoms in square antiprismatic geometry[16]. Because of the soft Lewis acid character of Bi(III) ion, the given metal ion is more deeply penetrated inside the cage of macrocyclic ligand than the smaller and harder Lu(III). In spite of the high thermodynamic stability of [Bi(DOTA)]⁻ (logK_{BiL}= 30.3)[16] the ligand has numerous drawbacks for the complexation of ²¹³Bi. The quantitative radiolabeling of DOTA with ²¹³Bi requires high temperature (e.g. 95°C at pH=4.0) longer reaction times (e.g. 30 – 60 min), and high DOTA concentration (10 µM), which is about 10 times higher than that of CHX-A''-DTPA (1 µM) for a similar radiolabeling yield [63]. Since ²¹³Bi is a short-lived isotope, the fast radiolabeling is crucial. However, the formation rate of [²¹²/²¹³Bi][Bi(DOTA)]⁻ is very low resulting in a significant loss of radioactivity during the 18abelled18. Furthermore, the high temperature is not suitable for heat-sensitive DOTA-bioconjugates because it may cause denaturation of the biological vector molecules.

Preclinical test was performed for some peptide bioconjugates. For instance [²¹³Bi]Bi(DOTA-TOC) has been shown to be effective in controlling the growth of small tumors and shows a dose-dependent response in large tumors over 20 days on STT receptor-expressing pancreatic tumors[64].

[²¹³Bi]Bi(DOTA-TATE) was tested in mice with pancreatic cancer (AR42J). The result has been reported by Chan et al[65]–[67]. Interestingly, preinjection of L-lysine was able to improve the kidney depuration and led to decreased renal dose during the [²¹³Bi]Bi(DOTA-TATE) treatments. A separate study investigated the influence of tumor size on the efficacy of [²¹³Bi]Bi(DOTA-TATE) treatment and it was shown

that smaller tumors generally received higher doses compared to large tumors (both for H69 and CA20948 cell lines).

[213Bi]Bi(PSMA-617) is promising candidate for the treatment of metastatic castration-resistant prostate cancer based on the results evidenced in a patient receiving a total dose of 592 MBq (in two cycles). After 11 months no accumulation of [68Ga]Ga(PSMA-617) used to monitor the therapeutical treatment was foud by PET/CT in cancerous regions [68].

PEPA is a 15 membered decadentate macrocyclic ligand possessing five ring N and five carboxylate O^- donor atoms. Comparison of the [205,206Bi][Bi(B3-PEPA)]$^{2-}$ with [213Bi][Bi(CHX-A''-DTPA)]$^{2-}$ reveals lower tumor and higher kidney uptake of [205,206Bi][Bi(B3-PEPA)]$^{2-}$, which in turn seriously questions the suitability of PEPA ligand for the chelation of Bi(III) ion [69].

Me-DO2PA is cyclen derivative ligand possessing two picolinic acid (PA) pendant arms and two methyl groups. According to the detailed physico-chemical studies [Bi(Me-DO2PA]$^+$ is characterized by somewhat higher stability constants ($\log K_{BiL}=34.2$)[70] and kinetic inertness comparable to that of [Bi(DOTA)]$^-$. Moreover, the serum stability test confirmed the presence of the intact [213Bi][Bi(Me-DO2PA)]$^+$ complex for at least 2 hours.

NEPA and **DEPA** are NOTA and DOTA derivative ligands possessing animino-diacetate moiety linked via ethylene bridge to one of the macrocyclic nitrogen atoms. These ligands are promising chelators for α and β^- emitters such as 90Y, 177Lu, 206Bi, 207Bi, 213Bi, and 212Pb[71], [72]. A common feature of these ligands is the combination of the macrocyclic NOTA and DOTA with the flexible imino-diacetate moiety which can accelerate the formation of the thermodynamically stable and inert

19

radiocomplexes [63], [72]. Moreover, the radiochemical studies reveal that the20abelled20 of it's a bifunctional version 3p-C-NETA with ^{213}Bi isotope takes place in quantitative yield at room temperature in the presence of low chelate concentration (≥1.5μM). *In vivo* experiments show lower dissociation of [$^{205/206}$Bi]Bi(NETA) derivatives than [$^{205/206}$Bi][Bi(CHX-A″-DTPA)]$^{2-}$. Interestingly,20abelled20nision of the kidney uptake revealed significantly lower accumulation of the seven-coordinated [$^{205/206}$Bi]Bi(C-NE3TA)]$^-$ than that observed for the eight coordinated [$^{205/206}$Bi][Bi(C-NETA)]$^-$ in nontumor-bearing mice [63], [73]. $^{205/206}$Bi labeled 3p-C-NETA-trastuzumab shows remarkable tumor accumulation without increasing kidney uptake in mice bearing subcutaneous tumors [74]. Radiochemical studies of [$^{205/206}$Bi]Bi(DEPA) derivatives indicate that the [$^{205/206}$Bi]Bi(DEPA-trastuzumab) complex remained completely intact, whereas 23% of [$^{205/206}$Bi]Bi(DTPA-trastuzumab) dissociated after 72 h in human serum[75]. Moreover, [$^{205/206}$Bi]Bi(3p-C-DEPA-trastuzumab) also showed remarkable tumor uptake in LS-174T tumor-bearing mice.

III. Experimental section

III.1. Materials

The chemicals used for the experiments were of analytical grade. $Bi(ClO_4)_3$ solution was prepared by dissolving Bi_2O_3 (99.9%, Fluka) in 6 M $HClO_4$. The concentration of the $Bi(ClO_4)_3$ solution was determined by complexometric titration with a standardized Na_2H_2EDTA solution and xylenol orange as indicator at pH=1. The H^+ concentration of the $Bi(ClO_4)_3$ solution was determined by using pH potentiometric titration in the presence of two fold excess of Na_2H_2EDTA.

H_4DOTA, H_5DTPA and H_3NTA were purchased from Sigma, while H_8DOTP, H_4AAZTA and H_5AAZTA-C4 ligands were synthesized following literature procedures [76]–[78]. H_4AAZTA-C4-TATE and H_3HP-DO3A was provided by Bracco Imaging spa. The concentration of the ligand stock solutions was determined by pH-potentiometric titration in the presence and absence of a large (40-fold) $CaCl_2$ excess. The pH-potentiometric titrations were made with standardized 0.2 M NaOH. The concentration of the AAZTA-C4-TATE stock solution was determined by spectrophotometry with the standardized $Bi(ClO_4)_3$ solution by following the formation of the $[Bi(AAZTA$-C4-TATE$)]^-$ complex at 280 nm and pH=7.4 (formation of the $[Bi(AAZTA$-C4-TATE$)]^-$ complex is rapid process).

Bi(III) complexes were prepared by the reaction of the ligand and equivalent amounts of $Bi(ClO_4)_3$. The $Bi(ClO_4)_3$ solution was slowly added dropwise to the intensively stirred solution of DOTA, DOTP, HP-DO3A, DTPA, AAZTA, AAZTA-C4 and AAZTA-C4-TATE. The pH of the

solution was controlled, and it was set to 5.0-7.0 by addition of concentrated NaOH solution.

III.2.   pH-potentiomtery

The protonation constants of the ligands and the Bi(III) complexes were determined by pH potentiometric titration with 0.2 M NaOH at 25°C using a constant ionic strength (0.15 M NaClO$_4$) in 6 mL samples. The concentration of the ligand and Bi(III) complexes was generally 0.002 M. For the pH measurements and titrations, *Metrohm 888 Titrando* titration workstation equipped with *Metrohm-6.0234.110* combined electrode loaded with 3 M NaCl solution was used. The solutions were stirred, and N$_2$ was bubbled through them. The titrations were made in the pH range of 1.7-12.0. KH-phthalate (pH=4.005) and borax (pH=9.177) buffers were used to calibrate the pH meter. For the calculation of [H$^+$] from the measured pH values, the method proposed by *Irving et al.* was used as follows:[79] 0.01M HClO$_4$ solution was titrated with standardized NaOH solution at 0.15 M NaClO$_4$ ionic strength. The differences (*A*) between the measured (pH$_{read}$) and calculated pH (-log[H$^+$]) value (*i.e.*, the average of A values in the pH-range of 1.75-2.20 was used to obtain the equilibrium H$^+$ concentration from the pH values measured in the titration experiments (typically *A*=-0.042). For the equilibrium calculations, the stoichiometric water ionic product (*pK$_w$*) was also calculated. The V$_{NaOH}$ – pH$_{read}$ data pairs of the HClO$_4$ – NaOH titration obtained in the pH range 10.8 – 12.0 were used to calculate the pK_w value (pK_w=13.65).

III.3. Determination of stability constants of Bi(III) complexes

The stability constants of the [Bi(NTA)] and $[Bi(NTA)_2]^{3-}$ complexes were determined by following the competition reactions in Bi(III) - NTA – H^+ systems with spectrophotometry at the absorption band of [Bi(NTA)] and $[Bi(NTA)_2]^{3-}$ complexes in the wavelength range of 240-300 nm. In these experiments two series of samples were prepared with $[Bi^{3+}]$=0.1 mM and [NTA]=0.1 mM or $[Bi^{3+}]$=0.1 mM and [NTA]=0.2 mM in 0.15 M $NaClO_4$ solution. In the first series the -log[H^+] values were adjusted to 0.1, 0.3, 0.6 and 1.0 M with the addition of calculated amounts of 3.0 M $HClO_4$ (ionic strength was not constant in these samples). In the second series, the pH values of the samples were adjusted by stepwise addition of the concentrated NaOH and $HClO_4$ solutions in the pH range 2.0 – 5.5.

The stability constants of $[Bi(DOTA)]^-$, $[Bi(DOTP)]^{5-}$, $[Bi(AAZTA)]^-$, $[Bi(AAZTA-C4-COO^-)]^{2-}$ complexes were determined by following the competition reactions of DOTA, DOTP, AAZTA and AAZTA-C4-COO$^-$ ligands with NTA for the Bi(III) ion with spectrophotometry at the absorption band of $[Bi(DOTA)]^-$, $[Bi(DOTP)]^{5-}$, $[Bi(AAZTA)]^-$, $[Bi(AAZTA-C4-COO^-)]^{2-}$ complexes in the wavelength range of 260-310 nm (10 wavelenghts). For Bi(III) -DOTA - NTA systems, six samples were prepared with $[Bi^{3+}]$=50 μM, [NTA]=50 mM and [DOTA]=0.0, 20, 40, 60, 80 and 100 μM in 0.15 M $NaClO_4$ solution. For Bi(III) - DOTP - NTA systems, eight samples were prepared with [Bi(III)]=50 μM, [NTA]=10 mM and [DOTP]=0.0, 30, 60, 90, 120, 150, 210 and 300 μM in 0.15 M $NaClO_4$ solution. The pH values of the samples were adjusted to 3.0 by stepwise addition of the concentrated NaOH and $HClO_4$ solutions. The samples were kept for a week at 50°C and eight weeks at 25°C in order to attain equilibrium. The time needed to reach the

equilibrium was determined by spectrophotometry. For Bi(III) -AAZTA - NTA systems, five samples were prepared with $[Bi^{3+}]$=30.2 μM, [NTA]=10 mM and [AAZTA]=0.0, 10, 20, 30 and 50 μM in 0.15 M NaClO$_4$ solution. For Bi^{III} - AAZTA-C4-COOH - NTA systems, six samples were prepared with $[Bi^{3+}]$=27.0 μM, [NTA]=30 mM and [AAZTA-C4-COO$^-$]=5.0, 10, 20, 30, 40 and 60 μM in 0.15 M NaClO$_4$ solution ($[Bi(NTA)_2]^{3-}$ was prepared at pH=7.4 in 10 or 30 mM solution of NTA). The pH values of the samples were adjusted to 7.4 by stepwise addition of the concentrated NaOH and HClO$_4$ solutions. The samples were kept at 50°C for a week and then at 25°C for two weeks in order to attain equilibrium. For the calculations of the stability constants of the Bi(III) complexes, the molar absorptivities of [Bi(NTA)], $[Bi(NTA)_2]^{3-}$, [Bi(DOTA)]$^-$, [Bi(DOTP)]$^{5-}$, [Bi(AAZTA)]$^-$ and [Bi(AAZTA-C4-COO$^-$)]$^{2-}$ complexes were determined by recording the spectra of 0.01, 0.05, 0.1 and 0.2 mM solutions of [Bi(NTA)], $[Bi(NTA)_2]^{3-}$, [Bi(DOTA)]$^-$, [Bi(DOTP)]$^{5-}$ in the presence of 0.15 M NaClO$_4$. ([Bi(NTA)] was prepared at pH=2.0 in the presence of two fold NTA excess). The spectrophotometric measurements were made with the use of *PerkinElmer Lambda 365* UV-Vis spectrophotometer at 25 °C, using 1.0 cm cells. The protonation and stability constants were calculated with the PSEQUAD program.

The thermodynamic properties of [Bi(AAZTA-C4-TATE)] complex were characterized by the conditional stability constant ($\log K^{cond}$) at pH=7.4 in 0.15 M NaClO$_4$ solution. To determine the $\log K^{cond}$ value of [Bi(AAZTA-C4-TATE)]$^-$ complex, the competition reaction of AAZTA-C4-TATE with NTA at pH=7.4 in 0.15 M NaClO$_4$ solution have been studied by Capillary Zone Electrophoresis (CZE) due to the high sensitivity

and the low material demand of the CZE method. For capillary electrophoresis *Hewlett-Packard HP^{3D}* capillary electrophoresis system was used. Separations were performed using bare fused-silica capillaries of 64 cm x 50 μm i.d. (*Agilent*). Before the first use of the capillary it was washed with 1.0 M NaOH (15 min), with 0.1 M NaOH (30 min) and with the buffer electrolyte (30 min). Prior to CE analysis all buffers were filtered through a 0.45 μm syringe filter and stored in refrigerator at +4ºC. In CZE the sample solutions were introduced at the anodic end of the capillary in normal mode (50 mbar, 6 s). The effective length of the capillary was 56 cm. The capillary was preconditioned with the buffer electrolyte (150 mM disodium hydrogen phosphate, pH=7.4) for 3 minutes. The separation was performed at 10°C with the application of 20 kV voltage. After analysis, the postconditioning (0.1 M NaOH (3 min) and buffer (3 min)) was applied to remove all possibly adsorbed materials from the capillary. In all measurements, 5 mM DMSO as internal standard was applied in order to correct the migration time of components on the electropherogram. The detection was carried out by on-column DAD measurement at 200 nm. The electropherograms were recorded and processed by ChemStation computer program of B.04.02 version (*Agilent*).

In CZE experiments, 5 samples were prepared in which the concentration of Bi(III) and NTA was 30.2 μM and 15.0 mM, respectvelly while that of the AAZTA-C4-TATE was varied between 0.0 and 50.4 μM. Samples were prepared by the addition of AAZTA-C4-TATE to the pre-prepared $[Bi(NTA)_2]^{3-}$ complex in 0.15 M NaClO$_4$ solution. The pH was adjusted to pH=7.4 by stepwise addition of concentrated NaOH or HClO$_4$. The samples were kept at 50°C for a week and then at 25°C for two weeks in order to attain the equilibrium (the time needed to reach the equilibria

25

was determined by capillary electrophoresis). For the equilibrium calculations, the molar integral values of the AAZTA-C4-TATE and [Bi(AAZTA-C4-TATE)]⁻ were used. The molar integral values of the AAZTA-C4-TATE and [Bi(AAZTA-C4-TATE)]⁻ were determined by recording the electropherograms of 10, 20, 30 and 40 μM AAZTA-C4-TATE and [Bi(AAZTA-C4-TATE)]⁻ solutions at pH=7.4 and 25°C in the presence of 0.15 M NaClO$_4$ ionic strength. The individual linear regression equations (response-concentration) for each component were determined according to four concentrations. The peak areas were found to be linear ($R^2 > 0.998$) in a concentration range specified in III.3.1 Table, in each case with a precision better than 4%. The limit of detection (LOD) and linear range values obtained at 200 nm are summarized in Table III.3.1.

Table III.3.1 Analytical performance data of the CZE determination of AAZTA-C4-TATE and Bi(AAZTA-C4-TATE) at pH=7.4 and 25°C in 0.15 M NaClO$_4$

	LOD[a] (μM)	molar integral (mAu⁻¹M⁻¹)	linear range (μM)
AAZTA-C4-TATE	0.467	$(1.6 \pm 0.1) \times 10^6$	10 - 40
Bi(AAZTA-C4-TATE	0.534	$(1.8 \pm 0.1) \times 10^6$	10 - 40

[a] LOD=3σ/μ molar integral

III.4. Formation kinetic studies of [Bi(DOTA)]⁻ and [Bi(DOTP)]⁵⁻ complexes

Formation rates of [Bi(DOTA)]⁻ and [Bi(DOTP)]⁵⁻ were studied by spectrophotometry at 308 nm in the presence and absence of citrate as an auxiliary ligand in order to avoid the hydrolysis of the Bi(III) ion. The formation of [Bi(DOTA)]⁻ was followed with a *PerkinElmer Lambda 365 UV-Vis* spectrophotometer at 25 °C, using 1.0 cm cells (pH=3.3–5.9).

However, the formation of $[Bi(DOTP)]^{5-}$ was too fast for the conventional spectrophotometry. Therefore, the formation of $[Bi(DOTP)]^{5-}$ was monitored with *Applied Photophisics DX-17MV* stopped-flow instrument using l=1.0 cm (pH=3.0–5.6) at 25°C in the presence of 0.15 M NaClO₄. The formation of Bi(III) complexes were studied in the presence of a 2- to 40-fold DOTA or DOTP excess in order to guarantee the pseudo-first order conditions ($[Bi(III)]_{tot}$=25 µM). The effect of citrate for the formation rate of $[Bi(DOTA)]^-$ and $[Bi(DOTP)]^{5-}$ was also investigated in the presence of 0.05 – 2.0 mM citrate in the pH range 3.0 – 5.6 ($[Bi(III)]_{tot}$=25 µM, $[DOTA]_{tot}$=1.0 mM, $[DOTP]_{tot}$=0.1 mM, 0.15 M NaClO₄, 25°C). pH values were maintained constant by the application of 0.01 M buffers (chloroacetic acid (CA), N-methyl-piperazine (NMP), N,N-dimethyl-piperazine (DMP), MES). The pseudo-first order rate constants (k_{obs}) were calculated by fitting the absorbance values to the Eq. III.4.1.

$$A_t = (A_0 - A_e)e^{(-k_{obs}t)} + A_e \qquad \text{III.4.1}$$

where A_0, A_e and A_t are the absorbance values at the start (t=0 s), at equilibrium and at the t time of the reaction, respectively.

To investigate the formation and the compostion of the diprotonated *[Bi(H₂DOTP)] intermediate in the Bi(III) -H₆DOTP reaction system ΔpH value was determined by spectrophotometry at 506 nm in the presence of methyl-orange as indicator ($[Bi(III)]_{tot}$=0.5 mM, [H₆DOTP], [methyl orange]$_{tot}$=12.5 µM, pH$_{end}$=3.17, 0.15 M NaClO₄, 0°C). ΔpH was calculated by considering the absorbance values of the Bi(III)-H₆DOTP reaction system at the start (A_0) and at equilibrium (A_e). A_0 and A_e were calculated by fitting of the absorbance values to Eq. (III.4.1). For the calculation of ΔpH, the protonation constant $(\log K^H$=3.52 (4)) and the

molar absorptivity of the protonated (ε_{HL}=42780 M^{-1}cm^{-1}) and deprotonated (ε_{L}=15483 M^{-1}cm^{-1}) methyl-orange at 506 nm was determined by recording the absorption spectra of methyl orange with *PerkinElmer Lambda 365 UV-Vis* spectrophotometer in the pH range 2.5-4.5 ([methyl orange]$_{tot}$=12.5 μM, 0.15 M NaClO$_4$, 0°C). The absorbance of the methyl orange at any wavelengths is a combination of the absorption of each protonated species and expressed by Eq. III.4.2.

$$A = \sum[H_iL]\varepsilon_{H_iL}\, l \qquad\qquad III.4.2$$

where, A is the absorbance at a given wavelength, [H$_i$L], ε_{HiL} and l are the concentration and the molar absorptivity of the species and the path length of the cell, respectively. The absorbance values (A) of methyl orange obtained at 506 nm have been fitted to the Eq (III.4.2) (the concentration of the different protonated species has been expressed by the protonation constants, K_i^H, Eq. (IV.1.1)). The calculations were performed by using the computer program Micromath Scientist, version 2.0 (Salt Lake City, UT, USA).

III.5.   Dissociation kinetic studies of Bi(III) complexes.

The kinetic inertness of the [Bi(DOTA)]$^-$, [Bi(DOTP)]$^{5-}$, [Bi(AAZTA)]$^-$, [Bi(AAZTA-C4-COO$^-$)]$^{2-}$, [Bi(AAZTA-C4-TATE)]$^-$ and [Bi(DTPA)]$^{2-}$ was characterized by the rates of the transchelation reactions taking place with transchelating AAZTA, DTPA, DOTP and HP-DO3A ligands in acidic and basic conditions. The exchange reactions in [Bi(DOTA)]$^-$ - AAZTA, [Bi(DOTP)]$^{5-}$ - AAZTA, [Bi(AAZTA)]$^-$ - DTPA, [Bi(AAZTA-C4-COO$^-$)]$^{2-}$ - DOTP and [Bi(DTPA)]$^{2-}$ - DOTP systems were studied by spectrophotometry, following the dissociation of the [Bi(DOTA)]$^-$ and

[Bi(DOTP)]$^{5-}$ complexes at 308 nm and the formation of [Bi(DTPA)]$^{2-}$ and [Bi(DOTP)]$^{5-}$ complexes at 278 and 308 nm. The concentration of the [Bi(DOTA)]$^{-}$ and [Bi(DOTP)]$^{5-}$ was 50 μM, while the concentration of AAZTA was 40 times higher, in order to guarantee pseudo-first order conditions. The temperature was kept at 25°C and the ionic strength of the solutions was kept constant, 0.15 M for NaClO$_4$. The exchange rates were studied in the pH range about 1.0 – 3.3. For keeping the pH values constant, mono-chloroacetic acid buffer (0.01 M) was used. In the transchelation reactions of the [Bi(AAZTA)]$^{-}$ - DTPA, [Bi(AAZTA-C4-COO^{-})]$^{2-}$ - DOTP and [Bi(DTPA)]$^{2-}$ - DOTP systems, the concentration of [Bi(AAZTA)]$^{-}$, [Bi(AAZTA-C4-COO^{-})]$^{2-}$ and [Bi(DTPA)]$^{2-}$ was 0.1 mM while the concentration of DTPA and DOTP was 10 - 20 and 20 - 40 times higher in order to guarantee pseudo-first order conditions. The temperature was maintained at 25°C and the ionic strength of the solutions was kept constant, 0.15 M for NaClO$_4$. The pH was adjusted to 8.5, 9.0, 9.5, 10.0, 10.5, 11.0 and 11.5 by stepwise addition of concentrated NaOH or HClO$_4$. For keeping the pH values constant 0.01 M N-methyl-piperazine - NMP (pH≤11) buffers were used. At pH>11, buffer was not used to keep the constant pH due to the presence of large [OH^{-}] excess. The pseudo-first order rate constants (k_d) were calculated by fitting the absorbance – time data sets to Eq. III.5.1.

$$A_t = (A_0 - A_e)e^{(-k_d t)} + A_e \qquad\qquad III.5.1$$

where A_0, A_e and A_t are the absorbance values at the start (t=0 s), at equilibrium and at the t time of the reaction, respectively.

The ligand exchange reaction of [Bi(DOTA)]$^{-}$ and [Bi(DOTP)]$^{5-}$ with HP-DO3A as an exchanging ligand have also been studied by *Capillary Zone Electrophoresis* (CZE) in the pH range 10.0 – 12.0. The

29

transchelation reactions of [Bi(DOTA)]$^-$ and [Bi(DOTP)]$^{5-}$ were studied by following the formation of the [Bi(HP-DO3A)] complex (migration time is 5.2 min) with *Hewlett-Packard HP^{3D}* capillary electrophoresis system. The concentration of the HP-DO3A was 5 and 10 mM, while the Bi(III) complexes was employed in high excess ([BiL]$_{tot}$=60 mM), in order to guarantee pseudo-first order conditions. The temperature was maintained at 25°C and the ionic strength of the solutions was kept constant, 0.15 M NaClO$_4$. The exchange rates were studied in the pH range about 9.0 – 11.5. For keeping the pH values constant, 0.01 M phosphate buffers were used. The rates of the transchelation reactions have been studied in the presence of Bi(III) complex excess, when the reactions can be regarded as pseudo-first order ones and the rates of transmetallation can be expressed by Eq. III.5.2.

$$-\frac{d[BiL]_t}{dt} = \frac{d[Bi(HP-DO3A)]_t}{dt} = k_d[BiL]_t \qquad III.5.2$$

where k_d is a pseudo-first order rate constant, [BiL]$_{tot}$ and [Bi(HP-DO3A)]$_{tot}$ are the concentration of complexes, containing the species [Bi(DOTA)]$^-$, [Bi(DOTP)]$^{5-}$ and [Bi(HP-DO3A)] at the time *t*, respectively. During the progress of the transchelation reactions the concentration of the [Bi(HP-DO3A)] complex increases. By the following the integral of the [Bi(HP-DO3A)] formed in transchelation reaction of the Bi(III) complex, the first-order rate constant, k_d can be expressed by Eq. III.5.3.

$$k_d = \frac{\Delta \int}{\Delta t} \times \frac{1}{\int^M_{Bi(HP-DO3A)}} \times \frac{1}{[BiL]_t} \qquad III.5.3$$

In the Eq. (III.5.3) $\Delta \int$ is the increase of the integral value of [Bi(HP-DO3A)] during the time Δt. $\int^M_{Bi(HP-DO3A)}$ is the molar integral value of the

[Bi(HP-DO3A)] ($\int^{M}_{Bi(HP-DO3A)}$=1.96×10^6 mAU^{-1}M^{-1}), which was determined by recording the CZE electropherograms of 0.2, 0.4, 0.6, 0.8, 1.0, 1.2, 1.4 and 1.7 mM solutions of [Bi(HP-DO3A)] complex at pH=7.4 and 25°C in the presence of 0.15 M NaClO$_4$ ionic strength.

The kinetic inertness of [Bi(AAZTA-C4-TATE)]$^-$ was determined by following the ligand exchange reaction of [Bi(AAZTA-C4-TATE)]$^-$ with AAZTA by CZE at pH=9.0 and 25°C in 0.15 M NaClO$_4$ solution. At pH=9.0 the degradation of the TATE unit in [Bi(AAZTA-C4-TATE)]$^-$ takes place slowly, whereas the transchelation reactions of [Bi(AAZTA-C4-TATE)]$^-$ was not too slow to be monitored by CZE method. For the kinetic experiments, two samples were prepared with 50.1 μM [Bi(AAZTA-C4-TATE)]$^-$ in the presence of 20 and 40 fold excess AAZTA ligand in order to guarantee the pseudo-first order kinetic condition. The pH was adjusted to pH=9.0 by stepwise addition of concentrated NaOH or HClO$_4$. The temperature was maintained at 25°C and the ionic strength of the solutions was kept constant, 0.15 M for NaClO$_4$. The pseudo-first order rate constants (k_{obs}=k_d) were calculated by fitting the absorbance data to Eq. (III.5.1). Calculation of the kinetic parameters were performed by the fitting of the absorbance and area - time data pairs to Eq. (III.5.1) with the *Micromath Scientist* computer program (version 2.0, Salt Lake City, UT, USA).

III.6. Radiolabeling of DOTA with ²¹³Bi isotope in the presence of citrate, acetate and MES buffers

In order to investigate the effect of different buffers on the formation of $[^{213}Bi(DOTA)]^{-}$, the labeling yield of DOTA ligand with ^{213}Bi isotope was determined by radio-TLC in the presence of trisodium-citrate, ammonium-acetate and MES buffers (MES: 2-(*N*-morpholino)ethanesulfonic acid). Radiolabeling of DOTA with ^{213}Bi isotope was performed by Prof. Johannes Notni in Technical University of Munich.

III.7. Radiolabeling of AAZTA-C4-TATE and DOTA-TATE with ²⁰⁵/²⁰⁶Bi isotope, *in vitro* and *ex vivo* studies of [²⁰⁵/²⁰⁶Bi][Bi(AAZTA-C4-TATE)]⁻

Suprapur nitric acid (s.p. HNO_3), $\geq 96\%$ ethanol and the human plasma type AB from male AB were obtained from Merck. Ultrapure ammonium acetate (CH_3CCONH_4) was purchased from VWR. TK-200 resin (a trioctyl-phosphine oxide (TOPO) based extractant) was purchased from TRISKEM. The Strata-X 33u Polymeric Reversed Phase cartridge was purchased from Phenomenex. Glass macrofiber chromatography paper impregnated with silica gel (iTLC-SG) was bought from Agilent Technologies. All other solvents and reagents were bought from ROTH. Labelling experiments were followed by Raytest miniGita Star TLC scanner with beta-positron detector.

The $^{205/206}Bi$ isotope mixture was produced in a GE PETtrace cyclotron with 16 MeV proton beam on natural Pb-foil target (99.995%, 0.9 by 0.9 cm, 0.25 mm thick). A 60 min irradiation with a 10 μA beam current yielded approx. 60 MBq activity. After a 24 hours decay period,

the irradiated Pb target was dissolved in 7 M suprapur HNO_3 (2 mL). Solutions were prepared with ultrapure (u.p.) water. $Pb(NO_3)_2$ precipitation was observed after the solution was concentrated to circa 1 mL. The solution was separated from the solid and diluted to 10 mL with u.p. water and filtered with Millipore 0.22-µm filter. This solution was transferred onto a column self-filled with TK 200 resin (150 mg), which is a trioctyl-phosphine oxide (TOPO) based extractant. The TK 200 column was preconditioned with 0.7 M s.p. HNO_3 (1 mL), 7 M s.p. HNO_3 (1 mL) and 0.7 M s.p. HNO_3 (5 mL). After loading the [205/206]Bi isotope solution the column was washed with 5 mL 0.7 M s.p. HNO_3 to remove the remaining Pb target contaminants and the [205/206]Bi isotopes were eluted with 7 M s.p. HNO_3 in 1 mL fractions. The fractions which contained [205/206]Bi isotopes (~30 MBq) were concentrated to dryness and were dissolved in 200 µL 0.1 M u.p. HCl. The activity of the solution was measured by ISOMED 2010 Dose calibrator at ^{18}F channel.

The effect of pH, temperature and ligand concentration on the labeling of AAZTA-TATE and DOTA-TATE ligands with [205/206]Bi(III) as a model of [213]Bi have been examined by radio-TLC method ([205]Bi: 100% β^+, $t_{1/2}$=15.31 d and [206]Bi: 100% β^+, $t_{1/2}$=6.24 d; [205]Bi:[206]Bi=1:2). 5 µl of the reaction mixture was dropped to a glass macrofiber chromatography paper impregnated with silica gel (iTLC-SG) strip. The strip has 12.5 cm length and 1.5 cm wide, start line was placed 1.5 cm and the front line was placed 1 cm. It was developed in 0.5 M sodium citrate eluent (pH=5.5). The [205/206]Bi[III] in the form of citrate complex was eluted with the solvent front (R_f= 0.8 – 1), whereas the retention factor of [[205/206]Bi(AAZTA-C4-TATE)][-] were found to be 0.1 - 0.2. The stability of [[205/206]Bi][Bi(AAZTA-C4-TATE)][-] has been investigated in PBS buffer, 0.01 M DTPA solution

at room temperature and in human plasma at 37°C. Radio labeling of AAZTA-C4-TATE and DOTA-TATE with [205/206]Bi isotope and the stability of [[205/206]Bi][Bi(AAZTA-C4-TATE)][-] in PBS buffer, 0.01 M DTPA solution and in human plasma were performed by Dr. Adrienn Vágner and Dr. Gábor Nagy in Scanomed Ltd. and by Dr. Dezső Szikra in Department of Nuclear Medicine, Universitiy of Debrecen.

The somatostatin receptor specificity of [[205/206]Bi][Bi(AAZTA-C4-TATE)][-] and [[205/206]Bi][Bi(DOTA-TATE)][-] was investigated *in vitro* using AR42J cell line. The efficiency of [[213]Bi][Bi(AAZTA-C4-TATE)][-] as TAT agent of neuroendocrine tumours have been investigated by monitoring the relative accumulated dose (%ID/g) obtained at 15, 60 and 90 min for [[205/206]Bi][Bi(AAZTA-C4-TATE)][-] in AR42J tumour-bearing mice (n=9). The localization of the dissociated [205/206]Bi isotope was determined by *ex vivo* biodistribution studies of free [205/206]Bi in healthy control mice (n=3). Radioactivity was measured with a calibrated gamma counter (*Perkin-Elmer Packard Cobra*, Waltham, MA, USA). *In vitro* and *ex vivo* studies were performed by Dr. György Trencsényi in Department of Nuclear Medicine, Universitiy of Debrecen.

III.8.   Multinuclear 1D and 2D NMR studies of DOTP ligand and Bi(III) complexes

^{1}H, ^{13}C and ^{31}P NMR measurements were performed with the Bruker Avance III (9.4 T) spectrometer, equipped with Bruker Variable Temperature Unit (BVT), Bruker Cooling Unit (BCU) and a BB inverse *z* gradient probe (5 mm). $\log K_1^H$ and $\log K_2^H$ values of DOTP[8-] ligand were determined by following the ^{1}H and ^{31}P NMR chemical shifts of DOTP ligand as a function of -log[H^{+}]. Since the protonation/deprotonation is fast

on the NMR time scale, the chemical shifts of the observed signals represent a weighted average of the shifts of the different species involved in a specific protonation step (Eq. (III.8.1)):[80]

$$\delta_{obs} = \sum x_i \delta^{H_i L} \qquad\qquad III.8.1$$

where, δ_{obs} is the observed chemical shift of a given signal (^{1}H and ^{31}P), x_i and $\delta^{H_i L}$ are the molar fraction and the chemical shift of the involved species, respectively. The observed chemical shifts (δ_{obs}) have been fitted to the Eq. (III.8.1), respectively (the molar fractions x_i and the concentration of the different protonated species have been expressed by the protonation constants K_i^H, Eq. (IV.1.1)).

For these experiments, a 0.01 M solution of DOTP in 0.15 M NaClO$_4$ aqueous solution was prepared (a capillary with D$_2$O was used for lock). The -log[H$^+$] values were adjusted by stepwise addition of NaOH and HClO$_4$ solutions (both prepared in H$_2$O). At -log[H$^+$]>12.0 the required -log[H$^+$] values of the DOTP solution were obtained by the addition of calculated amount of 19.3 M NaOH solution. The chemical shifts are reported in ppm, relative to DSS for ^{1}H and ^{13}C and 85% H$_3$PO$_4$ for ^{31}P as the external standard. The protonation constants were determined by fitting of the chemical shift versus -log[H$^+$] data using *Micromath Scientist, version 2.0* (Salt Lake City, UT, USA).

VT- NMR spectra of [Bi(DOTP)]$^-$ were aquired in 0.1 M samples prepared at pD=10 in D$_2$O. The ^{1}H-^{1}H COSY and [1]H-^{1}H EXSY spectra were collected by using gradient pulses in the z direction with the standard Bruker pulse program. The [1]H - [13]C correlation spectra were recorded by using gradient pulse in the z direction with the usual Bruker heteronuclear single quantum coherence (HSQC) pulse sequence. 1D and 2D NMR spectra of [Bi(DOTP)]$^{5-}$ obtained in the temperature range 273 - 333 K are

shown in the Appendix Figures A.2-A.6. ^{1}H and ^{13}C NMR signals of the [Bi(DOTP)]$^{5-}$ were assigned on the basis of ^{1}H – ^{1}H COSY (Figure A.8), ^{1}H – ^{1}H EXSY (Figure A.9) and ^{1}H – ^{13}C HSQC (Figure A.10) techniques at 273 and 298K. Dynamic properties of H$_6$DOTP^{2-} and [Bi(DOTP)]$^{5-}$ complexes were investigated by Band-shape analyses with the use of *DNMR* program included in the *Bruker Topspin* software package. The ^{31}P NMR signals of H$_6$DOTP and ^{13}C NMR signals of [Bi(DOTP)]$^{5-}$ were simulated. Values of the chemical shift, the spin-spin coupling constants, intensity and line width without chemical exchange were fixed input parameters during the fitting procedure. Agreement of the measured and calculated ^{31}P NMR and ^{13}C NMR spectra obtained at different temperature was >92%.

Solution structure and dynamic properties of [Bi(AAZTA)]$^-$ and [Bi(AAZTA-C4-COO$^-$)]$^{2-}$ complexes were investidted by multinuclear 1D and 2D NMR spectrosctopy. For these experiments, a 0.01 M solution of [Bi(AAZTA)]$^-$ and 0.02 M sample of [Bi(AAZTA-C4-COO$^-$)]$^{2-}$ was prepared in D$_2$O. The pD was adjusted to 7.4 by stepwise addition of the NaOD and DCl solutions. The chemical shifts are reported in ppm, relative to DSS for ^{1}H as an external standard. The ^{1}H-^{1}H (COSY) and ^{1}H - ^{13}C (HSQC and HMBC) correlation spectra of [Bi(AAZTA)]$^-$ and [Bi(AAZTA-C4-COO$^-$)]$^{2-}$ were collected by using gradient pulses in the *z* direction with the standard Bruker pulse programs.

III.9. X-Ray diffraction studies of the [Bi(*H*AAZTA)] and [Bi(AAZTA)]$^-$ complexes

Colourless single crystals of formula [Bi(*H*AAZTA)(H$_2$O)]·3H$_2$O ([Bi(*H*AAZTA)]) suitable for X-ray diffraction studies were grown from

an aqueous solution of [Bi(*H*AAZTA)] complex prepared by mixing stoichiometric amounts of Bi_2O_3 and H_4AAZTA in water. Single crystals of $\{[C(NH_2)_3][Bi(AAZTA)]\}\cdot3.5H_2O$ ([Bi(AAZTA)]⁻) were grown from an aqueous solution of [Bi(*H*AAZTA)] complex at pH=6.0 adjusted by guanidine carbonate.

Single crystal XRD data collections were performed at the X-ray diffraction beamline (XRD1) of the Elettra Synchrotron, Trieste (Italy).[81] The crystals were dipped in NHV oil (Jena Bioscience, Jena, Germany) and mounted on the goniometer head with kapton loops (MiTeGen, Ithaca, USA). Complete datasets were collected at 100 K (nitrogen stream supplied through an Oxford Cryostream 700 (Oxford Cryosystems Ltd., Oxford, United Kingdom) through the rotating crystal method. Data were acquired using a monochromatic wavelength of 0.700 Å, on a Pilatus 2M hybrid-pixel area detector (DECTRIS Ltd., Baden-Daettwil, Switzerland). The diffraction data were indexed and integrated using XDS.[82] Two different datasets have been merged for [Bi(*H*AAZTA)], collected from random orientations of the same crystal. Semi-empirical absorption corrections and scaling were performed on datasets, exploiting multiple measures of symmetry-related reflections, using SADABS program [83]. Both the samples were prone to radiation damage, especially for the thin needles of ([Bi(AAZTA)]⁻), that show also limited diffraction power (best dataset resolution of ~0.86 Å). The structures were solved by the dual space algorithm implemented in the SHELXT code.[84] Fourier analysis and refinement were performed by the full-matrix least-squares methods based on F2 implemented in SHELXL (Version 2018/3)[85]. The Coot program was used for modeling.[86] Anisotropic thermal motion refinement have been used for all atoms with

occupancy greater than 50%. Hydrogen atoms were included at calculated positions with isotropic Ufactors = 1.2·Ueq or Ufactors = 1.5·Ueq for methyl and hydroxyl groups (Ueq being the equivalent isotropic thermal factor of the bonded non hydrogen atom). Hydrogen atoms for solvent water molecules have not been included in the refined models since it was not possible to locate them unambiguously in electron-density peaks of Fourier difference maps (contributions of these missing H atoms are still included in the properties reported in appendix Table.A.22). Geometric and thermal motion parameters restrain (DFIX, DANG, SIMU) have been applied on disordered and poorly defined fragments. Pictures were prepared using Ortep3,[87] CCDC Mercury[88] and Pymol [89] software. Essential crystal and refinement data are reported in the appendix Table.A.22). Deposition numbers: 2115291 and 2115292 contain the supplementary crystallographic data for compounds [Bi(AAZTA)]⁻ and [Bi(*H*AAZTA)], which are provided free of charge by the joint Cambridge Crystallographic Data Centre and Fachinformationszentrum Karlsruhe Access Structures service.

IV.   Results and Discussion

IV.1.   Acid-base properties of ligands.

The protonation constants of ligands, defined by Eq. IV.1.1, have been determined by pH-potentiometry, ^{1}H- and ^{31}P-NMR spectroscopy.

$$K_i^H = \frac{[H_i L]}{[H_{i-1}L][H^+]} \qquad\qquad IV.1.1$$

where i=1, 2…7. Because of the high log K_1^H and log K_2^H values of DOTP^{5-} the protonation constant of DOTP has also been determined by ^{1}H and ^{31}P NMR spectroscopy, recording the chemical shift variations of the non-labile protons and phosphorous atoms as a function of -log[H$^+$] (Figure IV.1.1).

The protonation sequence of the AAZTA ligand was characterized in detail by both spectroscopic and potentiometric methods.[90] The first protonation occurs at both endo- and exocyclic nitrogen atoms of the ligand (all nitrogen atoms are partially protonated). The second proton is attached to the exocyclic nitrogen, whereas the first proton is shifted to the exocyclic nitrogen because of the electrostatic repulsion between the protonated nitrogen atoms. Further protonations take place at the carboxylate groups attached the unprotonated exocyclic nitrogen or the exocyclic nitrogen groups. According to the similarities one it can be assumed that the protonation sequence of AAZTA-C4-COOH is similar to that of the parent AAZTA. A comparison of the protonation constants obtained in the presence of the same background electrolyte (0.15 M NaClO$_4$, Table IV.1.1) indicated that the log K_3^H value of AAZTA-C4-COOH is slightly larger than the corresponding protonation constants of AAZTA. By taking into account the protonation constant of *n*-valeric acid (log K_1^H=4.69, 1.0

M NaClO$_4$, 25°C)[91]. it is reasonable to assume that the 3rd protonation of AAZTA-C4-COOH occurs at the "IMDA" carboxylate. The comparison of the log K_i^H values in Table IV.1.1 reveals that the log K_1^H value of AAZTA determined in 0.15 M NaClO$_4$ or NaCl solution is significantly lower than that value obtained in 0.1 M KCl or Me$_4$NCl solutions due to the competition between the first protonation process and the Na$^+$ complexes formed in the presence of Na$^+$ion.[90] The fitting of the experimental data points are shown in Figures IV.1.1. The obtained log K_i^H values are listed in Table IV.1.1.

Table IV.1.1 Protonation constant of NTA, DTPA, DOTA, DOTP, AAZTA and AAZTA-C4-COO ligands (25°C).

	NTA	DTPA	DOTA		DOTP		AAZTA-C4-COOH		AAZTA	
I	0.15M NaClO$_4$	0.1 M NaClO$_4$ [e]	0.15M NaClO$_4$	0.1M Me$_4$N(NO$_3$)[a]	0.15M NaClO$_4$	0.1M Me$_4$N(NO$_3$)[b]	0.15 M NaClO$_4$	0.15 M NaCl[d]	0.15M NaClO$_4$	0.1M NaCl[c]
log K_1^H	9.22 (2)	10.00	9.12	12.09	*13.6 (1)	13.7	10.21 (2)	10.48	10.29 (2)	10.06
log K_2^H	2.80 (2)	8.63	9.50	9.76	*12.21 (4)	12.2	6.85 (3)	6.90	6.51 (3)	6.50
log K_3^H	1.06 (3)	4.13	4.51	4.56	8.62 (2)	9.28	**4.73 (3)**	**4.68**	3.86 (3)	3.77
log K_4^H	–	2.90	4.05	4.09	7.53 (2)	8.09	3.91 (4)	3.73	1.94 (3)	2.33
log K_5^H	–	2.46	2.05	–	5.82 (3)	6.12	2.83 (4)	2.60	1.00 (6)	1.51
log K_6^H	–	–	1.14	–	5.11 (3)	5.22	2.11 (3)	1.80	–	–
log K_7^H	–	–	–	–	1.64 (3)	–	–	–	–	–
Σlog K_i^H	13.08	28.12	30.37	30.50	54.53	54.61	25.91 (Σlog K_i^H-log K_3^H)	25.51 (Σlog K_i^H-log K_3^H)	23.6	24.17

[a] Ref. [[92]]; [b] Ref. [[93]]; [c] Ref.[[94]]* ^{1}H and ^{31}P NMR spectroscopy [d] Ref[[95]] [e] Ref[[96]]

The protonation of DOTA-like ligands is fully characterized with both spectroscopic and potentiometric methods.[93], [97]–[99] These studies reveal that the first and second protonation takes place at nitrogen atoms positioned trans to each other. Third and fourth protonation steps take place at the carboxylate or basic phosphonate groups of the pendant arms attached to the non-protonated ring nitrogen atoms, because of the greater charge separation and lower electrostatic repulsion between the protonated donor atoms.[93], [97] Further protonation processes occur on the non-protonated carboxylate/basic phosphonate groups of DOTA and DOTP ligands.[93], [97] Acidic phosphonate groups of DOTP might be protonated at pH<2.[93] Since the deprotonation of the ring nitrogen atoms in H_2DOTP^{6-} species takes place at pH>12, the accurate determination of the protonation constants cannot be performed by pH-potentiometry. Therefore, $\log K_1^H$ and $\log K_2^H$ values of the DOTP ligand were determined by ^{1}H and ^{31}P NMR spectroscopy (Figure IV.1.1). In the ^{1}H NMR spectra of DOTP there are only two signals, which can be assigned to the ring methylen protons of the macrocycle (a singlet) and the methylene protons of the phosphonate group (a doublet, $^2J_{PH}=9.8$ Hz), respectively. Starting from the basic form (solution), the addition of the first and the second equivalent of acid to DOTP results in a significant downfield shift of the ^{1}H NMR signals of both the ring and phosphonate methylen protons and the upfield shift of the ^{31}P NMR signal of the phosphonate group. Since the largest changes of the chemical shifts take place on the ^{1}H NMR signals of the ring methylen protons, it can be safely assumed that the first and second protonation processes occur at two opposite ring nitrogen atoms of the DOTP ligand.
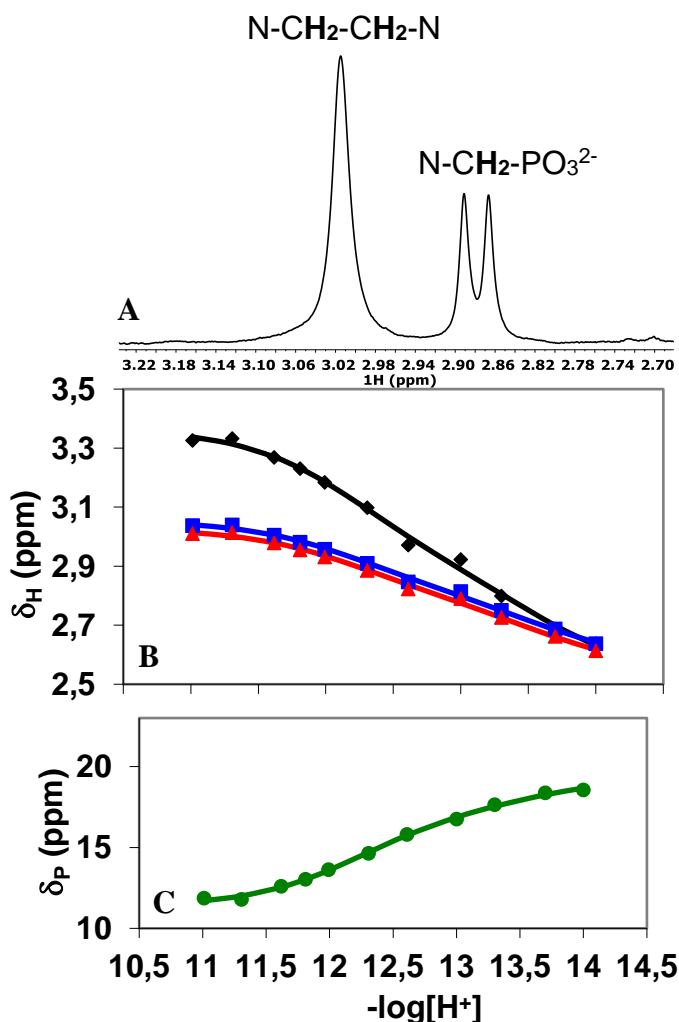
Figure IV.1.1 400 MHz ^{1}H-NMR spectra (**A**) at pH = 11.0 and the chemical shifts of the ring (◆) and the phosphonate (■, ▲) –CH$_2$- protons (**B**) and 162 MHz ^{31}P NMR shift of phosphorous atoms (●) of DOTP ligand at different pH (**C**). The solid lines and the symbols represent the calculated and the experimental δ_H and δ_P values, respectively ([DOTP]$_{tot}$=10 mM, pH=12.6, H$_2$O, [Na$^+$]$_{tot}$≤0.15 M→[NaOH]$_{tot}$+[NaClO$_4$]$_{tot}$=0.15 M, 25°C)

Comparison of the related protonation constants of DOTA ligand indicates that the log K_i^H values obtained in 0.15 M NaClO$_4$ and 0.15 M NaCl solutions are essentially identical confirming the negligible influence

of the anions of the background electrolyte for the protonation constants of the ligand. On the other hand, the log K_1^H value of DOTA obtained in 0.15 M NaClO$_4$ or 0.15 M NaCl is lower by about 3 log units than the constant determined in 0.1 M Me$_4$N(NO$_3$) solutions. The lower log K_1^H value obtained in NaClO$_4$ or NaCl solutions can be interpreted by the formation of the relatively stable [Na(DOTA)]$^{3-}$ complex (log$K_{Na(DOTA)}$=4.38).[100] The log K_i^H values of DOTP ligand determined in 0.15 M NaClO$_4$ and 0.1 M Me$_4$N(NO$_3$) solutions are essentially identical, which might be interpreted by the very weak interaction between the Na$^+$ ion and the DOTP ligand. Interestingly, the single resonance in ^{31}P NMR spectra of H$_6$DOTP is broadened and split into two resonances of equal area separated by about 14 ppm with the lowering of temperature from 313 K to 253 K at pH=2.5 in DMSO-D$_6$/H$_2$O: 40/60 vol % mixture (Figure IV.1.2). A similar behaviour for ligand DOTP was evidenced at pH=7.0.[76] By taking into account the structure of H$_6$DOTP species, it can be assumed that the broadening and coalescence of ^{31}P NMR signals is caused by the increased exchange rate of non-H-bonded and H-bonded phosphonate pendants with the protonated ring nitrogen atoms (Figure (IV.1.3.)). The ^{31}P-NMR signals of the –**PO**$_3$H$^-$ group were suitable to carry out line-shape analysis by simulating the ^{31}P NMR spectra obtained at different temperatures. The transverse relaxation time (T_2) of the –**PO**$_3$H$^-$ phosphorous signal was found to be T_2=0.016 s. The experimental spectra have been simulated using the chemical shift difference of the two phosphorous signals ($\Delta\delta$=2271 Hz). Examples for typical experimental and simulated spectra are shown in Figure IV.1.3.
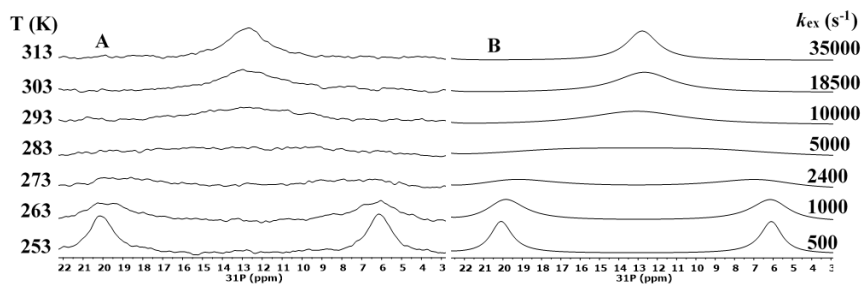
Figure IV.1.2. Experimental (**A**) and simulated (**B**) proton-decoupled ^{31}P NMR spectra of H_6DOTP in DMSO-D_6/ H_2O: 40/60 vol % mixture ([H_6DOTP]$_{tot}$=5.0 mM, 162 MHz.
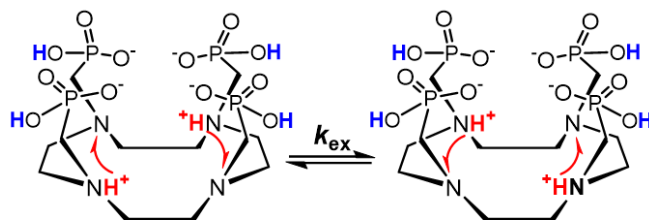
Figure IV.1.3. Proposed isomerization process of the H_6DOTP species

The activation parameters (Table IV.1.2) of the isomerization process for H_6DOTP species have been estimated with the *Eyring* equation by using the k_{ex} rate constant obtained by the line-shape analysis The Eyring plot for the determination of the activation parameters for H_6DOTP species is shown in the appendix Figure A.1.

Table IV.1.2 Rate constants and activation parameters of the isomerization process for H_6DOTP species obtained from the line-shape analysis of the ^{31}P NMR spectra.

	H$_6$**DOTP**
$\Delta H^{\ddagger}$ /kJ·mol^{-1}	45 ± 1
$\Delta S^{\ddagger}$ / J·mol^{-1}K^{-1}	-15 ± 2
$\Delta G^{\ddagger}_{298}$ /kJ·mol^{-1}	49 ± 1
k_{ex}^{298} /s^{-1}	13226

The activation energy ($\Delta G^{\ddagger}_{298}$) of the isomerization process of the H$_6$DOTP is 45 kJ·mol^{-1}, which is somewhat lower than that of H$_3$DOTP-H$_4$DOTP mixture obtained at pH=7.0 ($\Delta G^{\ddagger}_{298}$=56 kJ·mol^{-1}).[76] The lower $\Delta G^{\ddagger}_{298}$ value of H$_6$DOTP might be explained by the protonation of the phosphonate pendants results in the weaker interaction between the non-protonated phosphonate O$^-$ and the protonated ring nitrogen donor atoms. Our band shape analysis provides negative activation entropy ($\Delta S^{\ddagger}$), which is probably related to the reorganization of the hydration shell around the positively charged ring NH$^+$ donor atoms in the transition state.

IV.2. Equilibrium, kinetic and structural studies of [Bi(DOTA)]$^-$ and [Bi(DOTP)]$^{5-}$ complexes

The stability constants of Bi(III)-polyamino-policarboxylate complexes have been commonly determined by spectrophotometry relying on the competition or decomplexation reaction by Br$^-$ at acidic conditions (pH= 2-3) or by OH$^-$ at basic conditions (pH> 11).

Stepwise, cumulative and conditional stability and protonation constants of Bi(III) complexes are defined by Eq IV.2.1-IV.2.5, where $\alpha_H = K_1[\text{H}^+] + K_1 K_2[\text{H}^+] + \ldots K_1 K_2 .. K_n[\text{H}^+]^n$.

$$K_{\text{BiL}} = \frac{[\text{BiL}]}{[\text{Bi}^{3+}][\text{L}]} \qquad\qquad IV.2.1$$

$$\beta_{\text{BiL}} = \frac{[\text{BiL}_2]}{[\text{Bi}^{3+}][\text{L}]^2} \ \ (\text{L=NTA}) \qquad IV.2.2$$

$$K_{\text{Bi}(\text{H}_i\text{L})} = \frac{[\text{Bi}(\text{H}_i\text{L})]}{[\text{Bi}(\text{H}_{i-1}\text{L})][\text{H}^+]} \qquad IV.2.3$$

$$K_{\text{BiL}}^{\text{cond}} = \frac{K_{\text{BiL}}}{(1+\alpha_H)} \qquad\qquad IV.2.4$$

$$\beta_{\text{BiL}_2}^{\text{cond}} = \frac{\beta_{\text{BiL}_2}}{(1+\alpha_H)^2} \qquad\qquad IV.2.5$$

IV.2.1 Equilibrium studies of Bi(III) - NTA system

Karadakov and co-workers had determined the stability constants of the [Bi(NTA)] and $[Bi(NTA)_2]^{3-}$ complexes defined by Eqs. (IV.2.1) and (IV.2.2) by spectrophotometry in 1.0 M $NaClO_4$ solution ($\log K_{Bi(NTA)}=17.54$, $\log K_{Bi(NTA)2}=9.01$, $\log \beta_{Bi(NTA)2}=26.55$, 25°C, 1.0 M $NaClO_4$,[101]. To obtain equilibrium data for Bi(III) - NTA system in 0.15 M $NaClO_4$ solution, the stability constants of [Bi(NTA)] and $[Bi(NTA)_2]^{3-}$ complexes (Eqs. (IV.2.1) and (IV.2.2)) were also determined by spectrophotometry at 25 ºC in 0.15 M $NaClO_4$ solution.

The K_{BiL} and β_{BiL2} values have been calculated from the spectrophotometric titration data obtained at 1:1 and 1:2 metal to ligand concentration ratio. The equilibrium reaction has been studied in the – $\log[H^+]$ range of 0.0 – 5.3 (the ionic strength were constant I=$[NaClO_4]+[HClO_4]$=0.15 in the samples $[H^+]\leq0.15$ M), where the formation of Bi^{III}, BiL, BiL_2 and H_xL species was assumed (x=1 – 3, y=1 or 2). Some characteristic absorption spectra of Bi(III) - NTA systems are shown in Figure IV.2.1.1.

$$Bi^{3+} + yH_xNTA \rightleftharpoons Bi(NTA)_y + x \times yH^+ \qquad \textit{IV.2.1.1}$$
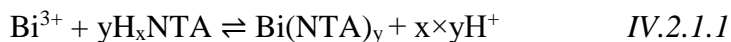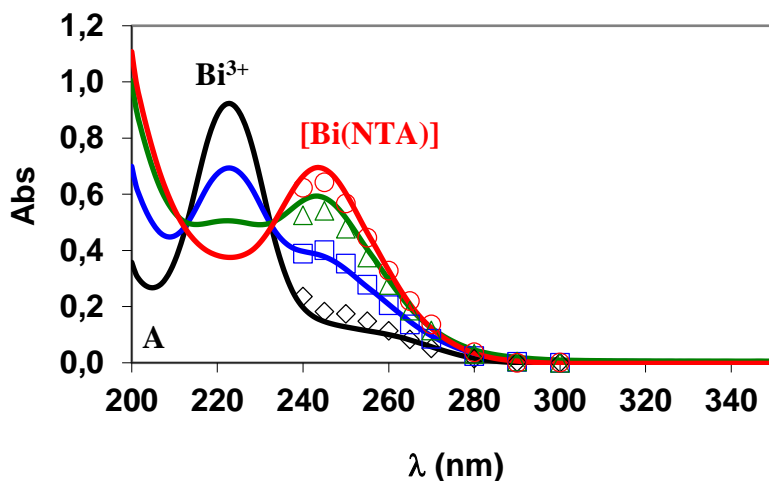
Figure IV.2.1.1 Absorption spectra of the Bi(III) - NTA system at 1:1 (**A**) metal to ligand concentration ratio. The solid lines and the open symbols represent the experimental and the calculated absorbance values, respectively. **A**: $[Bi(III)]_{tot}=[NTA]_{tot}=0.1$ mM, $-\log[H^+]=$**0.1**, **0.3**, **0.6** and **1.0** M.
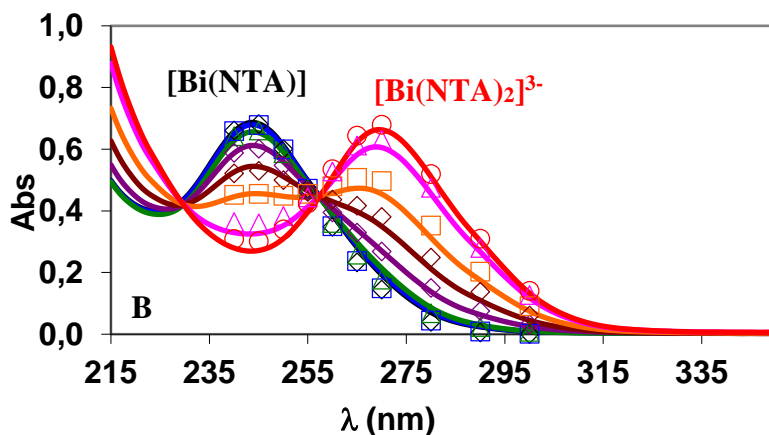
Figure IV.2.1.2. Absorption spectra of the Bi(III) - NTA system at 1:2 (**B**) metal to ligand concentration ratio. The solid lines and the open symbols represent the experimental and the calculated absorbance values, respectively.**B:** $[Bi(III)]_{tot}=0.1$ mM, $[NTA]_{tot}=0.2$ mM, pH=**2.01**, **2.41**, **2.95**, **3.52**, **3.96**, **4.42** and **5.15**, $[H^+] \leq 0.15$ M$\rightarrow[Na^+]+[H^+]=0.15$ M, l=1 cm, 25°C

Stability constant of the $[Bi(NTA)]$ and $[Bi(NTA)_2]^{3-}$ complexes at 25°C in 0.15 M NaClO$_4$ solution were found to be $K_{BiL}=16.97$ (3) and $\beta_{BiL2}=26.20$ (6), which are in a good agreement with the $K_{BiL}=17.53$ and

48

β_{BiL2}=26.56 values obtained at 25°C in 1.0 M NaClO$_4$ solution by Karadakov and co-workers.[101]

IV.2.2 Equilibrium studies of the of Bi(III)-DOTA-NTA and Bi(III)-DOTP-NTA systems

Based on our model calculations the nitrilotriacetic acid (H$_3$NTA) can efficiently compete with the H$_8$DOTP and H$_4$DOTA for the Bi(III) ion in the pH range of 1.8-3.2 regardless of the fact that the stability constant of the Bi(III) complexes are log$K_{BiL} > 30.0$, due to the comparatively low conditional stability constant of the protonated [Bi(H$_x$DOTP)]$^{x-5}$ and [Bi(DOTA)]$^-$ species. The four basic phosphonate O donor atoms, which do not participitate in the coordination of Bi(III) ion, enable the formation of different protonated [Bi(H$_x$DOTP)]$^{x-5}$ species (Eq IV.2.2.1).

$$Bi(NTA)_2 + H_xL \leftrightharpoons Bi(H_iL) + 2\ H_2NTA \qquad IV.2.2.1$$
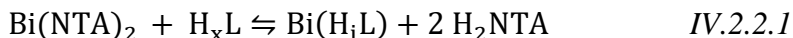
where x=6 and i=4 for DOTP , x=4 and i=0 for DOTA, at pH=3.0 where the [Bi(DOTA)]$^-$ and [Bi(H_4DOTP)]$^-$ species predominates. The stability constants can be determined by following the competition equilibria in the systems Bi(III) - NTA - H$_x$L with spectrophotometry due to the different absorption spectra (6p $\leftarrow$ 6s transitions) of the [Bi(NTA)$_2$]$^{3-}$, [Bi(DOTA)]$^-$ and [Bi(H_4DOTP)]$^-$ complexes. The competition equilibria could be monitored via the absorption band of both [Bi(DOTA)]$^-$ or [Bi(H_4DOTP)]$^-$ and the [Bi(NTA)$_2$]$^{3-}$ complexes. Some characteristic absorption spectra obtained in the systems Bi(III) - NTA - H$_4$DOTA and Bi(III) - NTA - H$_6$DOTP systems are shown in Figure IV.2.2.1
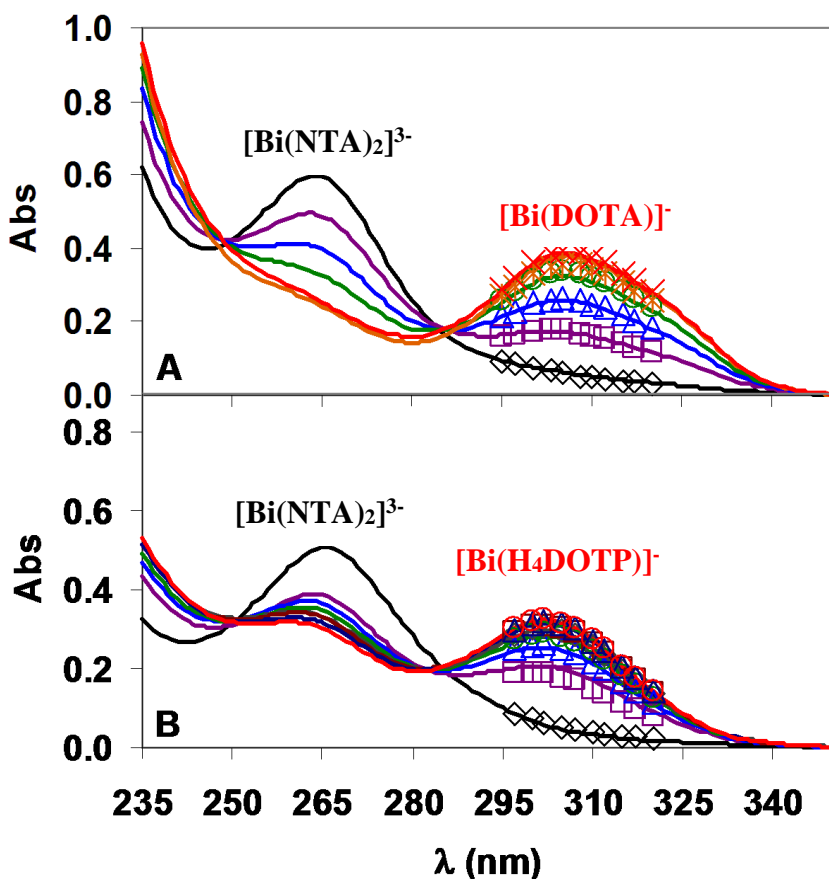
Figure IV.2.2.1 Absorption spectra of the Bi(III) - NTA – DOTA (**A**) and Bi(III) - NTA – DOTP (**B**) systems. The solid lines and the open symbols represent the experimental and the calculated absorbance values, respectively (**A**: $[Bi(III)]_{tot}$=0.05 mM, $[NTA]_{tot}$=50 mM, $[DOTA]_{tot}$=**0.0**, **20**, **40**, **60**, **80** and **100** μM; **B**: $[Bi(III)]_{tot}$=0.05 mM, $[NTA]_{tot}$=10 mM, $[DOTP]_{tot}$=**0.0**, **30**, **60**, **90**, **120**, **150**, **210** and **300** μM pH=3.0, $[NTA]_{tot}$+$[NaClO_4]_{tot}$=0.15 M, 25°C)

The absorbtion spectra indicate the presence of two absorbing species, $[Bi(NTA)_2]^{3-}$ and $[Bi(DOTA)]^-$ (A) or $[Bi(H_4DOTP)]^-$ (B) in equilibrium. Considering the molar absorptivities of $[Bi(DOTA)]^-$ and $[Bi(H_4DOTP)]^-$, the protonation constants of NTA, DOTA and DOTP ligand (Table IV.1.1), the stability product of $[Bi(NTA)_2]^{3-}$ ($\log\beta_{Bi(NTA)2}$, Table IV.2.2.1), the stability constants of $[Bi(DOTA)]^-$ and $[Bi(DOTP)]^{5-}$ are calculated, and

the log K_{BiL} values are presented in Table IV.2.2.1 For the equilibrium calculations, the protonation constants of [Bi(DOTA)]- and [Bi(DOTP)]$^{5-}$ complexes (log $K_{Bi(HiL)}$, Eq. (IV.2.3), Table IV.2.2.1) determined by pH-potentiometry at 25°C in 0.15 M NaClO$_4$ solution are also included in the model.

Table IV.2.2.1. Stability and protonation constants of the Bi(III) complexes (0.15 M NaClO$_4$, 25°C).

	NTA	DOTA		DOTP
log K_{BiL}	**16.97 (3)**	**30.86 (7)**	**30.3**[a]	**38.67 (2)**
log$K_{Bi(HL)}$	–	1.38 (4)	–	7.04 (3)
log$K_{Bi(H2L)}$	–	–	–	5.86 (3)
log$K_{Bi(H3L)}$	–	–	–	4.81 (4)
log$K_{Bi(H4L)}$	–	–	–	4.27 (2)
				(logβ=60.65)
log K_{BiL2}	**9.23 (6)**	**–**	**–**	**–**
	(logβ=26.21)			
logK_{FeL}	14.78 [b]	29.4 [e]		–
logK_{InL}	13.81 [c]	24.53 [f]		–
logK_{GdL}	11.11 [d]	24.7[g], 24.67[h], 25.58 [i]		28.8 [j]

[a]Ref [16](1.0 M NaBr, 25°C); [b] Ref.[[102]] (1.0 M NaClO$_4$, 25°C); [c] Ref.[[103]] (0.1 M KNO$_3$, 25°C); [d]Ref. [[104]] (0.5 M NaClO$_4$, 25°C); [e] Ref. [[105]] (0.1 M KCl, 25°C); [f] Ref. [[106]] (0.1 M KCl, 25°C); [g] Ref. [[107]] (0.1 M NaCl, 25°C); [h] Ref. [[108]] (0.1 M Me$_4$NCl, 25°C); [i] Ref. [[109]](0.1 M Me$_4$NCl, 25°C); [j] Ref. [[110]] (0.1 M Me$_4$NCl, 25°C).

Bi(III) is a soft or borderline metal ion and it usually forms stable complexes with ligands containing O, N and S donor atoms. Ionic radius of the Bi(III) ion in complexes is 124-133 pm and CN=8. Comparing the obtained stability constant of [Bi(DOTP)]$^{5-}$ with that of [Bi(DOTA)]- reveals that the substitution of the carboxylate with the phosphonate pendants results in about 8 log unit increase of the log K_{BiL} value due to the higher basicity of the ring nitrogen atoms and the higher total basicity of the DOTP ligand (Table IV.1.1).

The stability constants in Table IV.2.2.1 indicate that the log K_{BiL} values of the $[Bi(DOTP)]^{5-}$ and $[Bi(DOTA)]^-$ complexes are significantly higher than the log K_{ML} values of Fe(III), In(III) and Gd(III) complexes. Considering the size of Bi(III) (124-133 pm) and Gd(III) ion (100 pm), the higher stability constant of the $[Bi(DOTP)]^{5-}$ and $[Bi(DOTA)]^-$ complexes is probably accounted to the stronger interaction of the ring nitrogen atoms with the softer Bi(III) ion. It has been confirmed by the shorter Bi(III)-N bound distances than those observed in the Gd(III) complexes in the single crystals .

IV.2.3 Formation kinetic studies of $[Bi(DOTA)]^-$ and $[Bi(DOTP)]^{5-}$ complexes

The complex formation reactions of the trivalent metal ions with protonated macrocyclic DOTA-like ligands are usually slow[16], [111]–[113]. This slow formation is not favourable for the short-lived radiometals (e.g ^{213}Bi, ^{68}Ga). The phenomenon is well known in the literature that slow complexation of macrocyclic liagnds of trivalent metal ions is mostly caused by rigid structure of highly preorganized macrocycle, which can form the long lived protonated intermediate.

The formation of M(III) complexes and deprotonation of the intermediate takes place simultaneously by the slow penetration of the M(III) ion into the coordination cage formed by the four ring N atoms and the four O atoms of the pendant arms[109], [111]–[115]. The formation of the final in-cage complex occurs via deprotonation of the intermediate and by the rearrangement to the final M(III) complexes.

The formation of $[Bi(DOTA)]^-$ and $[Bi(DOTP)]^{5-}$ complexes was followed by spectrophotometry using the absorption bands of the

[Bi(DOTA)]$^-$ and [Bi(DOTP)]$^{5-}$ complexes (308 nm) in the pH range 3.0 – 6.0 (0.15 M NaClO$_4$, 25°C). Some characteristic absorption spectra obtained for the reacting systems Bi(III) - DOTA and Bi(III) - DOTP are shown in Figure IV.2.3.1.
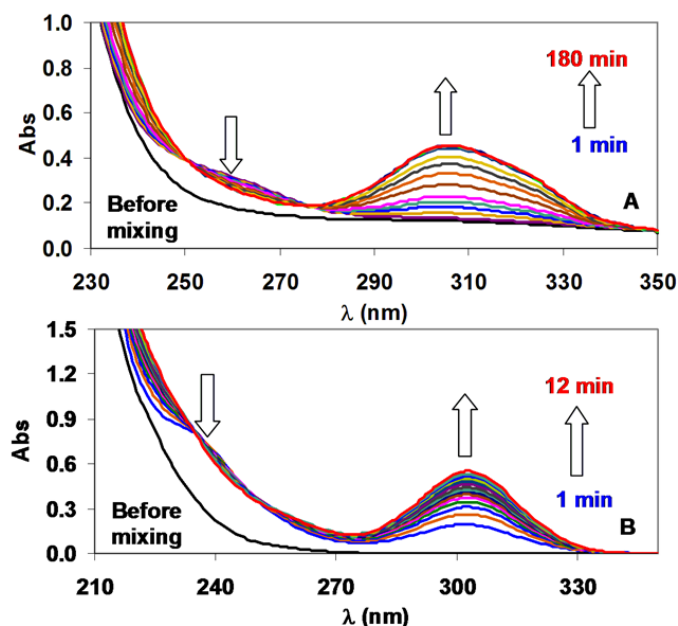
Figure IV.2.3.1. Absorption spectra of Bi(III) - DOTA (**A**) and and Bi^{III} - DOTP (**B**) reacting systems. (A: [Bi(III)]$_{tot}$=0.050 mM, [DOTA]$_{tot}$=5.0 mM, pH=4.0, [NMP]$_{tot}$=0.01 M, 25°C; B: [Bi(III)]$_{tot}$=0.05 mM, [DOTP]$_{tot}$=1.0 mM, pH=3.0, [CA]$_{tot}$=0.01 M, 0°C; 0.15 M NaClO$_4$).

Under these conditions the formation of the [Bi(DOTP)]$^{5-}$ was fast, thus the absorption spectra of the Bi(III)–DOTP reacting system were recorded at 0°C. In the reaction mixture of Bi(III)-DOTA at pH=4.0, two new absorption bands were observed with maxima at 260 and 308 nm. In the progress of the reaction the intensity of the band at 260 nm decreased, whereas the other band at 308 nm increased. Based on this phenomena the absorption bands at 260 and 308 nm were characteristic for the intermediate and the final [Bi(DOTA)]$^-$ complex, respectively. For the

reaction mixture of Bi(III)-DOTP at pH=3.0, absorption bands at 240 and 308 nm might be assigned in a similar manner. Since the structure of the ligands is similar, it can be assumed that the formation of $[Bi(DOTA)]^-$ occurs by coordination of four acetates to Bi(III) ion, to form a diprotonated intermediate $[Bi(H_2DOTA)]^+$, in which the Bi(III) ion is placed outside the coordination cage, meanwhile two opposite macrocyclic ring-N atoms are protonated.

To characterise the stoichiometry and the possible structure of the $[BiH_x(DOTP)]^{x-3}$ intermediate, ΔpH was monitored by spectrophotometry in the Bi(III) - H_6DOTP reaction system ($[Bi(III)]_{tot}$=0.5 mM, [H_6DOTP], pH_{end}=3.17, V_{tot}=1.8 mL, 0.15 M NaClO$_4$, 0°C) using methyl orange as indicator. The absorption spectra of methyl orange and the absorbance values of the Bi(III) - H_6DOTP reaction system at 506 nm as a function of time are shown in Figures IV.2.3.2 and IV.2.3.3.
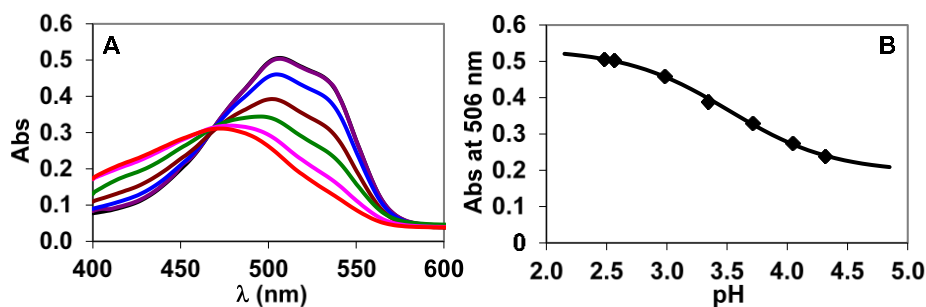
Figure IV.2.3.2 Absorption spectra (A) and absorbance values at 506 nm of methyl orange as a function of pH (B).
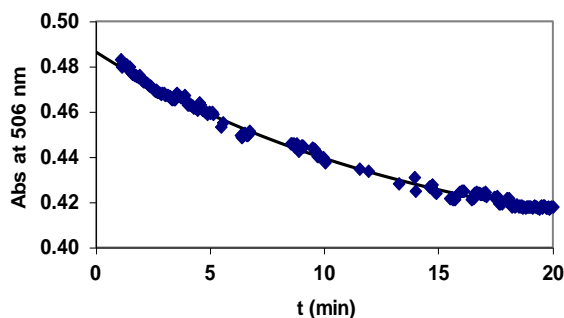
Figure IV.2.3.3. Absorbance values of the Bi(III) - H_6DOTP reacting system as a function of time ([Bi(III)]$_{tot}$=0.5 mM, [H_6DOTP]$_{tot}$=10 mM, [methyl orange]$_{tot}$=12.5 µM, pH_{end}=3.17, l=1 cm, 0.15 M NaClO$_4$, 0°C).

The absorbance values obtained at 506 nm decrease over time, which can be interpreted by the increase of the pH value in the Bi(III) - H_6DOTP reaction system (Figure IV.2.3.3). By taking into account the protonation constant (log K^H=3.52 (4)) and the molar absorptivity of the protonated (HL) and deprotonated (L) methyl-orange obtained at 506 nm (ε_L=15483 M^{-1}cm^{-1}; ε_{HL}=42780 M^{-1}cm^{-1}), the ΔpH was found to be +0.44 (Δ[H$^+$] = -1.2 mM) in the Bi(III) - H_6DOTP reaction system. Considering the large excess of H_6DOTP, it can be assumed that the intermediate is fully formed at the beginning of the reaction. So, the increase of the pH might be accounted to the transformation of the intermediate to the final [Bi(H_4DOTP)]$^-$ complex during the H$^+$ consuming process ([Bi(H_4DOTP)]$^-$ predominates at pH_{end}=3.17). By taking into account the concentration of Bi(III) ion ([Bi(III)]$_{tot}$=0.5 mM) and Δ[H$^+$]= -1.2 mM, the formation of the diprotonated *[Bi(H$_2$DOTP)]$^{3-}$ intermediate can be assumed in the Bi(III) - H_6DOTP reaction system. In the *[Bi(H_2DOTP)]$^-$

intermediate the Bi(III) ion is coordinated by the four more basic phosphonate –O$^-$ donor atoms, whereas two opposite macrocyclic ring N atoms are protonated (four weakly basic deprotonated phosphonate –O$^-$ donor atoms very likely do not take place in the coordination of the Bi(III) ion). The formation of *[Bi(H_2DOTP)]$^-$ intermediate is also supported by the structural characterization of H$_6$DOTP^{2-} ligand (Figure IV.1.1, Figure IV.1.2, Table IV.1.2,), which reveals the availability of the more basic phosphonate –O$^-$ donor atoms for the coordination of the Bi(III) ion, whereas four weakly basic deprotonated phosphonate –O$^-$ donor atoms might form the H-bonding with the protonated macrocyclic ring N atoms. The formation of the final in-cage Bi(III) complex occurs by the deprotonation of the two macrocyclic ring N atoms of the diprotonated *[Bi(H_2DOTP)]$^{3-}$ intermediate, which is followed by the rearrangement to the final [Bi(H_4DOTP)]$^-$ complex with the consumption of two equivalents of H$^+$.

The formation rates of Bi(III) complexes have been studied under pseudo-first order conditions that were ensured by the presence of a large excess of DOTA or DOTP ([Bi(III)]$_{tot}$=25 μM). In these cases, the rate of formation reactions can be expressed by Eq. IV.2.3.1

$$\frac{d[BiL]}{dt} = k_{obs}[\text{Bi(III)}]_t \qquad \textit{IV.2.3.1}$$

where [BiL] is the concentration of the [Bi(DOTA)]$^-$ and [Bi(DOTP)]$^{5-}$ complexes formed, [Bi(III)]$_{tot}$ is the total concentration of species containing Bi(III) ions and k_{obs} is the pseudo-first order rate constant. The formation reaction of [Bi(DOTA)]$^-$ and [Bi(DOTP)]$^{5-}$ was investigated by varying the concentrations of DOTA and DOTP at different pH values. As expected, the k_{obs} vs. [DOTA]$_{tot}$ and k_{obs} vs.

[DOTP]$_{tot}$ (Figures IV.2.3.4 and IV.2.3.5) were saturation curves indicating the fast formation of the *[Bi(H_2DOTA)]$^+$ and *[Bi(H_2DOTP)]$^{3-}$ intermediates in a pre-equilibrium characterized by a stability constant defined by Eq. IV.2.3.2.

$$K_{\text{Bi}(H_2\text{L})} = \frac{[^*\text{Bi}(H_2\text{L})]}{[\text{Bi}^{\text{III}}][H_2\text{L}]} \qquad\qquad IV.2.3.2$$

where [*Bi(H_2L)] is the concentration of *[Bi(H_2DOTA)]$^+$ and *[Bi(H_2DOTP)]$^{3-}$ intermediate and [H_2L] is the concentration of the H_2DOTA^{2-} and H_2DOTP^{6-}.
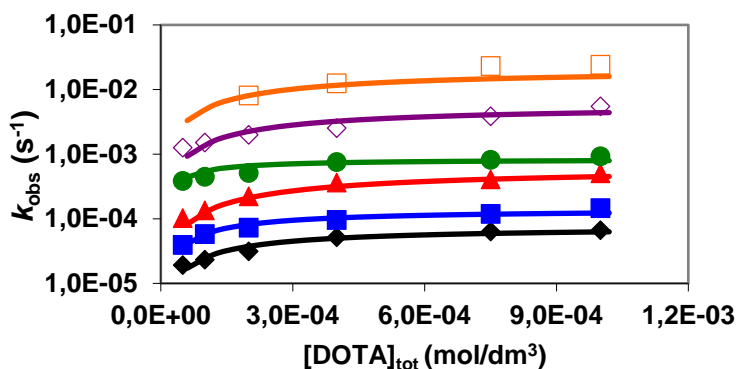
Figure IV.2.3.4 Pseudo-first order rate constants (k_{obs}) for the formation reaction of [Bi(DOTA)]$^-$ complex. The symbols and the solid lines represent the experimental and the calculated rate constants, respectively. ([Bi(III)]$_{tot}$=25 μM, pH=**3.3**, **3.9**, **4.5**, **4.9**, **5.4** and **5.9**, 0.15 M NaClO$_4$, 25°C).
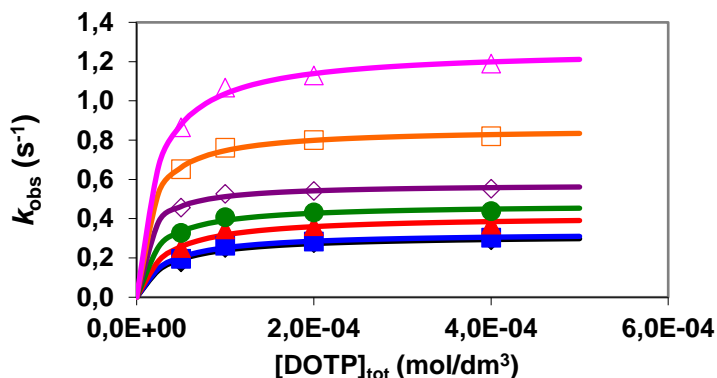
Figure IV.2.3.5 Pseudo-first order rate constants (k_{obs}) for the formation reaction of [Bi(DOTP)]$^{5-}$ complex. The symbols and the solid lines represent the experimental and the calculated rate constants, respectively. ([Bi(III)]$_{tot}$=25 μM, pH=**3.0**, **3.3**, **4.0**, **4.5**, **4.8**, **5.3** and **5.6**, 0.15 M NaClO$_4$, 25°C).

The rate-determining step of the reactions is the deprotonation and rearrangement of the *[Bi(H_2DOTA)]$^+$ and *[Bi(H_2DOTP)]$^{3-}$ intermediates by the entrance of the metal ion into the cavity of the DOTA or DOTP ligands:

$$\frac{d[BiL]}{dt} = k_{obs}[Bi(III)]_t = k_f[* Bi(H_2L)]_t \qquad IV.2.3.3$$

where [*Bi(H_2L)]$_{tot}$ is the concentration of [*Bi(H_2DOTA)]$^+$ and *[Bi(H_2DOTP)]$^{3-}$ intermediates and k_f is the rate constant characterizing the deprotonation and rearrangement of the intermediate to the final Bi^{III} complexes. The concentration of the non-complexed ligand can be expressed by Eq. (IV.2.3.4) using the protonation constants of DOTA and DOTP ligand (Table IV.1.1).

$$[L]_{free} = [H_2L]\big(1 + K_3^H[H^+] + K_3^H K_4^H[H^+]^2 + K_3^H K_4^H K_5^H[H^+]^3 +$$

$$K_3^H K_4^H K_5^H K_6^H[H^+]^4\big) = (1 + \alpha_{2H})[H_2L] \qquad IV.2.3.4.$$

where $\alpha_{2H} = K_3^H[H^+] + K_3^H K_4^H[H^+]^2 + K_3^H K_4^H K_5^H[H^+]^3 + K_3^H K_4^H K_5^H K_6^H[H^+]^4$.

By taking into account the hydrolysis of the Bi(III) ion the total metal ion concentration can be expressed by Eq. IV.2.3.5.

$[Bi(III)]_{tot} = [*Bi(H_2L)] + [Bi(OH)] + [Bi(OH)_2] + [Bi(OH)_3] + [Bi(III)]$

IV.2.3.5

      Under the experimental conditions (pH=3.0–6.0), the hydrolysis of Bi(III) ion may occur resulting in the formation of $[Bi(OH)]^{2+}$, $[Bi(OH)_2]^+$ and $Bi(OH)_3$ species. The formation of polymeric $Bi_x(OH)_y$ (x=6 and 9, y=12, 20 – 22) species does not take place under the experimental conditions applied in our kinetic studies.[15] Considering the hydrolysis of Bi(III) ion, the OH^- ion may compete with the ligands for the Bi(III) ions. By taking into account the protonation constants of DOTA and DOTP (Table IV.1.1 and (Eq. (IV.1.1)), the stability constant of $[*Bi(H_2L)]$ intermediates (Eq. (IV.2.3.2.)), the total concentration of the Bi(III) ion (Eq. (IV.2.3.5)) and Eq. (IV.2.3.3), the pseudo-first order rate constant can be expressed by Eq. IV.2.3.6.

$$k_{obs} = \frac{\frac{k_f K_{Bi(H_2L)}[L]_t}{1+\alpha_{2H}}}{1+\frac{K_{Bi(H_2L)}[L]_t}{1+\alpha_{2H}}+\alpha_{OH}} \qquad\qquad IV.2.3.6$$

where $[L]_{tot}$ is is the total concentration of DOTA and DOTP ligand and $\alpha_{OH} = \beta_1^{OH}/[H^+] + \beta_2^{OH}/[H^+]^2 + \beta_3^{OH}/[H^+]^3$ ($\log\beta_1^{OH}$=-1.09; $\log\beta_2^{OH}$=-4.0 and $\log\beta_3^{OH}$=-8.86 for Bi(III) ion).[116] The pseudo-first order rate constants determined at various pH, [DOTA] and [DOTP] values (Figures IV.2.3.4 and IV.2.3.5) were fitted to Eq. (IV.2.3.6) and the stability constant of the $[Bi(H_2L)]^+$ intermediates (K_{MH2L}) and the k_f rate constants were calculated. The calculated k_f rate constants obtained for the formation of the $[Bi(DOTA)]^-$ and $[Bi(DOTP)]^{5-}$ complexes are shown in Figure IV.2.3.6 as a function of pH and [OH^-].
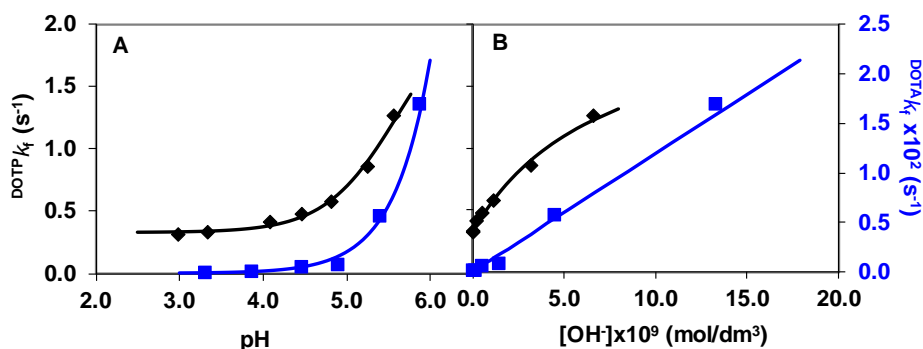
Figure IV.2.3.6 k_f rate constants characterize the formation of [Bi(DOTA)]$^-$ (■) and [Bi(DOTP)]$^{5-}$ (◆) complex as a function of pH (**A**) and [OH$^-$] (**B**). The symbols and the solid lines represent the experimental and the calculated k_f rate constants, respectively (0.15 M NaClO$_4$, 25°C).

The proposed mechanism for the formation of [Bi(DOTA)]$^-$ and [Bi(DOTP)]$^{5-}$ complexes is shown in Figure IV.2.3.7.
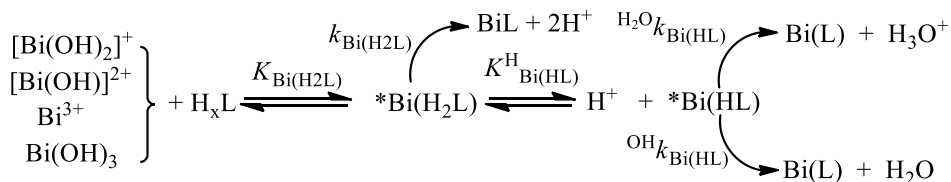

Figure IV.2.3.7 Formation mechanism of [Bi(DOTA)]$^-$ and [Bi(DOTP)]$^{5-}$ complexes (x= 2–4 for DOTA and x=4–6 for DOTP in the pH range 3–6).

Based on the reaction mechanism proposed for the formation of [M(DOTA)]$^-$ complexes with trivalent metal ions, the di- and the monoprotonated intermediates exist in equilibrium.[112]–[114] The dependence of the k_f values on the [OH$^-$] can be interpreted by the formation of the kinetically active monoprotonated *[Bi(HL)] intermediates via the dissociation of the diprotonated *[Bi(H_2L)] intermediates in an equilibrium characterized with the $K^H_{Bi(HL)}$ protonation constant Eq. IV.2.3.7.

$$K^H_{Bi(HL)} = \frac{[^*Bi(H_2L)]}{[^*Bi(HL)][H^+]} \qquad IV.2.3.7$$

60

The rate-controlling step of complex formation involves the H_2O or OH^- assisted deprotonation and rearrangement of the monoprotonated *[Bi(HL)] intermediates to the final [BiL] complex. However, the formation of [Bi(DOTP)]$^{5-}$ might occur by the spontaneous deprotonation of the *[Bi(H_2DOTP)]$^{3-}$ intermediates and rearrangement to the final [Bi(DOTP)]$^{5-}$ complex at pH<4.0 (Figure IV.2.3.6) According to the proposed reaction mechanism, the formation rate of the [Bi(DOTA)]$^-$ and [Bi(DOTP)]$^{5-}$ complexes can be given by Eq. IV.2.3.8.

$$\frac{d[BiL]}{dt} = k_f[^*Bi(H_2L)]_t = k_{Bi(H_2L)}[^*Bi(H_2L)] + {}^{H_2O}k_{Bi(HL)}[^*Bi(HL)]$$
$$+{}^{OH}k_{Bi(HL)}[^*Bi(HL)][OH^-] \qquad\qquad IV.2.3.8$$

By considering the total concentration of intermediates ([*Bi(H_2L)]$_{tot}$=[*Bi(HL)]+[*Bi(H_2L)]), the definition of $K^H{}_{Bi(HL)}$ protonation constant (Eq. IV.2.3.7), the k_f rate constant can be expressed by Eq. IV.2.3.9.

$$k_f = \frac{k_{Bi(H_2L)}K^H_{Bi(HL)}[H^+] + {}^{H_2O}k_{Bi(HL)} + {}^{OH}k_{Bi(HL)}K_w/[H^+]}{1+K^H_{Bi(HL)}[H^+]} \qquad IV.2.3.9$$

This equation was used for the fitting of the k_f values to determine the $k_{Bi(H2L)}$, ${}^{H2O}k_{Bi(HL)}$ and ${}^{OH}k_{Bi(HL)}$ rate constants and the $K^H{}_{Bi(HL)}$ protonation constants that characterize the formation of [Bi(DOTA)]$^-$ and [Bi(DOTP)]$^{5-}$ complexes. For [Bi(DOTA)]$^-$, the protonation constants of the monoprotonated *[Bi(HL)] intermediate ($K^H{}_{Bi(HL)}$) can not be calculated, which might be explained by the very low $K^H{}_{Bi(HL)}$ due to the high affinity of Bi(III) ion to the ring N donor atoms. The $k_{Bi(H2L)}$, ${}^{H2O}k_{Bi(HL)}$ and ${}^{OH}k_{Bi(HL)}$ rate constants and the $K^H{}_{Bi(HL)}$ protonation constants are shown in Table IV.2.3.1.

Table IV.2.3.1. Rate (k) and equilibrium (K) constants characterizing the formation of [Bi(DOTA)]⁻, [Bi(DOTP)]⁵⁻ [Ce(DOTA)]⁻ and [Gd(DOTP)]⁵⁻ complexes (0.15 M NaClO₄, 25°C)

	[Bi(DOTA)]⁻	[Bi(DOTP)]⁵⁻	[Ce(DOTA)]⁻ [a,b]	[Gd(DOTP)]⁵⁻ [d]
$k_{M(H2L)}$ (s⁻¹)	–	0.33 ± 0.01	–	–
$^{H2O}k_{M(HL)}$ (s⁻¹)	$(2\pm1)\times10^{-5}$	2.2 ± 0.2	18.5	–
$^{OH}k_{M(HL)}$ (M⁻¹s⁻¹)	$(1.2\pm0.2)\times10^{6}$	–	1.9×10^{7}	7.2×10^{3}
$\log K^{H}_{M(HL)}$	–	5.61 ± 0.05	8.64	–
$\log K_{M(H2L)}$	11.6 (3)	21.8 (1)	4.5[c]	–

[a] Ref. [[117]], [b] Ref. [[114]], [c] Ref. [[118]], [d] Ref. [[119]]

The $^{H2O}k_{M(HL)}$ and $^{HO}k_{M(HL)}$ rate constants relatied to the H₂O as Brønsted base and OH⁻ assisted deprotonation and rearrangement of the *[Bi(HDOTA)] intermediates via the formation of the final [Bi(DOTA)]⁻ complex is significantly lower than those of [Ce(DOTA)]⁻ complex. By taking into account the similar charge and size of Bi(III) and Ce(III) ions (Bi(III): 124–133 pm; Ce(III): 114 pm),[16] the slower formation of [Bi(DOTA)]⁻ is likely associated to the higher stability of the diprotonated *[Bi(H_2DOTA)]⁺ intermediate ($\log K_{Bi(H2L)}$=11.6), which results in slower H₂O- and OH⁻-assisted deprotonation and rearrangement processes to the final Bi(III) complex.

To confirm the role of the general base catalysis in the deprotonation of the *[Bi(H_2DOTA)]⁺ intermediate, the formation rate of [Bi(DOTA)]⁻ was followed by spectrophotometry at the absorption band of the final [Bi(DOTA)]⁻ complex (308 nm) in the presence of acetate as base (pH=3.3 – 5.5, 0.15 M NaClO₄, 25°C). The formation rates of Bi(III) complexes have been studied under pseudo-first order conditions that was ensured by the presence of a 40 fold excess of DOTA ([Bi(III)]$_{tot}$=25 μM,

[DOTA]$_{tot}$=1.0 mM). In these cases, the rate of formation reactions can be expressed by Eq. IV.2.3.1

The formation reaction of [Bi(DOTA)]⁻ was investigated by varying the concentrations of acetate [Ac] at different pH values. As expected, the k_{obs} values increase monotonously as a function of [Ac]$_{tot}$ (Figure IV.2.3.8). As it has been shown previously, the diprotonated *[Bi(H_2DOTA)]⁺ intermediate is fully formed in the presence of 40 fold excess of DOTA ([Bi(III)]$_{tot}$=25 µM, [DOTA]$_{tot}$=1.0 mM and [DOTP]$_{tot}$=0.1 mM, Figures IV.2.3.4 and IV.2.3.5). Moreover, the deprotonation of the diprotonated *[Bi(H_2DOTA)]⁺ intermediate takes place by the formation of the monoprotonated *[Bi(HDOTA)] intermediate in our experimental condition.
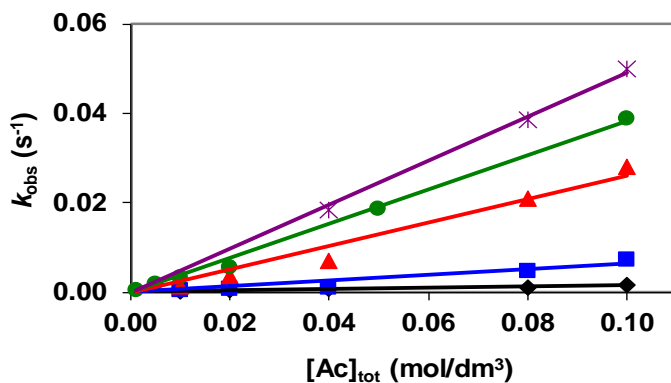
Figure IV.2.3.8. Pseudo-first order rate constants (k_{obs}) for the formation reaction of [Bi(DOTA)]⁻ complex. The symbols and the solid lines represent the experimental and the calculated rate constants, respectively. ([Bi(III)]$_{tot}$=25 µM, [DOTA]$_{tot}$=1.0 mM, pH=**3.3**, **4.0**, **4.6**, **4.8** and **5.4**, 0.15 M NaClO$_4$, 25°C).

Since the formation rate of the Bi(III) complexes is directly proportional to the concentration of the diprotonated *[Bi(H_2L)] intermediate (Eq. IV.2.3.3.), it can be assumed that the rate-determining step of the reactions is the acetate as general base assisted deprotonation

63

and rearrangement of the monoprotonated *[Bi(HDOTA)] intermediate (k'_{Ac}) and the entrance of the metal ion into the cavity of the DOTA. According to the proposed reaction mechanism, the formation rate of the [Bi(DOTA)]$^-$ complex in the presence of acetate buffer can be given by Eq. IV.2.3.10.

$$\frac{d[BiL]}{dt} = k_{obs}[Bi^{III}]_{tot} = k'_{Ac}[* Bi(HL)]_t[Ac]_{tot} \qquad \textit{IV.2.3.10}$$

Under the experimental conditions and at pH between 3.3 and 5.4, the H_2O and OH$^-$ assisted deprotonation of the *[Bi(HDOTA)] intermediates is very slow process, so their contribution to the formation rate of [Bi(DOTA)]$^-$ can be neglected. By considering the total concentration of Bi(III) ([Bi(III)]$_{tot}$=[*Bi(HL)]$_{tot}$) and Eq. (IV.2.3.10.), the pseudo-first order rate constant can be expressed by Eq. IV.2.3.11.

$$k_{obs} = k'_{Ac}[Ac]_{tot} \qquad \textit{IV.2.3.11}$$

This equation was used for the fitting of the k_{obs} values in Figure IV.2.3.9 to determine the k'_{Ac} rate constants characterizing the acetate anion assisted formation of [Bi(DOTA)]$^-$ complexes at given pH. The k'_{Ac} rate constants are shown as a function of pH in Figure IV.2.3.9.
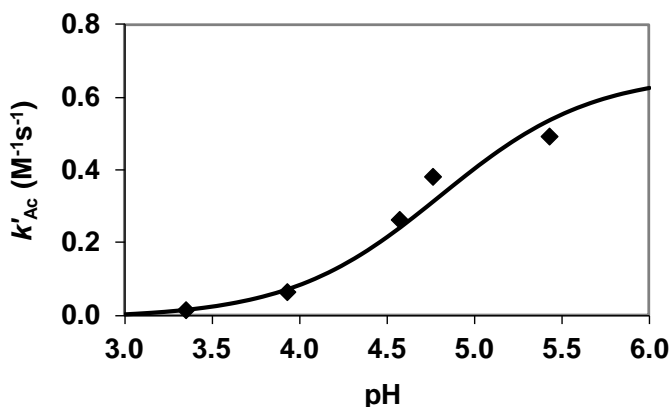
Figure IV.2.3.9. k'_{Ac} rate constants characterizes the acetate assisted deprotonation and transformation of the *[Bi(HDOTA)] intermediate to the final [Bi(DOTA)]⁻ complex The symbols and the solid lines represent the experimental and the calculated rate constants, respectively. (0.15 M NaClO₄, 25°C).

The k'_{Ac} rate constants increase with the increase of the pH. The dependence of the k'_{Ac} values on the pH can be interpreted by the formation of the kinetically active deprotonated acetate anion, which might assist the deprotonation *[Bi(HDOTA)] intermediate via proton exchange processes. By considering the total concentration of acetate ($[Ac]_{tot}=[HAc]+[Ac^-]$), and the definition of protonation constant of the acetate anion (Eq. (IV.1.1), the k'_{Ac} rate constant can be expressed by Eq.IV.2.3.12

$$k'_{Ac} = \frac{k_{Ac}}{1+^{Ac}K_1^H[H^+]} \qquad IV.2.3.12$$

where k_{Ac} is the rate constant characterizing the acetate anion assisted deprotonation of *[Bi(HDOTA)] intermediate, whereas $^{Ac}K_1^H$ is the protonation constant of the acetate anion. This equation was used for the fitting of the k'_{Ac} values to determine the k_{Ac} rate constant and the $^{Ac}K_1^H$ protonation constant of the acetate anion. The protonation constant of the acetate anion obtained by the fitting of the kinetic data in Figure IV.2.3.9 is $\log^{Ac}K_1^H = 4.8(2)$, which is in reasonable agreement with the published data ($\log^{Ac}K_1^H= 4.52$, 25°C, 0.15 M NaClO₄).[120] The k_{Ac} rate constants

characterizing the acetate assisted deprotonation and transformation of *[Bi(*H*DOTA)] intermediate to the final [Bi(DOTA)]⁻ complex is $k_{Ac} = 0.7 \pm 0.1$ M⁻¹s⁻¹. The k_{Ac} rate constant that characterise the acetate-assisted formation of [Bi(DOTA)]⁻ is about six orders of magnitude lower than the $^{OH}k_{Bi(HL)}$ rate constant relatied to the OH⁻-assisted formation of [Bi(DOTA)]⁻ due to the much lower basicity of acetate compared to OH⁻ (Ac: log $^{Ac}K_1^H$= 4.8 (2); OH⁻: log K^H= 15.4, 0.15 M NaClO₄, 25°C).

Surprisingly, the stability constant of diprotonated *[Bi(H_2DOTP)]³⁺ intermediate (log $K_{M(H2L)}$) is about two times higher than that of *[Bi(H_2DOTA)]⁺ intermediate, in which the Bi(III) ion is coordinated by four highly basic phosphonate –O⁻ donor atoms A comparison of the formation rate (k_{obs}) of the [Bi(DOTP)]⁵⁻ (Figure IV.3.4) to [Gd(DOTP)]⁵⁻ [119] indicates that the k_{obs} values of [Bi(DOTP)]⁵⁻ are more than hundred times higher than those of the [Gd(DOTP)]⁵⁻, *i.e.*: the Bi(III) complex is formed more rapidly at pH < 6. However, the faster formation of [Bi(DOTP)]⁵⁻ in the pH range 3–6 cannot be explained by the higher concentration of the kinetically active monoprotonated *[Bi(*H*DOTP)]⁴⁻ intermediate, since its protonation constant is relatively high (log $K^H_{Bi(HL)}$ = 5.61, Table IV.2.3.1). Thus, the faster formation of [Bi(DOTP)]⁵⁻ can be attributed by the rapid proton exchange between protonated ring-*N* atoms of the deprotonated *[Bi(H_2DOTP)]³⁺ and the monoprotonated *[Bi(*H*DOTP)]⁴⁻ intermediates and H₂O ($k_{M(H2L)}$ and $^{H2O}k_{M(HL)}$), which might be assisted by the four weakly basic deprotonated phosphonate –O⁻ donor atom in the general base catalyzed process.

IV.2.4 Formation kinetics of [Bi(DOTA)]⁻ and [Bi(DOTP)]⁵⁻ complexes in the presence of citrate

In order to avoid the precipitation of Bi_2O_3, the Bi(III) ion must be pre-complexed at pH > 2.5 in a form of a weak complex because of its strong tendency to hydrolysis.[116] Citrate was used previously as auxiliary ligand [121]–[125]. The effect of citrate on the formation rate of [Bi(DOTA)]⁻ and [Bi(DOTP)]⁵⁻ complexes was followed by spectrophotometry at the absorption band of the final [Bi(DOTA)]⁻ and [Bi(DOTP)]⁵⁻ complexes (308 nm) in the presence of 0.25 – 2.0 mM citrate (pH=3.0 – 5.6, 0.15 M $NaClO_4$, 25°C). Some characteristic absorption spectra of the Bi(III) - DOTA – citrate reacting system are shown in Figure IV.2.4.1.
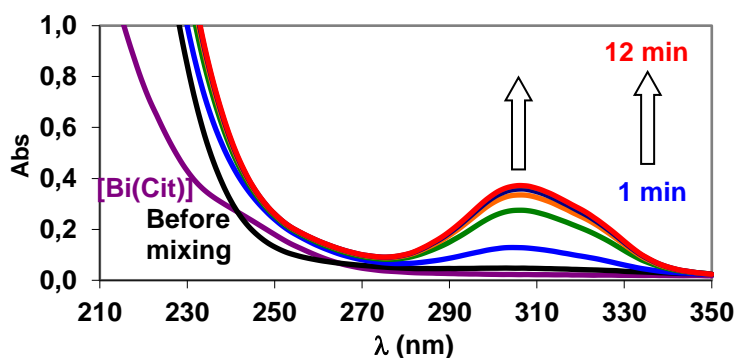
Figure IV.2.4.1 Absorption spectra of Bi(III) - DOTA - citrate reacting system ([Bi(III)]$_{tot}$=50 μM, [DOTA]$_{tot}$=2.0 mM, [Cit]$_{tot}$=4.0 mM; at pH=4.0, 0.15 M $NaClO_4$, 25°C) l =1 cm.

The formation reaction of [Bi(DOTA)]⁻ and [Bi(DOTP)]⁵⁻ was investigated by varying the concentrations of citrate between 0.25 – 2.0 mM at different pH values in the presence of DOTA and DOTP excess guaranteeing the pseudo-first-order kinetic condition ([Bi(III)]$_{tot}$=25 μM, [DOTA]$_{tot}$=1.0 mM, [DOTP]$_{tot}$=0.1 mM). The k_{obs} vs. [Cit]$_{tot}$ for the

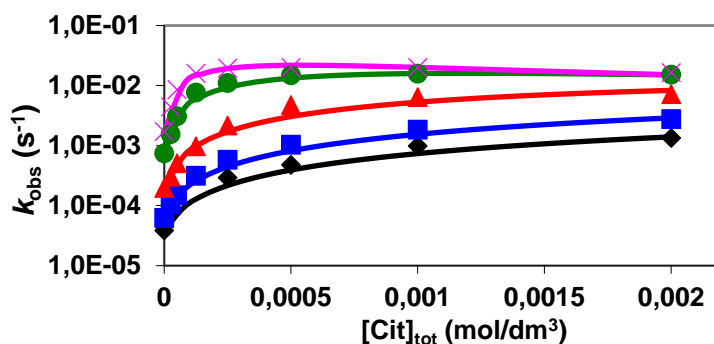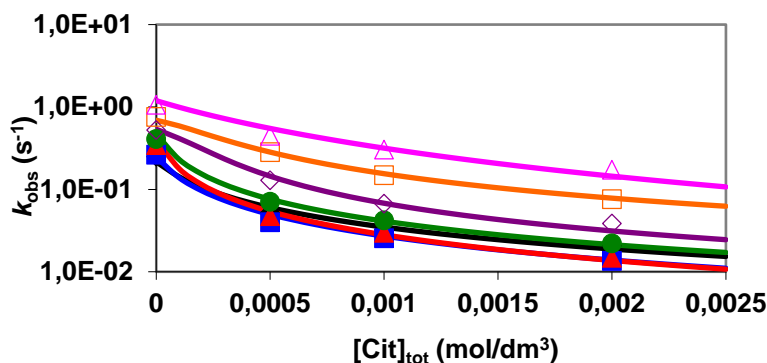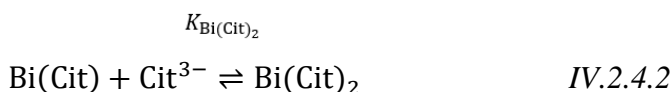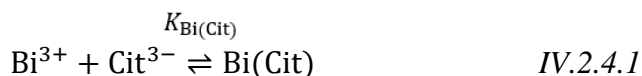formation of $[Bi(DOTA)]^-$ and $[Bi(DOTP)]^{5-}$ are shown in Figures IV.2.4.2 and IV.2.4.3.

Figure IV.2.4.2 Pseudo-first-order rate constants (k_{obs}) for the formation reaction of $[Bi(DOTA)]^-$ complex in the presence of citrate at different pH. The symbols and the solid lines represent the experimental and the calculated rate constants, respectively. ($[Bi(III)]_{tot}$=25 μM, $[DOTA]_{tot}$=1.0 mM, pH=**3.0**, **3.4**, **4.0**, **4.6** and **5.0**, 0.15 M NaClO$_4$, 25°C).

Figure IV.2.4.3 pseudo-first-order rate constants (k_{obs}) for the formation reaction of $[Bi(DOTP)]^{5-}$ complex in the presence of citrate at different pH. The symbols and the solid lines represent the experimental and the calculated rate constants, respectively. ($[Bi(III)]_{tot}$=25 μM, $[DOTP]_{tot}$=0.1 mM, pH=**3.0**, **3.3**, **4.0**, **4.5**, **4.8**, **5.3** and **5.6**, 0.15 M NaClO$_4$, 25°C).
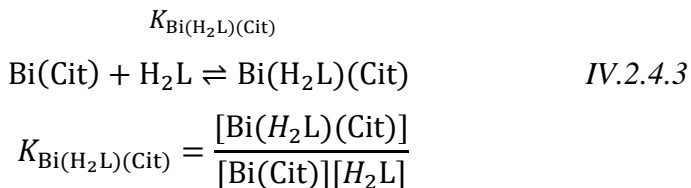
Interestingly, the formation rate (k_{obs}) of $[Bi(DOTA)]^-$ increase with the citrate concentration showing the saturation curve (Figure IV.2.4.2). However, the k_{obs} values that characterize the formation of the $[Bi(DOTP)]^{5-}$ decrease with the increase of $[Cit]_{tot}$ (Figure IV.2.4.3). The comparison of the absolute values of the k_{obs} reaction rate constants

obtained in the absence and presence of 2.0 mM citrate indicates that citrate accelerates the formation of [Bi(DOTA)]$^-$ by a factor of 8 - 10 in the pH range pH 3.0-5.0. The presence of 2.0 mM citrate slows down the formation of [Bi(DOTP)]$^{5-}$ by a factor of 10 at pH between 3.0 and 4.5, and by about 5 times in the pH range 4.8-5.6. Under the experimental conditions and at pH between 3.0 and 5.6, the Bi(III) ion might form [Bi(Cit)] and [Bi(Cit)$_2$]$^{3-}$ complexes characterized by Eqs. IV.2.4.1 and IV.2.4.2 (log$K_{Bi(Cit)}$=10.78, log$K_{Bi(Cit)2}$=5.05, 37°C, 0.15 M NaClO$_4$).[126]

$$\mathrm{Bi^{3+} + Cit^{3-} \overset{K_{Bi(Cit)}}{\rightleftharpoons} Bi(Cit)} \qquad \textit{IV.2.4.1}$$

$$\mathrm{Bi(Cit) + Cit^{3-} \overset{K_{Bi(Cit)_2}}{\rightleftharpoons} Bi(Cit)_2} \qquad \textit{IV.2.4.2}$$

As it has been shown previously, the diprotonated *[Bi(H_2L)] intermediate is fully formed in the presence of DOTA and DOTP excess ([Bi(III)]$_{tot}$=25 μM, [DOTA]$_{tot}$=1.0 mM and [DOTP]$_{tot}$=0.1 mM). Since the formation rate of the Bi(III) complexes is directly proportional to the concentration of the diprotonated *[Bi(H_2L)] intermediate, it can be assumed that the slower formation of [Bi(DOTP)]$^{5-}$ in the presence of citrate is caused by the formation of [Bi(Cit)] and [Bi(Cit)$_2$]$^{3-}$ complexes, i.e decreasing the concentration of the kinetically active diprotonated *[Bi(H_2DOTP)]$^{3-}$ intermediate. To explain the faster formation of [Bi(DOTA)]$^-$ in the presence of citrate, we hypothesize the intermediate contains a citrate ligand coordinated to the Bi(III) ion (*[Bi(H$_2$DOTA)(citrate)], Eq. (IV.2.4.3)), which deprotonates and transforms to the final [Bi(DOTA)]$^-$ complex in the rate determining step. The rate determining deprotonation and transformation of the *[Bi(H_2DOTA)(citrate)]) intermediate takes

place simultaneously with release of the coordinated citrate ligand. The formation of similar ternary *[Ga(*H*NOTA)(citrate)] intermediate has been found in the Ga(citrate) – NOTA reacting system.[127]

$$\text{Bi(Cit)} + \text{H}_2\text{L} \overset{K_{\text{Bi(H}_2\text{L)(Cit)}}}{\rightleftharpoons} \text{Bi(H}_2\text{L)(Cit)} \hspace{2cm} \textit{IV.2.4.3}$$

$$K_{\text{Bi(H}_2\text{L)(Cit)}} = \frac{[\text{Bi(H}_2\text{L)(Cit)}]}{[\text{Bi(Cit)}][H_2\text{L}]}$$

The formation rates of Bi(III) complexes have been studied under pseudo-first order conditions in the presence of a large excess of DOTA or DOTP ([Bi(III)]$_{\text{tot}}$=25 μM, [DOTA]$_{\text{tot}}$=1.0 mM and [DOTP]$_{\text{tot}}$=0.1 mM). Under these conditions the rate of formation reactions can be expressed by Eq. (IV.2.4.4.) The rate-determining step of the reactions is the deprotonation and rearrangement of the *[Bi(*H$_2$*DOTA)]$^+$ and *[Bi(*H$_2$*DOTA)(citrate)] intermediates followed by the entrance of the metal ion into the cavity of the DOTA ligand:

$$\frac{d[\text{BiL}]}{dt} = k_{\text{obs}}[\text{Bi}^{3+}]_t = k_{\text{Bi}(H2L)}[\text{Bi(H}_2\text{L)}] + {}^{\text{H}_2\text{O}}k_{\text{Bi}(HL)}[\text{Bi(}H\text{L)}] +$$

$${}^{\text{HO}}k_{\text{Bi}(HL)}[\text{Bi(}H\text{L)}] + k_{\text{Bi(Cit)}(H2L)}[\text{Bi(H}_2\text{L)(Cit)}] \hspace{1cm} \textit{IV.2.4.4}$$

where [*Bi(H$_2$L)], [*Bi(*H*L)] and [*Bi(H$_2$L)(Cit)] are the concentrations of *[Bi(H$_2$L)], *[Bi(*H*L)] and *[Bi(H$_2$L)(citrate)]) intermediates. $k_{\text{Bi(H2L)(Cit)}}$ and $k_{\text{Bi(H2L)}}$ are the rate constants characterizing the spontaneous deprotonation and rearrangement of the *[Bi(H$_2$L)(citrate)] and *[Bi(H$_2$L)] intermediate, whereas ${}^{\text{H2O}}k_{\text{Bi(HL)}}$ and ${}^{\text{OH}}k_{\text{Bi(HL)}}$ are the rate constants characterizing H$_2$O and OH$^-$ assisted deprotonation and rearrangement of the [*Bi(*H*L)] intermediate. The concentration of the noncomplexed citrate can be expressed by Eq. (IV.2.4.5).

[Cit]$_f$=[Cit](1+$^{\text{cit}}K_1{}^{\text{H}}$[H$^+$]+$^{\text{cit}}K_1{}^{\text{Hcit}}K_2{}^{\text{H}}$[H$^+$]^2+$^{\text{cit}}K_1{}^{\text{Hcit}}K_2{}^{\text{Hcit}}K_3{}^{\text{H}}$[H$^+$]^3)=

$(1+\alpha_{Cit})[Cit]$ $\qquad\qquad\qquad\qquad\qquad\qquad\qquad$ *IV.2.4.5*

where $^{cit}K_1^H$=5.58 (1), $^{cit}K_2^H$=4.33 (2), $^{cit}K_3^H$=2.93 (2) (0.15 M NaClO$_4$, 25°C) are the corresponding protonation constants of citrate, whereas $\alpha_{Cit}=$ $^{cit}K_1^H[H^+]+{}^{cit}K_1^H$ $^{cit}K_2^H[H^+]^2+{}^{cit}K_1^H$ $^{cit}K_2^H$ $^{cit}K_3^H[H^+]^3$. By taking into account the concentration of the noncomplexed H$_2$L ligand and citrate (Eqs. (IV.2.3.4) and (IV.2.4.5)), stability constants of [Bi(Cit)] and [Bi(Cit)$_2$]$^{3-}$ complexes and *[Bi(H_2L)(citrate)]) intermediates ((Eqs. (IV.2.4.1) - (IV.2.4.3)) and the hydrolysis of the Bi(III) ion (Eq. (IV.2.3.5)), the total metal ion concentration can be expressed by Eq. (IV.2.4.6):

$[Bi(III)]_{tot}=[*Bi(H_2L)]+[*Bi(HL)]+[Bi(Cit)]+[Bi(Cit)_2]+[Bi(Cit)(H_2L)]+[Bi(OH)]+[Bi(OH)_2]^++[Bi(OH)_3]+[Bi^{3+}])=[Bi^{III}]\times\gamma$

$$\gamma = \left(1 + \frac{K^*_{Bi(H_2L)}[L]_{tot}}{1+\alpha_{2H}} + \frac{\frac{K^*_{Bi(H_2L)}[L]_{tot}}{(1+\alpha_{2H})}}{K^H_{Bi(HL)}[H^+]} + \frac{K_{Bi(Cit)}[Cit]_{tot}}{1+\alpha_{cit}} + K_{Bi(Cit)}K_{Bi(Cit)_2}\left(\frac{[Cit]_{tot}}{1+\alpha_{cit}}\right)^2 \right.$$

$$\left. + \frac{K^*_{Bi(H_2L)(Cit)}K_{Bi(Cit)}[L]_{tot}}{(1+\alpha_{2H})} \times \frac{[Cit]_{tot}}{(1+\alpha_{cit})} + \alpha_{OH} \right)$$

IV.2.4.6

By taking into account the concentration of the noncomplexed H$_2$L ligand and citrate (Eqs. (IV.2.3.4) and (IV.2.4.5)), the stability constant of *[Bi(H_2L)] and *[Bi(H_2L)(citrate)]) intermediates (Eqs. (IV.3.1.2) and (IV.2.4.1)), the definition of $K^H_{Bi(HL)}$ protonation constant (Eq. (IV.2.3.2)), the total concentration of the Bi(III) ion (Eq. (IV.2.4.4)) and Eq. (IV.2.4.6), the pseudo-first order rate constant can be expressed by Eq. (IV.2.4.7).

$$k_{obs} = \left[\frac{k_{Bi(H2L)}K^*_{Bi(H_2L)}[L]_t}{1 + \alpha_{2H}} + \frac{\dfrac{{}^{H_2O}k_{Bi(HL)}K^*_{Bi(H_2L)}[L]_t}{1 + \alpha_{2H}}}{K^H_{Bi(HL)}[H^+]} \right.$$

$$+ \frac{\dfrac{{}^{OH}k_{Bi(HL)}K^*_{Bi(H_2L)}[L]_t[OH]}{1 + \alpha_{2H}}}{K^H_{Bi(HL)}[H^+]}$$

$$\left. + \frac{k_{Bi(Cit)(H_2L)}K^*_{Bi(H_2L)(Cit)}K_{Bi(Cit)}[L]_{tot}}{1 + \alpha_{2H}} \times \frac{[Cit]_{tot}}{(1 + \alpha_{cit})} \right] \times \frac{1}{\gamma}$$

IV.2.4.7

Eq. (IV.2.4.7) was used for the fitting of the k_{obs} values at Figures IV.2.4.2 and IV.2.4.3 In the fitting procedure of the kinetic data characterizing the formation of [Bi(DOTP)]$^{5-}$ and [Bi(DOTA)]$^{-}$, the $k_{Bi(H2L)(Cit)}$ rate constant attributed to the deprotonation and transformation of *[Bi(H_2DOTA)(citrate) intermediate, the stability constant of *[Bi(H_2L)(citrate)]) intermediate and [Bi(Cit)] complex was calculated, whereas the log$K_{Bi(Cit)2}$ was fixed (log$K_{Bi(Cit)2}$=5.05, 37°C, 0.15 M NaClO$_4$).[126] The formation of the *[Bi(H_2L)(citrate)]) intermediates has been neglected in the Bi(III) - DOTP – citrate reacting system. The stability constant of the *[Bi(H_2DOTP)] intermediate, the $k_{Bi(H2L)}$, $^{H2O}k_{Bi(HL)}$ and $^{OH}k_{Bi(HL)}$ rate constants and the $K^H_{Bi(HL)}$ protonation constants that characterize the formation of [Bi(DOTA)]$^{-}$ and [Bi(DOTP)]$^{5-}$ complexes obtained in the absence of citrate were fixed in the calculations. The stability constant of the [Bi(Cit)] complex obtained by the fitting of the kinetic data at Figures IV.2.4.2 and IV.2.4.3 are log$K_{Bi(Cit)}$= 11.55 (8) and 11.08 (6), which are in acceptable agreement with the stability constant of [Bi(Cit)] complex published in the literature (log$K_{Bi(Cit)}$=10.78, 37°C, 0.15

M NaClO$_4$).[126] The stability constant of the *[Bi(H_2DOTA)(citrate) intermediate was $\log K_{Bi(H2L)(Cit)}$=4.5 (1) ($\log \beta_{Bi(H2L)(Cit)}$=[Bi($H_2$DOTA)(citrate)]/[Bi^{3+}][H$_2$DOTA][citrate]=16.1), which is very similar to that of *[Ga(HNOTA)(citrate)] intermediate ($\log \beta_{Ga(HNOTA)(Cit)}$=14.9 – 16.7.[127] The $k_{Bi(H2L)(cit)}$ rate constant characterizing the deprotonation and transformation of *[Bi(H_2DOTA)(citrate)] intermediate to the final [Bi(DOTA)]$^-$ complex are shown in Figure IV.2.4.4
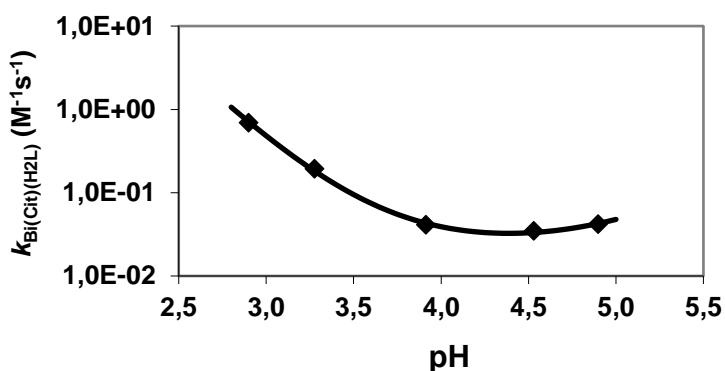
Figure IV.2.4.4 $k_{Bi(Cit)(H2L)}$ rate constants characterizing the transformation of the
*[Bi(H_2DOTA)(citrate)] intermediate to the final [Bi(DOTA)]$^-$ complex as a function of
pH. The symbols and the solid lines represent the experimental and the calculated rate
constants, respectively. (0.15 M NaClO$_4$, 25°C).

The variation of the $k_{Bi(H_2L)(Cit)}$ values as a function pH (Figure IV.2.4.4) shows an unusual pH dependency. We assume that the final [Bi(DOTA)]$^-$ complex from *[Bi(H_2DOTA)(citrate)] occurs by protonation and dissociation of the coordinated citrate (Hcitrate and H$_2$citrate species dominant in the pH range of 3.0–5.6), with the deprotonation of the ring nitrogen atoms and transformation of the intermediate to the final Bi(III) complex. These processes might occur simultaneously or consecutively. Protonation of the citrate ligand might be assisted by H$^+$ (k_1 and k_2), while

the deprotonation of the ring N donor atoms occurs via the assistance of H_2O and OH^- (characterized by k_0 and k_3 rate constants). Inspection of the pH-dependency of $k_{Bi(H2L)(cit)}$ values (shown in Figure IV.2.4.4) confirms that the assistance of H^+ dominates below pH=4, whereas the H_2O and OH^- assisted pathways has an important role in the formation of $[Bi(DOTA)]^-$ above pH=4. By taking into account the possible pathways for the transformation of the *[Bi(H_2DOTA)(citrate)] intermediate to the final $[Bi(DOTA)]^-$, the $k_{Bi(H2L)(cit)}$ rate constant can be expressed by Eq IV.2.4.9

$$k_{\mathrm{Bi}(H_2\mathrm{L})(\mathrm{Cit})} = k_0 + k_1[\mathrm{H^+}] + k_2[\mathrm{H^+}]^2 + k_3[\mathrm{OH^-}] \qquad IV.2.4.9$$

The rate constants characterizing the H_2O, H^+ and OH^- assisted transformation of the *[Bi(H_2DOTA)(citrate)] intermediate to the final $[Bi(DOTA)]^-$ are $k_0=(2.0 \pm 0.7) \times 10^{-2}$ s^{-1}, $k_1= 13 \pm 6$ $M^{-1}s^{-1}$, $k_2= (3.3 \pm 0.7) \times 10^5$ $M^{-1}s^{-1}$ and $k_3= (1.5 \pm 0.6) \times 10^7$ $M^{-1}s^{-1}$, respectively. Comparison of the $^{H2O}k_{Bi(HL)} = (2 \pm 1) \times 10^{-5}$ s^{-1} and $^{HO}k_{Bi(HL)}= (1.2 \pm 0.2) \times 10^6$ $M^{-1}s^{-1}$ values characterizing the H_2O and OH^- assisted transformation of the monoprotonated *[Bi(HDOTA)] intermediate with those values characteristic for the *[Bi(H_2DOTA)(citrate)] intermediate ($k_0=(2.0 \pm 0.7) \times 10^{-2}$ s^{-1} and $k_3= (1.5 \pm 0.6) \times 10^7$ $M^{-1}s^{-1}$) indicates that the faster formation of $[Bi(DOTA)]^-$ in the presence of citrate auxiliary ligand can be explained by the faster H_2O and OH^- assisted transformation of the *[Bi(H_2DOTA)(citrate)] intermediate at pH>4.0.

IV.2.5 Radiolabeling of DOTA with ^{213}Bi isotope in the presence of citrate, acetate and MES buffers

The radiolabeling of DOTP and DOTA ligands with ^{213}Bi(III) isotope in NaOAc buffer was studied in detail.[128] According to the

literature data the labeling properties of cyclen-based phosphonate ligands are better than those of the cyclic DOTA or acyclic CHX-A"-DTPA chelators for [213]Bi(III), resulting comparable labeling yields at 2–4 orders of magnitude lower concentrations both at ambient and elevated temperatures.[128] To investigate the role of citrate for the formation rate of [Bi(DOTA)]$^-$, the labeling of DOTA with [213]Bi(III) was investigated by determining the fraction of [213]Bi(III) incorporated by DOTA with radio-TLC at different concentrations of DOTA (0.3–100 µM) and citrate (0–100 µM) at 25°C in acetate and MES buffers (Figure IV.2.5.1).
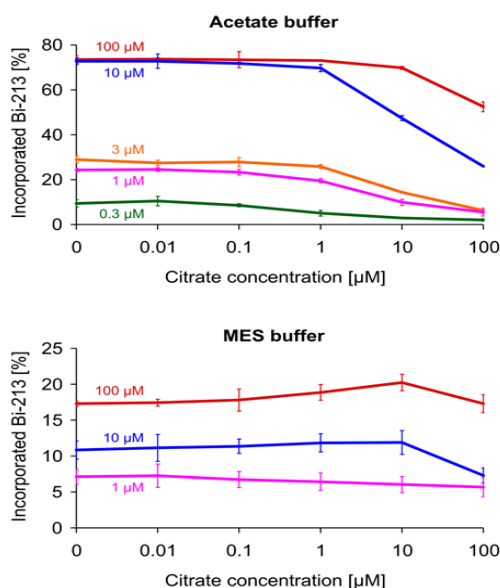

Figure IV.2.5.1 Complexation of [213]Bi(III) (reaction time: 10 min, 25°C) by H$_4$DOTA (concentrations of 0.3-100µM see lables on the figures) in ammonium acetate (pH 5.3 top) or MES (pH 5.6 bottom) buffers as a function of citrate concentration.

The percentages of complexed [213]Bi(III) ion indicated in Figure IV.2.5.1 refer only to the [Bi(DOTA)]$^-$ signal and exclude any non-DOTA coordinated [213]Bi(III) isotope. Suprisingly, we found that in the MES-buffered solutions, large amounts of activity were distributed almost over

the entire TLC ($R_f = 0.2 - 1$), which can be explained by the presence of oligomeric and polymeric ^{213}Bi(III) hydroxo species. On the other hand, TLCs of the acetate buffered solutions only contained distinct signals of $[^{213}Bi][Bi(DOTA)]^-$ and $[^{213}Bi]Bi(Cit)$ or $[^{213}Bi][Bi(Cit)_2]^{3-}$ formed bythe non-complexed ^{213}Bi(III) ion.

Based on the percentages of incorporated ^{213}Bi(III) ion in Figure IV.2.5.1 the labeling yields of DOTA increase with the increase of [DOTA] by reaching about 74 and 21% at $[DOTA]_{tot} = 100$ μM and $[Cit]_{tot} = 10$ μM in acetate and MES buffer, respectively. The presence of citrate has practically no effect on the amount of incorporated ^{213}Bi(III) ion at [Cit]<0.1 μM in both buffers. The labeling yields of DOTA decrease with the increase of the citrate concentration at [Cit]>0.1 μM in acetate buffer. However, the percentages of incorporated ^{213}Bi(III) ion increase with the increase of the citrate concentration from 0.1 to 10 μM by about 3-4 % in the presence of 100 μM DOTA in MES buffer. To explain the different effect of citrate for the radiolabeling of DOTA with ^{213}Bi(III) ion in acetate and MES buffer, we shoud consider that the ^{213}Bi(III)-ion does not interact with the MES, whereas the acetate might be coordinated to the ^{213}Bi(III) ion and *[Bi(*H*DOTA)] intermediate by accelerating its deprotonation and transformation to the final [Bi(DOTA)]$^-$ complex. In the presence of a large excess of acetate (0.15 M), the formation of $[^{213}Bi][Bi(DOTA)]^-$ takes places with a higher yield due to the acetate-assisted deprotonation of the *$[^{213}Bi][Bi(H$DOTA)] intermediate. Since the effect of acetate is higher than that of *$[^{213}Bi][Bi(H_2$DOTA)(Cit)] intermediate for the formation rate of $[^{213}Bi][Bi(DOTA)]^-$, the formation of the *$[^{213}Bi][Bi(H_2$DOTA)(Cit)] intermediate decreases the amount of the incorporated ^{213}Bi at [Cit]>1.0 μM. In contrast, MES as general base

cannot catalyze the deprotonation of the $*[^{213}Bi][Bi(HDOTA)]$ intermediate, since its protonated form is predominated at pH=5.6 (log $K_1^H =$ 6.11 (1), 0.15 M NaClO$_4$, 25°C). At [Cit]>0.1 μM and [DOTA]>1.0 μM, the formation of the $*[^{213}Bi][Bi(H_2DOTA)(Cit)]$ intermediate takes places with a higher incorporation yield of ^{213}Bi(III) ion in MES buffer. The decrease of the labeling yield at [Cit]>10 μM might be attributed to the formation of $[^{213}Bi][Bi(Cit)_2]^{3-}$ species, which can prevent the formation of both $*[^{213}Bi][Bi(HDOTA)]$ and $*[^{213}Bi][Bi(H_2DOTA)(Cit)]$ intermediates in acetate and MES buffers.

The effect of acetate and MES buffer for the formation rate of non-radioactive [Bi(DOTA)]$^-$ complex was also studied by spectrophotometry at the absorption band of the final [Bi(DOTA)]$^-$ complex (308 nm) in the presence of 0.25 mM citrate ([Bi(III)]$_{tot}$=25 μM, [DOTA]$_{tot}$=1.0 mM, pH=5.0, 0.15 M NaClO$_4$, 25°C). The k_{obs} vs. [Ac]$_{tot}$ and k_{obs} vs. [MES]$_{tot}$ for the formation of [Bi(DOTA)]$^-$ are reported in Figures IV.2.5.2.

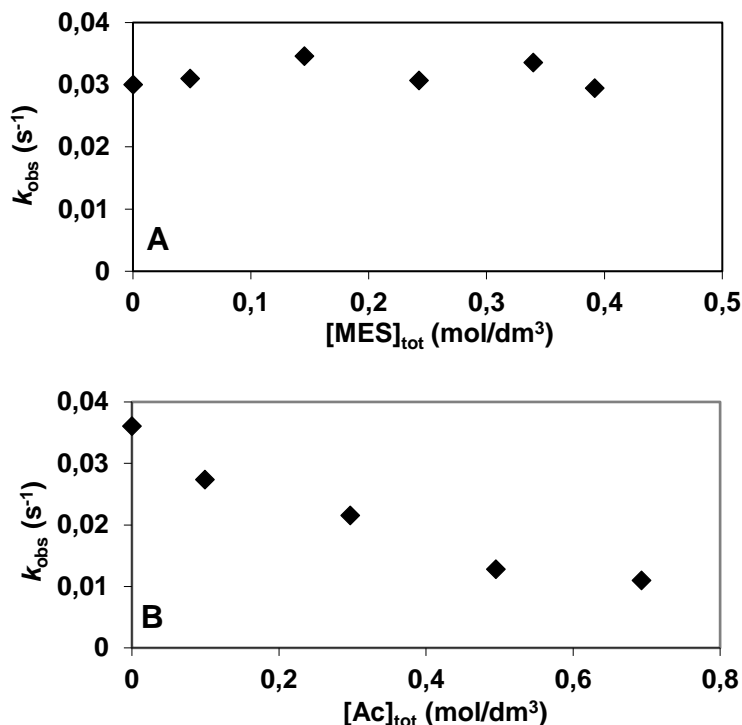**Figure IV.2.5.2** Pseudo-firstorder rate constants (k_{obs}) for the formation reaction of [Bi(DOTA)]$^-$ complex in the presence of MES buffer (**A**) and acetate buffer (**B**). ([Bi(III)]$_{tot}$=25 μM, [DOTA]$_{tot}$=1.0 mM, [citrate]$_{tot}$=0.25 mM pH= 5.0, 0.15 M NaClO$_4$, 25°C).

Interestingly, the k_{obs} values decrease with the increase of [Ac]$_{tot}$ in Bi(III) - DOTA – citrate system (Figure IV.2.5.2 B). Unfortunately, there is no literature data exists on the interaction of Bi(III) ion with acetate ligand[129]. However, it can be assumed that acetate as ligand in high excess ([Ac]$_{tot}$>0.1 M) might compete with the citrate for the coordination to Bi(III) ion in the intermediate, which can reduce the formation rate of [Bi(DOTA)]$^-$ complex by lowering the concentration of the kinetically active *[Bi(H_2DOTA)(citrate)] intermediate. On the other hand, MES buffer does not alter the formation rate of the [Bi(DOTA)]$^-$ complex (Figure IV.2.5.2 A). To the best of our knowledge, MES buffer does not interact with Bi(III) ion.

IV.2.6 Dissociation kinetic studies of [Bi(DOTA)]⁻ and [Bi(DOTP)]⁵⁻ complexes.

The safe and efficient *in vivo* applications of metal complexes require their stability and inertness in order to avoid the release of the metal ion and of the free ligand and to deliver the radiotracer in the form of intact complex to the target site. The extremely low concentration of the radiopharmaceuticals and the high excess of the possible endogenous competitors (transmetallation and transchelation reactions) might promote the *in vivo* dissociation of the metal complexes characterized by high thermodanymic stability constant. To investigate the inertness of Bi(III) complexes the rates of the transchelation reactions (Eq. IV.2.6.1) occurring between [Bi(DOTA)]⁻ or [Bi(DOTP)]⁵⁻ complexes and AAZTA and HP-DO3A were studied at acidic and basic conditions, respectively. Transchelation reactions of the Bi(III) complexes with AAZTA have been monitored by spectrophotometry at acidic condition on the absorption band of the Bi(DOTA)]⁻ and [Bi(DOTP)]⁵⁻ complexes complexes (308 nm) in the presence of 40-fold AAZTA excess.

$$\text{BiL} + \text{AAZTA} \rightleftharpoons \text{Bi(AAZTA)} + \text{L} \qquad (\text{L} = \text{DOTA, DOTP}) \qquad \textit{IV.2.6.1}$$

Some characteristic absorption spectra of the [Bi(DOTA)]⁻-AAZTA and [Bi(DOTP)]⁵⁻-AAZTA reacting systems are shown in Figure IV.2.6.1
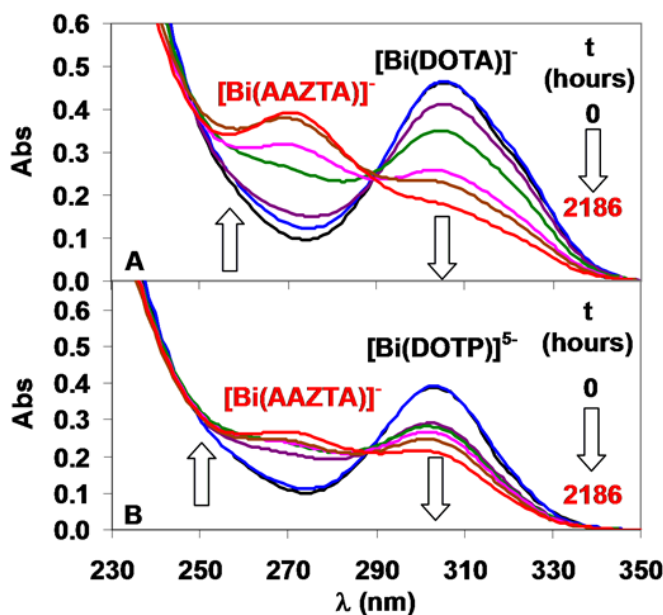
Figure IV.2.6.1 Absoprtion spectra of $[Bi(DOTA)]^-$-AAZTA (**A**) and $[Bi(DOTP)]^{5-}$-AAZTA (**B**) reacting system ($[Bi(DOTA)]_{tot}=[Bi(DOTP)]_{tot}= 0.05$ mM, $[AAZTA]_{tot}= 2.0$ mM, pH=1.5, l=1 cm, 0.15 M $NaClO_4$, 25°C).

In the presence of exchanging ligand AAZTA excess the transchelation can be treated as a pseudo-first order process and the rate of reactions can be expressed with the Eq. IV.2.6.2, where k_d is a pseudo-first order rate constant and $[BiL]_{tot}$ is the total concentration of the Bi(III) complexes.

$$-\frac{d[BiL]_t}{dt} = k_d[BiL]_t \qquad IV.2.6.2$$

The rates of the transchelation reactions have been studied in the pH range 1.0 – 3.3. The pseudo-first order rate constants (k_d) obtained are presented in Figure IV.2.6.2 as a function of pH and $[H^+]$.
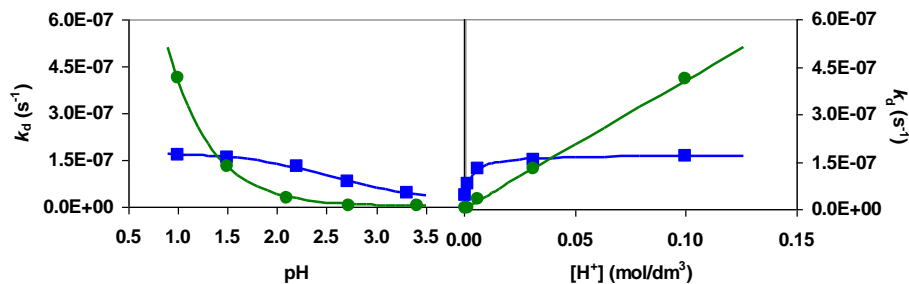
Figure IV.2.6.2 k_d pseudo-first order rate constant characterizing the transchelation reactions of **[Bi(DOTA)]**⁻ and **[Bi(DOTP)]**⁵⁻ with AAZTA ligand. Solid lines and the symbols represent the calculated and measured k_d rate constants. ([Bi(DOTA)]⁻$_{tot}$ = [Bi(DOTP)]⁵⁻$_{tot}$ =50 μM, [AAZTA]$_{tot}$=2.0 mM, [CA]$_{tot}$=0.01 M, 0.15 M NaClO₄, 25°C).

The kinetic data presented in Figure IV.2.6.2. show that the k_d values increase with increasing H⁺ ion concentration. On the basis of literature data,[130] the rate-determining step of the transchelation reactions is the dissociation of the Gd(III) complexes with DOTA derivatives, followed by the fast reaction between the free Gd(III) ion and the exchanging ligand or by the rapid reaction between the free chelate and the exchanging metal ion. The exchanging metal ions or ligand do not take place directly in the transmetallation or transchelation reactions.[111], [130]–[132] By taking into account the speciation of Bi(III) - DOTA and Bi(III) - DOTP systems, the dependence of the k_d values on pH and [H⁺] (Figure IV.2.6.2) can be interpreted as spontaneous ($^{dis}k_0$, Eq. IV.2.6.3) and H⁺-ion assisted dissociation ($^{dis}k_H$, Eq. IV.2.4.4) of Bi(III) complexes via the formation of [Bi(*H*DOTA)] and [Bi(*H₅*DOTP)] intermediates (K^H_{BiL}, Eq. IV.2.6.4) in the investigated pH ranges.

$$BiL \longrightarrow Bi^{3+} + L \qquad\qquad IV.2.6.3$$

$$BiL + H^+ \rightleftharpoons Bi(HL)$$
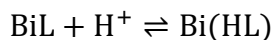
$$K^H_{BiL} = \frac{[Bi(HL)]}{[BiL][H^+]} \qquad\qquad IV.2.6.4$$

$$Bi(HL) \longrightarrow Bi^{3+} + HL \qquad\qquad IV.2.6.5$$

where [Bi(HL)] represents the concentration of the [Bi(HDOTA)] and [Bi(H_5DOTP)] complexes. By taking into account all possible pathways and Eq. IV.4.1.2, the rate of the dissociation of [Bi(DOTA)]⁻ and [Bi(DOTP)]⁵⁻ can be expressed by Eq. IV.2.6.6.

$$-\frac{d[BiL]_t}{dt} = k_d[BiL]_t = {}^{dis}k_0[BiL] + {}^{dis}k_H[Bi(H_xL)] \qquad IV.2.6.6$$

where x=1 and 5 for [Bi(DOTA)]⁻ and [Bi(DOTP)]⁵⁻, respectively. Considering the total concentration of the [Bi(DOTA)]⁻ and [Bi(DOTP)]⁵⁻ complexes ([BiL]_tot=[BiL]+[Bi(HL)]) and the protonation constant of BiL ((K^H_{BiL}, Eq. IV.2.6.4), the k_d pseudo-first order rate constants presented can be expressed by Eq. (IV.2.6.7).

$$k_d = \frac{{}^{dis}k_0 + {}^{dis}k_1[H^+]}{1 + K^H_{BiL}[H^+]} \qquad IV.2.6.7$$

where $^{dis}k_0$, $^{dis}k_1 = k_H \times K^H_{BiL}$ and K^H_{BiL} are the rate and protonation constants characterizing the spontaneous and H⁺ assisted dissociation of the [Bi(DOTA)]⁻ and [Bi(H_4DOTP)]⁻ species. The rate and protonation constants characterizing the transchelation reactions of [Bi(DOTA)]⁻ complex with AAZTA have been calculated by fitting of the corresponding k_d values presented in Figure IV.2.6.2 to the Eq. (IV.2.6.7). The protonation constant (K^H_{BiL}) of [Bi(H_4DOTP)]⁻ species is relatively small ($K^H_{BiL} < 10$) due to the protonation of the coordinated and weakly basic phosphonate O⁻ donor atom. Therefore, this protonation process could not be detected in the pH-potentiometric studies of [Bi(DOTP)]⁵⁻ complex. By taking into account the very low protonation constant of [Bi(H_4DOTP)]⁻ species ($K^H_{BiL} < 10$), the denominator of Eq. (IV.2.6.7) ($1 >> K^H_{BiL}[H^+]$) can be neglected, so Eq. (IV.2.6.7) can be simplified in the form of Eq. (IV.2.6.8). The $^{dis}k_0$

and $^{dis}k_1$ rate constants characterizing the spontaneous and H$^+$ assisted dissociation of the [Bi(H_4DOTP)]$^-$ species have been calculated by fitting of the corresponding kinetic data (Figure IV.2.6.2) to Eq. (IV.2.6.8).

$$k_d = {}^{diss}k_0 + {}^{diss}k_1[H^+] \qquad \qquad IV.2.6.8$$

The $^{dis}k_0$, $^{dis}k_1$ and K^H_{BiL} rate and protonation constants characterizing the spontaneous and H$^+$ assisted dissociation of the [Bi(DOTA)]$^-$ and [Bi(H_4DOTP)]$^-$ species are shown in Table IV.2.6.1.

The rates of the transchelation reactions between [Bi(DOTA)]$^-$ or [Bi(DOTP)]$^{5-}$ and HP-DO3A as exchanging ligand were also studied by CZE method under basic conditions on the signal of the [Bi(HP-DO3A)] complex (migration time: 5.2 min) in the presence of excess of the Bi(III) complexes (pH=10.0–12.0, 0.15 M NaClO$_4$, 25°C). Because of the similar absorption spectra of the [Bi(DOTA)]$^-$, [Bi(DOTP)]$^{5-}$ and [Bi(HP-DO3A)] CZE method was selected to monitor the transchelation reactions between [Bi(DOTA)]$^-$ or [Bi(DOTP)]$^{5-}$ and HP-DO3A ligand. The rates of the transchelation reactions (Eq. (IV.2.6.9)) between Bi(III) complexes and HP-DO3A were studied by CZE at basic condition on the signal of [Bi(HP-DO3A)] in the presence of the Bi(III) complex excess ([Bi(DOTA)]$_{tot}$=[Bi(DOTP)]$_{tot}$=60 mM, [HP-DO3A]$_{tot}$= 5.0 and 10 mM, pH=10.0 – 12.0, 0.15 M NaClO$_4$, 25°C). Some characteristic electropherograms of the [Bi(DOTA)]$^-$ - HP-DO3A reacting system are shown in Figure IV.2.6.3

$$BiL + HP-DO3A \rightleftharpoons Bi(HP-DO3A) + L \quad (L = DOTA, DOTP) \quad IV.2.6.9$$
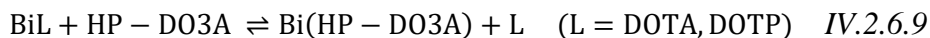
Under our experimental conditions ([Bi(DOTP)]$_{tot}$=60 mM, [HP-DO3A]$_{tot}$=5 and 10 mM) and at pH between 10.0 – 12.0, the transchelation

of [Bi(DOTP)]$^{5-}$ with HP-DO3A does not occur indicating the outstanding inertness of the given complex. In the presence of excess of the Bi(III) complexes the transchelation of [Bi(DOTA)]$^-$ can be treated as a pseudo-first order process and the rate of reactions can be expressed with the Eq. (IV.2.4.6). The rates of the transchelation reactions of [Bi(DOTA)]$^-$ were studied at different concentrations of the HP-DO3A ligand in the pH range 10.0 – 12.0. The pseudo-first order rate constants (k_d) obtained from the integral values of [Bi(HP-DO3A)] by Eq. (III.5.3) are presented in Figure IV.2.6.3 as a function of pH and [OH$^-$].
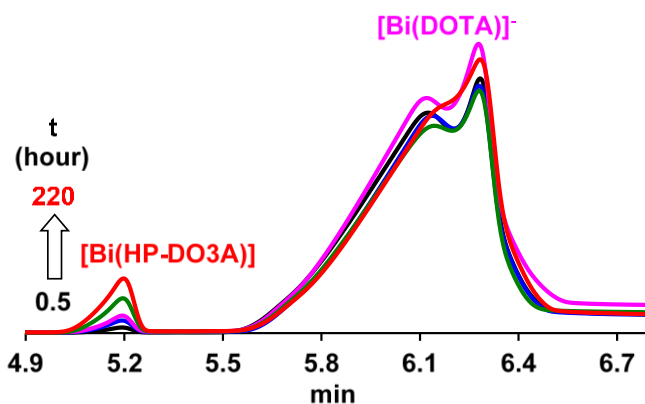

Figure IV.2.6.3 Electropherograms of the [Bi(DOTA)]$^-$ - HP-DO3A reacting system at **0.5**, **50**, **60**, **150** and **220** hours after the start of the reaction. ([Bi(DOTA)]$_{tot}$=53.2 mM, [HP-DO3A]$_{tot}$=10 mM, pH=12.0, 10 mM Na$_3$PO4, 0.15 M NaClO$_4$, 25°C).

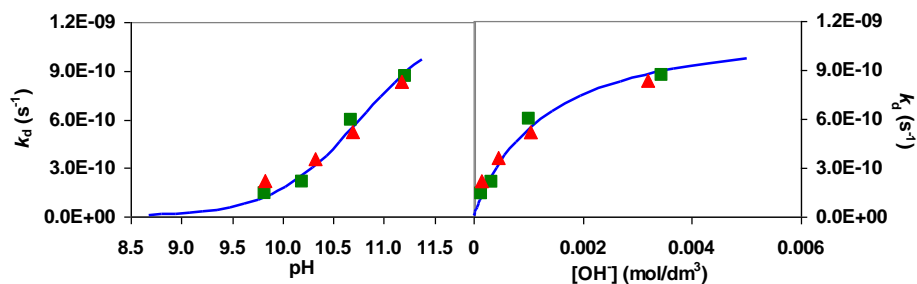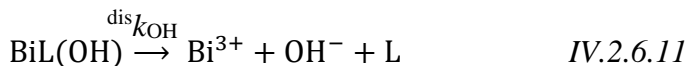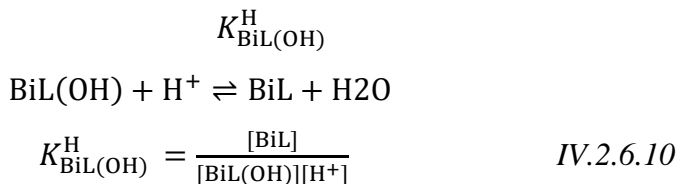**Figure IV.2.6.4** k_d pseudo-first order rate constant characterizing the transchelation reactions of [Bi(DOTA)]$^-$ with HP-DO3A ligand. Solid lines and the symbols represent the calculated and measured k_d rate constants. ([Bi(DOTA)]$^-_{tot}$=60 mM, [HP-DO3A]$_{tot}$=5.0 mM (■) and 10 mM (▲) [Na$_3$PO$_4$]$_{tot}$=0.01 M, 0.15 M NaClO$_4$, 25°C).

The kinetic data presented in Figure IV.2.6.4 show that the k_d values are independent of [HP-DO3A] and increase with pH and [OH⁻], indicating that the rate-determining step of the transchelation reactions is the dissociation of the [Bi(DOTA)]⁻ complex, followed by the fast reaction between the free Bi(III) ion and the exchanging HP-DO3A ligand. The dependence of the k_d values on pH can be interpreted by the formation (K^H_{BiLH-1} Eq. (IV.2.6.10)) and the spontaneous dissociation of the [Bi(DOTA)(OH)]²⁻ species ($^{dis}k_{OH}$, Eq. (IV.2.6.11)). The formation of [Bi(DOTA)(OH)]²⁻ species might be interpreted by the substitution of the carboxylate O⁻ donor atom by the OH⁻ ion in the inner sphere of the Bi(III) ion.

$$K^H_{BiL(OH)}$$

$$BiL(OH) + H^+ \rightleftharpoons BiL + H2O$$

$$K^H_{BiL(OH)} = \frac{[BiL]}{[BiL(OH)][H^+]} \qquad \qquad IV.2.6.10$$

$$BiL(OH) \xrightarrow{^{dis}k_{OH}} Bi^{3+} + OH^- + L \qquad \qquad IV.2.6.11$$

By taking into account all possible pathways and Eq. (III.5.2), the rate of the dissociation of [Bi(DOTA)]⁻ can be expressed by Eq. (IV.2.6.12).

$$-\frac{d[BiL]_t}{dt} = k_d[BiL]_t = {}^{dis}k_{OH}[BiL(OH)] \qquad IV.2.6.12$$

Considering the total concentration of the [Bi(DOTA)]⁻ complex ([BiL]_tot=[BiL]+[BiL(OH)]) and the protonation constant of [Bi(DOTA)(OH)]²⁻ species (K^H_{BiLH-1}, Eq. (IV.2.6.10)), the k_d pseudo-first order rate constants presented can be expressed by Eq. IV.2.6.13.

$$k_d = \frac{^{dis}k_{OH}}{1+K_{BiL(OH)}[H^+]} \qquad \qquad IV.2.6.13$$

wherein $K^H_{BiL(OH)}$ and $^{diss}k_{OH}$ are the equilibrium and rate constants characterizing the formation and the spontaneous dissociation of $[Bi(DOTA)(OH)]^{2-}$ species. The rate and protonation constants characterizing the transchelation reactions of $[Bi(DOTA)]^-$ complex with HP-DO3A have been calculated by fitting the k_d values presented in Figure IV.2.6.4 to the Eq. (IV.2.6.13). The $K^H_{BiL(OH)}$ and $^{diss}k_{OH}$ protonation and rate constants characterizing the formation and the spontaneous dissociation of $[Bi(DOTA)(OH)]^{2-}$ species are shown in Table IV.2.6.1.The assumed pathways for the transchelation of $[Bi(DOTA)]^-$ and $[Bi(DOTP)]^{5-}$ complexes are shown in Figure IV.2.6.5.
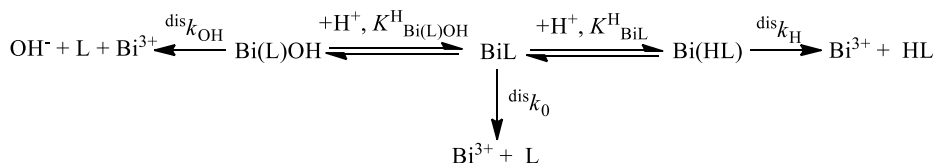
$$OH^- + L + Bi^{3+} \xleftarrow{^{dis}k_{OH}} Bi(L)OH \underset{}{\overset{+H^+,\ K^H_{Bi(L)OH}}{\rightleftharpoons}} BiL \underset{}{\overset{+H^+,\ K^H_{BiL}}{\rightleftharpoons}} Bi(HL) \xrightarrow{^{dis}k_H} Bi^{3+} + HL$$

$$\downarrow {^{dis}k_0}$$

$$Bi^{3+} + L$$

Figure IV.2.6.5 Acid and base catalysed dissociation of $[Bi(DOTA)]^-$ and $[Bi(DOTP)]^{5-}$ complexes. For the H^+ assisted dissociation of $[Bi(DOTP)]^{5-}$, BiL represents the $[Bi(H_4DOTP)]^-$ species dominates in our experimental condition. The reaction path in the left side is valid for the $[Bi(DOTA)]^-$ complex only.

Table IV.2.6.1 Rate (k_i) and equilibrium constants (K_i), and half-lives ($t_{1/2}=\ln2/k_d$) for the dissociation reactions of $[Bi(DOTA)]^-$, $[Bi(DOTP)]^{5-}$, $[Gd(DOTA)]^-$ and $[Gd(DOTP)]^{5-}$ complexes (25°C)

	$[Bi(DOTA)]^-$	$[Bi(DOTP)]^{5-}$	$[Gd(DOTA)]^-$ [b]	$[Gd(DOTP)]^{5-}$ [d]
I	0.15 M NaClO$_4$		0.15 M NaCl	1.0 M Me$_4$NCl
$^{dis}k_0$ (s^{-1})	$(2.4\pm0.3)\times10^{-8}$	–	6.7×10^{-11}	–
$^{dis}k_1$ [a] (M^{-1}s^{-1})	$(5.8\pm0.6)\times10^{-5}$	$(4.0\pm0.7)\times10^{-6}$	1.8×10^{-6}	5.4×10^{-4}
$^{dis}k_{OH}$ (M^{-1}s^{-1})	$(1.0\pm0.2)\times10^{-9}$	–	–	–
K^H_{ML}	337 ± 43	–	14 [c]	1.7 (Gd(H$_4$L))
$K^H_{ML(OH)}$	$(1.0\pm0.2)\times10^{11}$	–	–	–
$t_{1/2}$ (h) pH=3	3.1×10^3	4.8×10^4	1.0×10^5	3.6×10^2
$t_{1/2}$ (h) pH=11	2.5×10^5	–	–	–

[a] $^{dis}k_1 = K^H_{BiL} \times {^{dis}k_H}$; [b] Ref. [[130]]; [c] Ref. [[118]] (3.0 M NaClO$_4$, 25°C); [d] Ref. [[119]]

The $^{dis}k_1$ rate constants characterizes the H$^+$-assisted dissociation of the [Bi(DOTP)]$^{5-}$ is significantly lower than that of [Bi(DOTA)]$^-$. The H$^+$ catalysed dissociation might take place via proton transfer from the protonated pendant arm to the nitrogen atom of the macrocycle, forcing the release of the Bi(III) ion. By takint into account the stronger interaction of Bi(III) with the more basic ring-N donor atoms of DOTP ligand, it can be assumed that the proton transfer is less probable from the weakly basic phosphonate -O$^-$ to the ring-N donor atom than from the less acidic carboxylate oxygen to the weakly basic ring nitrogen in the [Bi(DOTA)]$^-$. The slow dissociation of the Bi(III) complex with DO3A and dipicolinate cyclen ligand is also interpreted by the low protonation constant and structural rigidity of the picolinate pendant arms .[133], [134] Suprisingly, the proton-assisted dissociation of [Bi(DOTP)]$^{5-}$ is about two orders of magnitude slower than that of [Gd(DOTP)]$^-$, possibly due to the higher affinity of   the ring-N donor atoms to   Bi(III) than to Gd(III) ion. Suprisingly, the $^{dis}k_1$ value of [Bi(DOTA)]$^-$ is about 30-times higher than that of [Gd(DOTA)]$^-$, which is more resistent to the H$^+$-assisted dissociation.

The spontaneous dissociation of *[Bi(DOTA)(OH)]$^{2-}$ intermediate in basic condition might take place by the simultaneous decoordination of the carboxylate -O$^-$ donor atoms due to the electrostatic repulsion between the carboxylate -O$^-$ and OH$^-$ ion coordinated to Bi(III) ion. The spontaneous dissociation ($^{dis}k_{OH}$) of the [Bi(DOTA)(OH)]$^{2-}$ intermediate occures in very slow process.

IV.2.7 ^{1}H, ^{13}C and ^{31}P NMR studies of [Bi(DOTP)]$^{5-}$ complex.

In order to acquire deeper insight into the solution properties, multinuclear 1D and 2D NMR studies of [Bi(DOTP)]$^{5-}$ have been performed in the temperature range 273 - 333 K. Structure and the possible conformation of the [Bi(DOTP)]$^{5-}$ with the assignment of the ^{1}H and ^{13}C NMR signals are shown in Figure IV.2.7.1
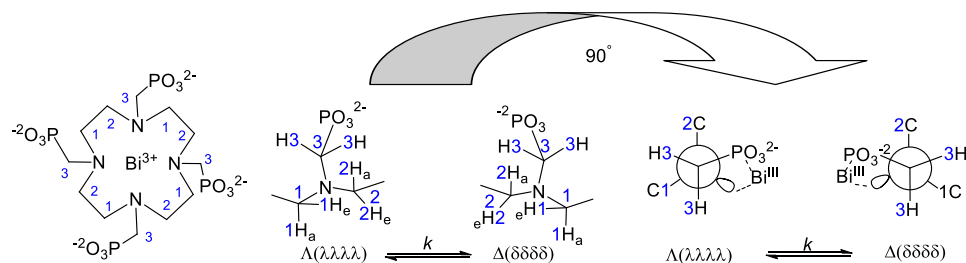

Figure IV.2.7.1. Structure and the possible conformation of the [Bi(DOTP)]$^{5-}$

Based on the result of the multinuclear NMR studies that the [Bi(DOTP)]$^{5-}$ complex in solution has C_{4V} symmetry, which might be very similar to that of the solid state structure found in the single crysta. X-ray diffraction studies of the sigle crystal with the formula Na[Bi(H_4DOTMP)(H$_2$O)$_4$)][135] reveal that the Bi(III) ion is octacoordinated by the four phosphonate oxygen and the four amine nitrogen donor atoms of the macrocycle.. Four protons are attached to the more basic and non-coordinated phosphonate O$^-$ donor atoms. As it was found for [Bi(DOTA)]$^-$ and [Bi(DO3A)],[16], [134] the five-membered chelate rings formed upon coordination of the ethylenediamine groups to Bi(III) adopt identical conformations [(δδδδ) or (λλλλ)], whereas the coordination of the phosphonate-O$^-$ to Bi(III) results in a counter-clockwise (Λ) or clockwise (Δ) orientation of the pendant arms in [Bi(DOTP)]$^{5-}$. The Δ(δδδδ) and Λ(λλλλ) enantiomers are present in the single crystal of [Bi(DOTP)]$^{5-}$. The coordination polyhedron around the

Bi(III) ion in $[Bi(DOTP)]^{5-}$ is twisted square antiprismatic similarly to $[Bi(DOTA)]^{-}$ and $[Bi(DO3A)]$ complexes. The torsion angle between the two square planes defined by phosphonate-O^{-} and ring N donor atoms of the macrocycle is 25.4° in $[Bi(DOTP)]^{5-}$.[135] In the ^{1}H and ^{13}C NMR spectra of $[Bi(DOTP)]^{5-}$ obtained at 273 K, the four ethylene protons ($1H_a$, $1H_e$, $2H_a$ and $2H_e$) and two ethylene carbons ($1C$ and $2C$) of the macrocyclic ring are non-equivalent (showing different resonances), which can be interpreted by rigid structure of the $[Bi(DOTP)]^{5-}$ complex (Figures A.2 and A.3). The ^{1}H and ^{13}C signals of the four ethylene protons ($1H_a$, $1H_e$, $2H_a$ and $2H_e$) and two ethylene carbons ($1C$ and $2C$) in $[Bi(DOTP)]^{5-}$ remain narrow up to 298 K, with a slight down- and upfield shift, respectively (Figures A.5 and A.6). However, the ^{1}H and ^{13}C NMR signals of $1H_a$, $1H_e$, $2H_a$ and $2H_e$ protons and $1C$ and $2C$ carbons gradually broaden and ^{13}C signals of $1C$ and $2C$ carbons collapse to a broad signal above 298 K due to the exchange between $\delta\delta\delta\delta$ and $\lambda\lambda\lambda\lambda$ conformations of the macrocyclic ring (Figure IV.2.7.1). Since the ^{1}H and ^{13}C NMR spectra of $[Bi(DOTP)]^{5-}$ contain only one set of signals, it might be assumed that the ring inversion ($\delta\delta\delta\delta \rightleftharpoons \lambda\lambda\lambda\lambda$) induced arm rotation process ($\Delta \rightleftharpoons \Lambda$) results in a $\Delta(\delta\delta\delta\delta) \rightleftharpoons \Lambda(\lambda\lambda\lambda\lambda)$ interconversion between the two enantiomers of $[Bi(DOTP)]^{5-}$ (the concentration of the other $\Delta(\lambda\lambda\lambda\lambda) - \Lambda(\delta\delta\delta\delta)$ enantiomeric pair is very low). The ring inversion and the arm rotation processes of $[Bi(DOTP)]^{5-}$ might occur subsequently or simultaneously. Similar phenomena of $[Bi(DOTA)]^{-}$ have been observed for by multinuclear NMR spectroscopy in aqueous solution.[16] The ^{31}C NMR signals of the $1C$ and $2C$ carbons were suitable to performe a full line-shape analysis by simulating the ^{13}C NMR spectra of $[Bi(DOTP)]^{5-}$ obtained in the temperature range 298–333 K (Figure A.6). The activation

parameters (Table IV.2.7.1) of the ring inversion process ($\delta\delta\delta\delta \rightleftharpoons \lambda\lambda\lambda\lambda$) of [Bi(DOTP)]$^{5-}$ have been estimated by the *Eyring* equation with the use of the *k* rate constant obtained in the line-shape analysis (Figure A.7).

Table IV.2.7.1 Rate constants and activation parameters of the ring inversion $\delta\delta\delta\delta \rightleftharpoons$ $\lambda\lambda\lambda\lambda$ process for [Bi(DOTP)]$^{5-}$ and [Bi(DOTA)]$^{-}$ complexes.

	[Bi(DOTP)]$^{5-}$	**[Bi(DOTA)]$^{-}$ [a]**
$\Delta H^{\ddagger}$ /kJ·mol^{-1}	64 ± 1	40
$\Delta S^{\ddagger}$ / J·mol^{-1}K^{-1}	−14 ± 2	−76
$\Delta G^{\ddagger}_{298}$ /kJ·mol^{-1}	68	63
k_{ex}^{298} /s^{-1}	8	65

[a] Ref. [16]

The activation enthalpy ($\Delta H^{\ddagger}$) and entropy ($\Delta S^{\ddagger}$) of the ring inversion process ($\delta\delta\delta\delta \rightleftharpoons \lambda\lambda\lambda\lambda$) in [Bi(DOTP)]$^{5-}$ are higher than those of [Bi(DOTA)]$^{-}$.[16] These data confirm the higher rigidity of [Bi(DOTP)]$^{5-}$ compared to [Bi(DOTA)]$^{-}$. Interestingly, the activation enthalpy of the ring inversion process for [La(DOTP)]$^{5-}$ is significantly higher than that of [Bi(DOTP)]$^{5-}$ ([La(DOTP)]$^{5-}$: $\Delta H^{\ddagger}$=101 kJ mol^{-1}).[136] The lower $\Delta H^{\ddagger}$ value of [Bi(DOTP)]$^{5-}$ might be interpreted by the larger size of the Bi^{III} ion, causing a less favourable size match between the Bi^{III} ion and the coordination cage of the DOTP ligand.

The methylene phosphonate protons (3H) of [Bi(DOTP)]$^{5-}$ give two multiplets (ABX, where X is ^{31}P nucleus) with chemical shifts of 2.90 and 3.10 ppm. The ^{31}P nuclei (T_1=1.02 ± 0.05 s at 298 K) are coupled to the two methylene phosphonate protons, with $^2J_{HP}$ couplings of − 15.4 and -15.7 Hz. The ring exhibits four proton signals: 1H$_a$ at 2.55 ppm (a doublet with $^2J_{HH}$\{1H$_e$\}=13.6 Hz), 1H$_e$ at 3.04 ppm (a "pseudotriplet" with $^2J_{HH}$\{1H$_a$\}=14.5 Hz and $^3J_{HH}$\{2H$_e$\}=14.3 Hz; i.e., the geminal and the

vicinal coupling constants are very similar), $2H_a$ at 2.65 ppm (a doublet with $^2J_{HH}\{2H_e\}$=13.6 Hz), $2H_e$ at 3.65 ppm (a "pseudotriplet" with $^2J_{HH}\{2H_a\}$=13.2 Hz and $^3J_{HH}\{1H_e\}$ = 13.3 Hz). The vicinal $^2J_{HH}$ and geminal $^3J_{HH}$ coupling constants of [Bi(DOTP)]$^{5-}$ are very similar to those of [Ln(DOTP)]$^{5-}$, [Bi(DOTA)]$^-$ and [Ln(DOTA)]$^-$ complexes.[16], [136], [137] The ^{31}P NMR spectra of the [Bi(DOTP)]$^{5-}$ complex is shifted by +1.6 ppm with the respect to the ^{31}P NMR signal of the free DOTP^{8-} ligand as a result of complex formation. $\Delta\delta_P$ value of [Bi(DOTP)]$^{5-}$ is somewhat lower than those of [Ln(DOTP)]$^{5-}$ complexes ([La(DOTP)]$^{5-}$: $\Delta\delta_P$=+7.2 ppm; [Lu(DOTP)]$^{5-}$: $\Delta\delta_P$ =+8.7 ppm).[136] [Bi(DOTP)]$^{5-}$ has a relatively simple ^{13}C NMR spectrum with a doublet for the methylene phosphonate 3C carbon (doublet with $^1J_{CP}$ = 136.5 Hz), a doublet for the ring 1C carbon (doublet with $^3J_{C1P}$ = 16.7 Hz) and a broad singlet for the C2 carbon ($^3J_{C2P}$ < 2 Hz). The T_1 relaxation time of the ^{13}C nuclei was found to be 0.12 ± 0.01 s at 298 K. Considering the coupling constants of the ring 1C and 2C carbons with ^{31}P nucleus ($^3J_{C1P}$ = 16.7 Hz and $^3J_{C2P}$ < 2 Hz), the dihedral angles (ϕ) of the 1C – N – 3C – P and 2C – N – 3C – P bonds have been calculated by using the Karplus equation as follows: $^3J_{CP} = 17.3\cos^2\phi - 4.7\cos\phi - 0.9$.[138] The dihedral angles were found to be $\phi = 46.7°$ and 151.8° for 2C – N – 3C – P and 1C – N – 3C – P "fragments".

IV.3. Equilibrium, kinetic and structural studies of [Bi(AAZTA)]$^-$, [Bi(AAZTA-C4-COO$^-$)], [Bi(AAZTA-C4-TATE)]$^-$ and [Bi(DTPA)]$^{2-}$ complexes

According to the detailed equilibrium and kinetic studies, [Bi(DOTA)]$^-$ and [Bi(DOTP)]$^{5-}$ are characterized by high thermodynamic

stability and kinetic inertness. However, the formation of Bi(III) complexes with DOTA and similar macrocyclic amino-polycarboxylates is extremely slow and requires high temperatures and long times to be completed. These conditions are hardly compatible with the preparation of labile and thermosensitive bioconjugates of short-lived isotopes[67]. Although, the fast formation of $[Bi(DOTP)]^{5-}$ is suitable for the application of the DOTP chelate to the complexation of the short lived $^{212/213}Bi(III)$ isotopes, but the presence of the phosphonate pendants results in the bone accumulation of the $[^{212/213}Bi][Bi(DOTP)]^{5-}$ which can pave the way for its usage in the treatment of bone cancer[132], [139]. In general the TAT application of the $^{212/213}Bi(III)$-based radiopharmaceuticals in oncology requires a chelate which can rapidly form a stable and inert $^{212/213}Bi(III)$ complexes without uncontroled targeting of tissues and organs. Among them, 6-amino-6-methylperhydro-1,4-diazepinetetraacetic acid (AAZTA)[140] proved to be an efficient coordinating ligand for several metal ions of the transition, post-transition metals and lanthanoids.. Moreover, the mesocyclic AAZTA-based systems form stable and inert complexes quickly and quantitatively around room temperature. These mild conditions are especially valuable for the preparation of radiobioconjugates with short-lived isotopes, limiting the degradation of the biomolecules and ensuring the maximum and correct dosage to the patient[141]. Moreover, bifunctional ligands derived from the parent AAZTA including AAZTA-C4-COOH and AAZTA-C9-COOH are commertially available for the preparation of targeted agents in nuclear oncology. Based on these considerations, the physico-chemical properties of Bi(III) complexes formed with AAZTA and its derivatives (AAZTA-C4-COOH and AAZTA-C4-TATE) have been investigated for the

potential application of AAZTA as a platform for the development of Bi(III)-based TAT agents.

IV.3.1 Equilibrium studies of the Bi(III) - AAZTA – NTA, Bi(III) – AAZTA-C4-COO$^-$ – NTA and Bi(III) – AAZTA-C4-TATE - NTA systems

Based on model calculations, NTA^{3-} can compete with AAZTA^{4-}, AAZTA-C4-TATE and AAZTA-C4 for Bi(III) (Eq IV.2.8) at pH=7.4 in the presence of large excess of NTA ([Bi(III)]=30.2 μM, [AAZTA]=10 - 50 μM, [NTA]=10 mM, 0.15 M NaClO$_4$, 25 °C). At such NTA concentrations, the species [Bi(NTA)$_2$]$^{3-}$ predominates.

$$Bi(NTA)_2 + H_xL \leftrightharpoons BiL + 2\ H_yNTA \qquad\qquad IV.3.1.1$$
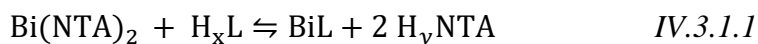
where L= AAZTA^{4-} and (AAZTA-C4-COO$^-$)$^{5-}$; x=1 and 2, y=0 and 1 at pH=7.4 in 0.15 M NaClO$_4$ solution. The stability constants of [Bi(AAZTA-C4-COO$^-$)]$^{2-}$ and [Bi(AAZTA)]$^-$ defined by Eq. (IV.2.1) have been determined by following the exchange reactions in the Bi(III)-NTA-H$_x$L system with spectrophotometry due to the different absorption spectra (6p ← 6s transitions) of the [Bi(NTA)$_2$]$^{3-}$, [Bi(AAZTA)]$^-$ and [Bi(AAZTA-C4-COO$^-$)]$^{2-}$ complexes. Some characteristic absorption spectra obtained in the systems Bi(III)-NTA- H$_x$L are shown in Figure IV.3.1.1-IV.3.1.2
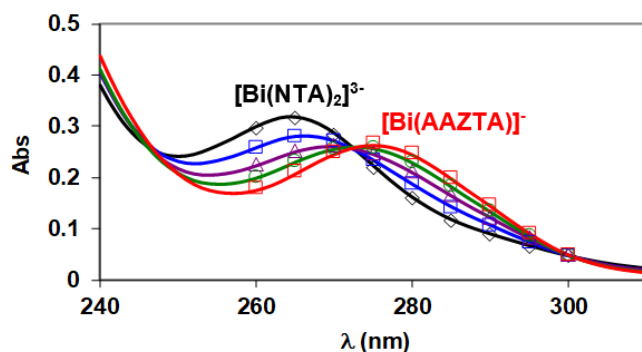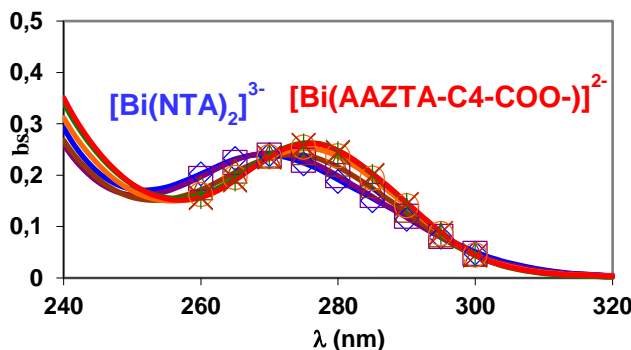
Figure.IV.3.1.1 The absorption spectra of the Bi(III) - NTA -AAZTA systems. The curves and the open symbols represent the experimental and the calculated absorbance values, respectively. ([Bi(III)]=30.2 μM, [NTA]=10 mM; [AAZTA] = **0.0** (◇), **10** (□), **20** (△), **30** (■) and **50** μM (□); pH=7.4, 25 °C, 0.15 M NaClO$_4$, l=1 cm).

Figure IV.3.1.2. The absorption spectra of the Bi(III) - NTA -AAZTA-C4-COOH systems. The curves and the open symbols represent the experimental and the calculated absorbance values, respectively. ([Bi(III)]=27.0 mM, [NTA]=30 mM; [AAZTA-C4-COO$^-$] = **5.0** (□), **10** (□), **20** (□), **30** (○), 40 (✳) and **60** □M (×); pH=7.4, 25 °C, 0.15 M NaClO$_4$, l=1 cm).

Isosbestic point in the spectra (Figures IV.3.1.1 and IV.3.1.2) indicate the only two absorbing species present in equilibrium: [Bi(AAZTA-C4-COO$^-$)]$^{2-}$, [Bi(AAZTA)]$^-$ and [Bi(NTA)$_2$]$^{3-}$. By taking into account the molar absorptivities of [Bi(AAZTA-C4-COO$^-$)]$^{2-}$, [Bi(AAZTA)]$^-$ and [Bi(NTA)$_2$]$^{3-}$, the protonation constants of (AAZTA-C4-COO$^-$)$^{5-}$, AAZTA^{4-} and NTA^{3-} (Table IV.1.1) and the stability product of [Bi(NTA)$_2$]$^{3-}$ (β_{BiL_2}=26.20, Table IV.2.2.1), the stability constants of

[Bi(AAZTA)]$^-$ and [Bi(AAZTA-C4-COO$^-$)]$^{2-}$ were calculated. For the complete description of equilibrium, the protonation constants of [Bi(AAZTA-C4-COO$^-$)]$^{2-}$ and [Bi(AAZTA)]$^-$ complex ($\log K_{Bi(H_iL)}$, Eq. (IV.2.3)) were also determined by pH-potentiometry at 25 °C in 0.15 M NaClO$_4$.

The competition reactions between AAZTA-C4-TATE and NTA for Bi(III) ion (Eq. (IV.3.1.1)) have been studied by CZE at pH=7.4 in 0.15 M NaCl solution. The separation of AAZTA-C4-TATE and [Bi(AAZTA-C4-TATE)]$^-$ is possible by CZE, since their charge-to-size ratios are slightly different. Because AAZTA-C4-TATE and [Bi(AAZTA-C4-TATE)]$^-$ are negatively charged, their migration velocities are smaller than the electroosmotic flow (EOF). However, the presence of the large TATE fragment require a low EOF for the separation of AAZTA-C4-TATE and [Bi(AAZTA-C4-TATE)]$^-$. In order to obtain a good resolution of AAZTA-C4-TATE and [Bi(AAZTA-C4-TATE)]$^-$, 150 mM disodium hydrogen phosphate buffer (pH=7.4) is optimal with the application of normal CE mode at 10 °C. The CZE electropherograms of the Bi(III)- AAZTA-C4-TATE - NTA equilibrium systems are shown in Figure IV.3.1.2 The signals of free NTA and [Bi(NTA)$_2$]$^{3-}$ are not observable in CZE electropherograms due to the very high differences between the LOD values of NTA, Bi(NTA)$_2$, AAZTA-C4-TATE and [Bi(AAZTA-C4-TATE)]$^-$.
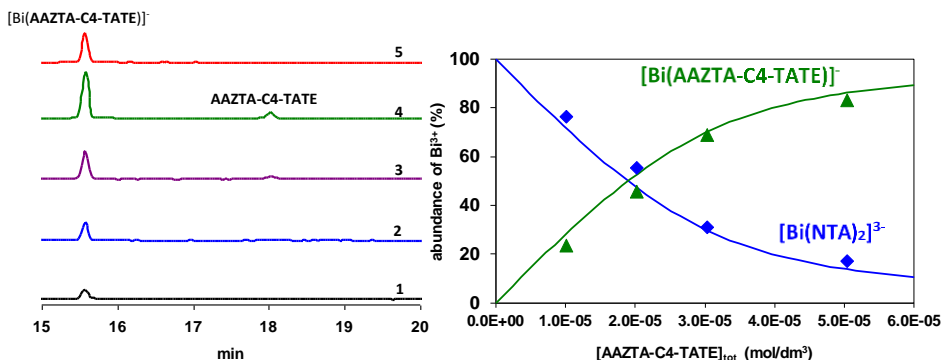
Figure IV.3.1.3. CZE electropherograms and species distribution of Bi(III) - AAZTA-C4-TATE - NTA equilibrium systems. The curves and the symbols represent the calculated and the experimental abundance of Bi(III), respectively ([Bi(III)]=36.2 μM, [NTA]= 15.0 mM, [AAZTA-C4-TATE]=10 (**1**), 20 (**2**), 30 (**3**), and 50 μM (**4**), [Bi(AAZTA-C4-TATE)]=30.2 μM (**5**), [DMSO]=5.0 mM, pH=7.4, 0.15 M NaClO₄, Conditions: 20 kV, 50 mbars, λ=200 nm; 150 mM disodium hydrogen phosphate, pH=7.4, 10 °C).

Figure IV.3.1.3 shows that the amount of the [Bi(AAZTA-C4-TATE)]⁻ complex increases with the increase of [AAZTA-C4-TATE]$_{tot}$ according to the competition reaction between AAZTA-C4-TATE and NTA for Bi(III) ion Eq. IV.3.1.1, characterized by the K_{BiTATE} equilibrium constant.

$$\text{Bi(NTA)}_2 + \text{AAZTA} - \text{C4} - \text{TATE} \leftrightharpoons \text{Bi(AAZTA} - \text{C4} - \text{TATE)} + 2\,\text{HNTA}$$
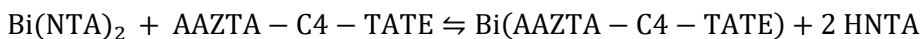
$$K_{\text{BiTATE}} = \frac{[\text{Bi(AAZTA}-\text{C4}-\text{TATE)}][\text{HNTA}]^2}{[\text{Bi(NTA)}_2][\text{AAZTA}-\text{C4}-\text{TATE}]} \qquad \textit{IV.3.1.1}$$

By taking into the definition of the stability and the conditional stability constants (Eqs. (IV.2.1), (IV.2.4) and (IV.2.5)) for [Bi(AAZTA-C4-TATE)] and [Bi(NTA)₂]³⁻ complexes, K_{BiTATE} equilibrium constant can be expressed by Eq. IV.3.1.2.

$$K_{\text{BiTATE}} = \frac{K_{\text{Bi(AAZTA}-\text{C4}-\text{TATE)}}(1+\alpha_H^{\text{NTA}})^2}{\beta_{\text{Bi(NTA)}_2}(1+\alpha_H^{\text{AAZTA}-\text{C4}-\text{TATE}})} = \frac{K_{\text{Bi(AAZTA}-\text{C4}-\text{TATE)}}^{\text{cond}}}{\beta_{\text{Bi(NTA)}_2}^{\text{cond}}} \qquad \textit{IV.3.1.2}$$

Considering the molar integral values of AAZTA-C4-TATE and [Bi(AAZTA-C4-TATE)] (Table IV.3.1), the total concentration of NTA ($[NTA]_{tot}=[HNTA]+2[Bi(NTA)_2]$), Bi(III)-ion ($[Bi^{3+}]_{tot}=[Bi(NTA)_2]+[Bi(AAZTA-C4-TATE)]$) and AAZTA-C4-TATE ($[AAZTA-C4-TATE]_{tot}=[Bi(AAZTA-C4-TATE)]+[H_xAAZTA-C4-TATE]$) the K_{BiTATE} value was calculated by Eq. (IV.2.9) ($K_{BiTATE}=51$ (9), pH=7.4, 0.15 M NaClO$_4$, 25 °C). Using the stability constant of [Bi(NTA)$_2$]$^{3-}$ ($\log\beta_{Bi(NTA)2}=26.21$, 0.15 M NaClO$_4$, 25 °C, Table IV.2.2.1) and the protonation constants of NTA ligand (Table IV.1.1) the conditional stability constant of [Bi(NTA)$_2$] was calculated by Eq. (IV.2.5) ($\log K^{cond}_{Bi(NTA)2}=22.5$, pH=7.4, 0.15 M NaClO$_4$, 25 °C). Considering the K_{BiTATE} equilibrium constant ($K_{BiTATE}=51$) and the conditional stability constant of [Bi(NTA)$_2$]$^{3-}$ ($\log K^{cond}_{Bi(NTA)2}=22.5$, 0.15 M NaClO$_4$, 25 °C), the conditional stability constant of [Bi(AAZTA-C4-TATE)] complex ($\log K^{cond}_{Bi(AAZTA-C4-TATE)}= \log K_{BiTATE} + \log K^{cond}_{Bi(NTA)2}$, Eq. (IV.3.1.2)) was found to be 24.3 at pH=7.4 and 25 °C in 0.15 M NaClO$_4$. The stability, protonation and conditional stability constants of the complexes are presented in the Table IV.3.1.1.

Table IV.3.1.1 Stability (log K_{BiL}), protonation (log $K_{Bi(HiL)}$) and conditional stability constants (log K_{BiL}^{cond}) of the complexes. A: [Bi(AAZTA)]$^-$, B: [Bi(AAZTA-C4-TATE)], C: [Bi(AAZTA-C4-COO$^-$)]$^{2-}$ D: [Bi(NTA)$_2$]$^{3-}$, E: [Bi(DTPA)]$^{2-}$, F: [Bi(DOTA)]$^-$ (0.15M NaClO$_4$ 25°C).

|	A	B	C	D	E [a]	F
log K_{BiL}	**26.45 (6)**	**–**	**28.75 (8)**	**16.97**	**29.29**	**30.86**
log $K_{Bi(HL)}$	1.63 (3)	–	4.74(4)	-	2.55 (1)	1.38
log K_{BiL2}	-	-	-	9.23	-	-
log K_{BiL}^{cond} (pH=7.4)	**23.5**	**24.3 (2)**	**25.6**	**22.5**	**25.4**	**27.0**

[a] Ref. [142] (0.6 M NaClO$_4$, 25°C);

The thermodynamic parameters in Table IV.3.1.1 indicates that the stability constant of [Bi(AAZTA)]$^-$ is lower than that of [Bi(DOTA)]$^-$ [Bi(DTPA)]$^{2-}$ and [Bi(AAZTA-C4-COO$^-$)]$^{2-}$ complexes by about 4, 3 and 2.5 log units, respectively (0.15 M NaClO$_4$, 25°C). To compare the Bi(III) affinity of AAZTA, AAZTA-C4-COOH, AAZTA-C4-TATE, DTPA and DOTA ligands the apparent stability of Bi(III) complexes have been calculated near to physiological conditions by considering the protonation constants of AAZTA-C4-COOH, AAZTA, DTPA and DOTA and the stability constants of [Bi(AAZTA-C4-COO$^-$)]$^{2-}$, [Bi(AAZTA)]$^-$, [Bi(DTPA)]$^{2-}$ and [Bi(DOTA)]$^-$ complexes. Suprisingly, the logK_{BiL}^{cond} values at pH=7.4 and 25°C show that the apparent stability of [Bi(AAZTA-C4-COO$^-$)]$^{2-}$ is higher than those of [Bi(AAZTA)]$^-$ and [Bi(DTPA)]$^{2-}$ by 2.1 and 0.2 log units. Furthermore, favorable thermodynamic property of [Bi(AAZTA-C4-COO-)]$^{2-}$ is maintained for the [Bi(AAZTA-C4-TATE)]$^-$ conjugate, which is characterised by about 1 log unit higher apparent stability constant than that of [Bi(AAZTA)]$^-$ and it is being similar to that of [Bi(DTPA)]$^{2-}$. The higher apparent stability constant of [Bi(AAZTA-C4-COO-)]$^{2-}$ and [Bi(AAZTA-C4-TATE)]$^-$ with respect to [Bi(AAZTA)]$^-$ might be interpreted by the higher basicity of the ring N donor atoms (Table IV.1.1) causing the higher affinity of AAZTA-C4-COO$^-$ and AAZTA-C4-TATE to Bi(III) ion. The lack of the interaction between the Bi(III) ion and the *n*-valeric acid residue of the AAZTA-C4-COO$^-$ is confirmed by the similar protonation constant of the distant carboxylate group of the free ligand and the Bi(III) complex (the protonation constant of the *n*-valeric acid residue of the AAZTA-C4-COOH free ligand and its Bi(III) complex are shown in Table IV.1.1 and Table IV.3.1.1). The similarity in the

apparent stability constant of the $[Bi(AAZTA-C4-COO-)]^{2-}$, $[Bi(AAZTA-C4-TATE)]^{-}$ and $[Bi(DTPA)]^{2-}$ complexes is rather surprising, by considering the lower denticity of AAZTA in a respect to DTPA (7 *vs* 8). On the other hand, the $\log K_{BiL}^{cond}$ values in Table IV.3.1.1 indicate that $[Bi(DOTA)]^{-}$ has slightly higher apparent stability constant, which can be interpreted by the stronger interaction between the ring N donor atoms ofmacrocycle and Bi(III) as well as the better size match between the preformed cage of the DOTA ligand and Bi(III) ion.

IV.3.2 Transchelation reactions of $[Bi(AAZTA)]^{-}$, $[Bi(AAZTA-C4-COO-)]^{2-}$, $[Bi(AAZTA-C4-TATE)]^{2-}$ and $[Bi(DTPA)]^{2-}$

Based on the results of the equilibrium studies, $[Bi(AAZTA)]^{-}$, $[Bi(AAZTA-C4-COO^{-})]^{2-}$ and $[Bi(AAZTA-C4-TATE)]^{-}$ are characterized by high thermodynamic stability (Table IV.3.1.1.) which support their applications as suitable alternative of $[^{212/213}Bi][Bi(DOTA)]^{-}$ and $[^{212/213}Bi][Bi(DOTP)]^{5-}$ in TAT. However, the targeted application requires the kinetic inertness of $[Bi(AAZTA)]^{-}$ and its derivatives. To obtain information about the kinetic inertness, the transchelation reactions of the, $[Bi(AAZTA)]^{-}$, $[Bi(AAZTA-C4-COO^{-})]^{2-}$, $[Bi(AAZTA-C4-TATE)]^{-}$ and $[Bi(DTPA)]^{2-}$ the transchelation reactions were studied in the presence of a large exchanging ligands excess in order to ensure the pseudo-first order rate conditions. Transchelation reactions of Bi(III) complexes with DTPA or DOTP (Eq. (IV.3.2.1)) were monitored by UV-spectrophotometry at 278 and 308 nm in the pH range 8.0 – 11.0. (25 °C, 0.15 M NaClO₄).

$$BiA + L \rightleftharpoons BiA + L \qquad \qquad \textit{IV.3.2.1}$$
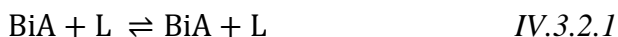
where A=DTPA, AAZTA-C4-COOH and AAZTA, L=DOTP or DTPA. Some absorption spectra are shown in Figure IV.3.2.1, IV.3.2.2. and IV.3.2.3.
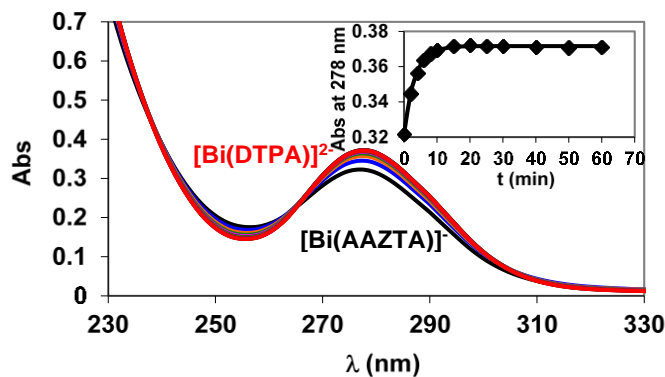

Figure IV.3.2.1 Absorption spectra and absorbance values of [Bi(AAZTA)]⁻ - DTPA reacting system ([Bi(AAZTA)]=0.1 mM, [DTPA]=1.0 mM, pH=10.5; 0.15 M NaClO₄, 25 °C).
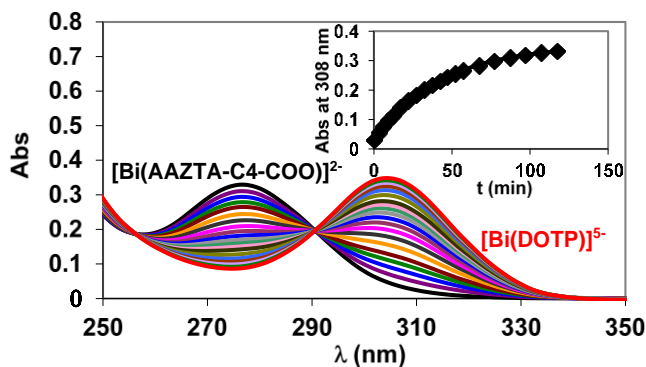
Figure IV.3.2.2 Absorption spectra and absorbance values of [Bi(AAZTA-C4-COO-)]²⁻ - DOTP , [Bi(AAZTA-C4-COO-)]=0.05 mM, [DOTP]=1.0 mM, pH=11.0; 0.15 M NaClO₄, 25 °C, l=1 cm).
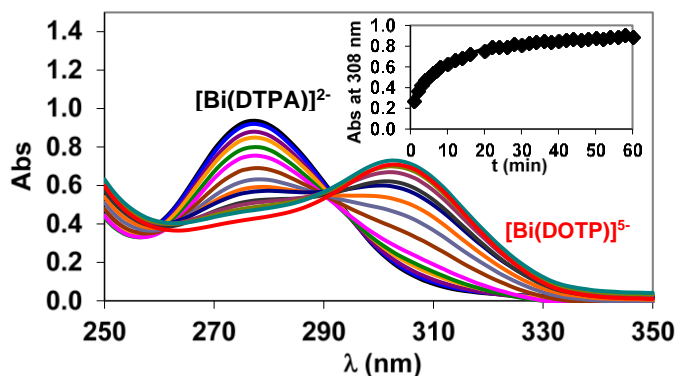
Figure. **IV.3.2.4** Absorption spectra and absorbance values of [Bi(DTPA)]$^{2-}$ - DOTP reacting system ([Bi(DTPA)]=0.1 mM, [DOTP]=2.0 mM, pH=10.8, 0.15 M NaClO$_4$, 25°C)

In the presence of large DTPA and DOTP excess, the transchelation can be accounted as a pseudo-first order process and the rate of reactions can be expressed by the Eq. IV.2.6.2, where k_d is a pseudo-first order rate constant and [BiL]$_{tot}$ is the total concentration of [Bi(AAZTA)]$^-$, [Bi(AAZTA-C4-COO$^-$)]$^{2-}$ or [Bi(DTPA)]$^{2-}$. The obtained pseudo-first order rate constants k_d in [Bi(AAZTA)]$^-$ - DTPA, [Bi(AAZTA-C4-COO$^-$)]$^{2-}$ - DOTP and [Bi(DTPA)]$^{2-}$ - DOTP reacting systems are presented as a function of pH and [OH$^-$] in Figure IV.3.2.5, left and right.
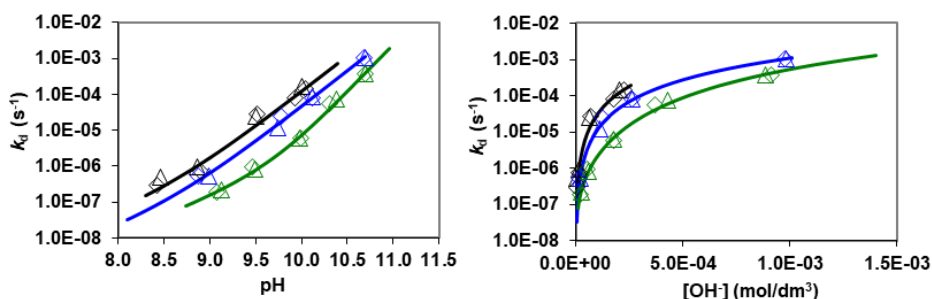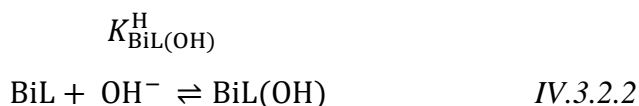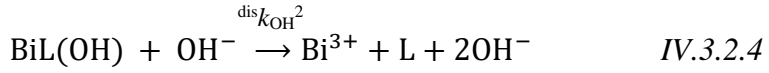

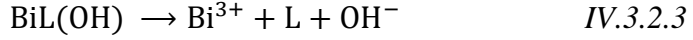**Figure IV.3.2.5** Pseudo-first order rate constant k_d characterizing the transchelation reactions in **[Bi(AAZTA)]$^-$ - DTPA**, **[Bi(DTPA)]$^{2-}$ - DOTP** and **[Bi(AAZTA-C4-COO$^-$)]$^{2-}$ - DOTP** systems. Solid lines and the symbols represent the calculated and measured k_d rate constants. ([Bi(AAZTA)]= 0.1 mM, [DTPA]=1.0 mM ($\Diamond$) and 2.0 mM ($\triangle$); [Bi(DTPA)]$^{2-}$= 0.1 mM, [DOTP]=2.0 mM ($\Diamond$) and 4.0 mM ($\triangle$); [Bi(AAZTA-C4-COO$^-$)]$^{2-}$= 0.05 mM, [DOTP]=1.0 mM ($\Diamond$) and 2.0 mM ($\triangle$), [NMP]=0.01 M, 0.15 M NaClO$_4$, 25 °C).

The pseudo-first order rate constants (k_d) plotted in Figure IV.3.2.5 indicate that the k_d values are independent of [DTPA] and [DOTP]. The rates increase with pH and [OH$^-$], confirming that the rate-determining step of the transchelation reactions is the dissociation of the [Bi(AAZTA)]$^-$, [Bi(AAZTA-C4-COO$^-$)]$^{2-}$ and [Bi(DTPA)]$^{2-}$ complexes, followed by the fast reaction between the free Bi(III) ion and the exchanging DTPA or DOTP ligands. The dependence of the k_d values on pH and [OH$^-$] can be interpreted by the formation ($K^H_{BiL(OH)}$ Eq. IV.3.2.2.) and the spontaneous dissociation of the [Bi(L)(OH)] species ($^{dis}k_{OH}$ Eq. IV.3.2.3). Moreover, the dissociation of the [Bi(L)(OH)] species might take place by OH$^-$ assisted pathway, which is characterized with $^{dis}k_{OH}^2$ rate constant (Eq. IV.3.2.4). According to the X-ray structure of [Bi(HAAZTA)(H$_2$O)] and [Bi(AAZTA)]$^-$ (see in section VII) the Bi(III) ion is coordinated by 3 amino-N and four carboxylate-O$^-$ donor atoms of AAZTA ligand, whereas the apical coordination site is occupied by H$_2$O molecule to complete the dodecahedron coordination environment around the Bi(III) ion. Based on the X-ray diffraction data of [Bi(H$_2$DTPA)], the Bi(III) ion is coordinated by 3 amino-N and 5 carboxylate-O donor atoms in a square antiprism geometry.[143] The [Bi(L)(OH)] species might be formed by the replacement of the inner-sphere water molecule with the OH$^-$ ion in [Bi(AAZTA)(H$_2$O)]$^-$ or following the substitution of the weakly coordinated -COO$^-$ group by the OH$^-$ ion in [Bi(DTPA)]$^{2-}$.

$$K^H_{BiL(OH)}$$

$$BiL + OH^- \rightleftharpoons BiL(OH) \qquad\qquad IV.3.2.2$$

$$K^H_{BiL(OH)} = \frac{[BiL(OH)]}{[BiL][OH^-]}$$

$$^{dis}k_{OH}$$

102

$$BiL(OH) \longrightarrow Bi^{3+} + L + OH^- \qquad\qquad IV.3.2.3$$

$$BiL(OH) + OH^- \overset{^{dis}k_{OH}2}{\longrightarrow} Bi^{3+} + L + 2OH^- \qquad IV.3.2.4$$

By taking into account all possible pathways and Eq. IV.2.6.2, the rate of the dissociation of [Bi(AAZTA-C4-COO$^-$)]$^{2-}$, [Bi(AAZTA)]$^-$ and [Bi(DTPA)]$^{2-}$ can be expressed by Eq. IV.3.2.5.

$$-\frac{d[BiL]_t}{dt} = k_d[BiL]_t = {}^{dis}k_{OH}[BiL(OH)\,] + {}^{dis}k_{OH^2}[BiL(OH)\,][OH^-]$$

$$IV.3.2.5$$

Considering the total concentration of the [Bi(AAZTA)]$^-$, [Bi(AAZTA-C4-COO$^-$)]$^{2-}$ and [Bi(DTPA)]$^{2-}$ complexes ([BiL]$_{tot}$=[BiL]+[BiL(OH)]) and the formation constant of [Bi(L)(OH)] species ($K^H_{BiL(OH)}$, Eq. IV.3.2.2), the k_d pseudo-first order rate constants presented can be expressed by Eq.IV.3.2.6

$$k_d = \frac{{}^{dis}k_1[OH^-] + {}^{dis}k_2[OH^-]^2}{1 + K_{BiL(OH)}[OH^-]} \qquad\qquad IV.3.2.6$$

wherein $K^H_{BiL(OH)}$, ${}^{dis}k_1 = {}^{dis}k_{OH} \times K^H_{BiL(OH)}$ and ${}^{dis}k_2 = {}^{dis}k_{OH}{}^2 \times K^H_{BiL(OH)}$ are the equilibrium and rate constants characterizing the formation, the spontaneous and OH$^-$-assisted dissociation of [Bi(AAZTA)(OH)]$^{2-}$ and [Bi(DTPA)(OH)]$^{3-}$ species, respectively. The formation constant ($K^H_{BiL(OH)}$) of [Bi(L)(OH)] species for Bi(DOTA)-like complexes are relatively small ($K^H_{BiL(OH} = 478$). However, the formation of [Bi(L)(OH)] species could not be detected under basic conditions in the pH-potentiometric studies of [Bi(AAZTA)]$^-$ and [Bi(DTPA)]$^{2-}$ complexes.

Considering the very low protonation constant of [Bi(L)(OH)]⁻ species ($K^H_{BiL(OH)} = 478$) and the pH range of the kinetic studies (pH=8.5 – 11), the denominator of Eq. (V.3.2.6) ($1 \gg K^H_{BiL(OH)}$ [OH⁻]) can be neglected, so Eq. IV.3.2.6 can be simplified in the form of Eq. IV.3.2.7. The $^{dis}k_1$ and $^{dis}k_2$ values have been calculated by fitting of the kinetic data to Eq. IV.3.2.7.

$$k_d = {}^{dis}k_1[OH^-] + {}^{dis}k_2[OH^-]^2 \qquad\qquad IV.3.2.7$$

In Eq. IV.3.2.7 $^{dis}k_1$ and $^{dis}k_2$ are the rate constants characterizing the formation, the spontaneous and OH⁻-assisted dissociation of the [Bi(AAZTA)(OH)]²⁻ and [Bi(DTPA)(OH)]³⁻ species have been calculated by fitting the k_d values presented in Figure IV.3.2.5 to the Eq. IV.3.2.6. The $^{diss}k_1$ and $^{diss}k_2$ rate and K^H_{BiLH-1} formation constants characterizing the formation and the dissociation of [Bi(L)(OH)] species of [Bi(AAZTA)]⁻, [Bi(AAZTA-C4-COO⁻)]²⁻, [Bi(DTPA)]²⁻ and [Bi(DOTA)]⁻ are shown in Table IV.3.2.1.

The inertness of [Bi(AAZTA-C4-TATE)]⁻ had been investigated by following the transchelation reactions between [Bi(AAZTA-C4-TATE)]⁻ complex and AAZTA (Eq. IV.3.2.1) with CZE at pH=9.0 and 25 °C in the presence of 20 and 40 fold AAZTA excess used in order to guarantee the pseudo-first order kinetic condition. For keeping the pH values constant 0.01 M N-methyl-piperazine (NMP) buffer was used (signal of NMP in the electropherograms was also used as an internal standard for the calibration of the migration times and injections). The temperature was maintained at 25 °C and the ionic strength of the solutions was kept constant, 0.15 M for NaClO₄. The CZE electropherograms of the [Bi(AAZTA-C4-TATE)]⁻ – AAZTA reacting systems are shown in Figure IV.3.2.6. The signals of free

AAZTA and [Bi(AAZTA)]⁻ are not observable in CZE electropherograms. Area$_{Bi(AA-TATE)}$ / Area$_{NMP}$ values of the [Bi(AAZTA-C4-TATE)]⁻ complex as a function of time in [Bi(AAZTA-C4-TATE)]⁻ – AAZTA reacting systems are shown in Figure IV.3.2.7.
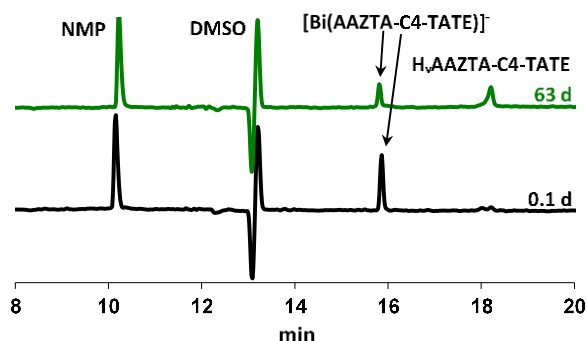
$$[Bi(AAZTA\_C4\_TATE)]^- + H_xAAZTA \rightleftharpoons [Bi(AAZTA)]^- + H_xAAZTA\_C4\_TATE$$
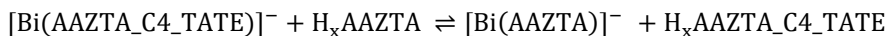
IV.3.2.8

Figure IV.3.2.6 CZE electropherograms of [Bi(AAZTA-C4-TATE)]⁻ – AAZTA reacting system (Samples: [Bi(AAZTA-C4-TATE)]=50.1 μM, [AAZTA]= 1.0 mM, [NMP]=0.01 M, pH=9.0, 0.15 M NaClO₄, Conditions: 20 kV, 50 mbars, λ=200 nm; 150 mM Na₂HPO₄, pH=7.4, 10 °C)
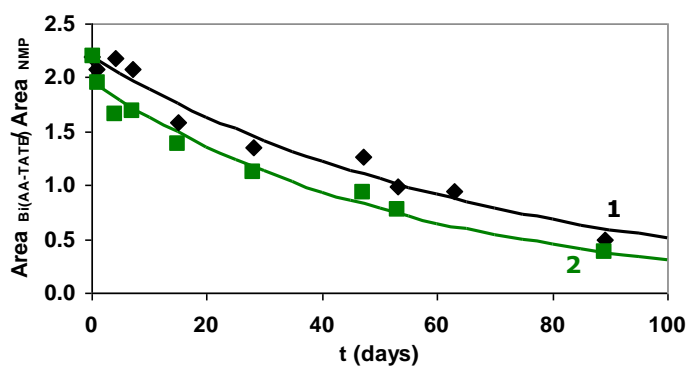
Figure IV.3.2.7 Area$_{Bi(AA-TATE)}$ / Area$_{NMP}$ values of the [Bi(AZTA-C4-TATE)]⁻ – AAZTA reacting system as a function of time (**1:** [Bi(AAZTA-C4-TATE)]=50.1 μM, [AAZTA]= 1.0 mM; **2:** [Bi(AAZTA-C4-TATE)]=50.1 μM, [AAZTA]= 2.0 mM; [NMP]=0.01 M, pH=9.0, 25 °C 0.15 M NaClO₄).

The rates of the ligand exchange reactions were studied at different concentrations of the AAZTA in order to obtain the information for the effect of [AAZTA] for the rate of the reaction (Eq. (III.5.1)). The pseudo-first order rate constant (k_d) characterizing the transchelation reactions between [Bi(AAZTA-C4-TATE)]$^-$ and AAZTA obtained in the presence of 20 and 40 fold excess of AAZTA are $(1.7\pm0.1)\times10^{-7}$ s^{-1} and $(2.0\pm0.2)\times10^{-7}$ s^{-1}, respectively ([Bi(AAZTA-C4-TATE)]=50.1 μM, pH=9.0, [NMP]=0.01 M, 25 °C, 0.15 M NaClO$_4$). These kinetic data clearly indicates that [AAZTA] has practically no effect for the dissociation rate of [Bi(AAZTA-C4-TATE)]$^-$ as it was found for [Bi(AAZTA)]$^-$, [Bi(AAZTA-C4-COO$^-$)]$^{2-}$ and [Bi(DTPA)]$^{2-}$. According to these experimental evidences, it can be assumed that the rate determining step is the OH$^-$-assisted dissociation of [Bi(AAZTA-C4-TATE)]$^-$ complex which is followed by the fast reaction between the free Bi(III) ion and the exchanging AAZTA ligand. The dissociation rate and the half-life of the complexes are shown in Table IV.3.2.1.

Table IV.3.2.1 Rate ($^{diss}k_i$ and k_d) and equilibrium constants (K^H_{BiLH-1}) and dissociation half-life values ($t_{1/2}$=ln2/k_d) characterizing the dissociation reactions of [Bi(AAZTA)]$^-$ (**A**) [Bi(AAZTA-C4-COO$^-$)]$^{2-}$ (**B**), [Bi(AAZTA-C4-TATE)]$^-$ (**C**), [Bi(DTPA)]$^{2-}$ (**D**) and [Bi(DOTA)]$^-$ (**E**) complexes (0.15 M NaClO$_4$, 25 °C)

	A	B$^-$	C	D	E [a]
$^{diss}k_1$ (M^{-1}s^{-1})	(2.5 ± 1.0) $\times10^{-2}$	(7 ± 1) $\times10^{-3}$	–	(1.0 ± 0.2) $\times10^{-2}$	(1.0 ± 0.2) $\times10^{-9}$
$^{diss}k_2$ (M^{-2}s^{-1})	(2.8 ± 0.7) $\times10^{3}$	86 ± 30	–	(1.2 ± 0.1) $\times10^{3}$	–
K^H_{BiLH-1} (M^{-1})	–	338 ± 100	–	–	473 ± 100
k_d (s^{-1}) $t_{1/2}$ (d) at pH=7.4	1.3×10^{-8} **601**	3.2×10^{-9} **2507**	–	5.3×10^{-9} **1500**	3.4×10^{-13} **2.4×10^7**
k_d (s^{-1}) $t_{1/2}$ (d) at pH=9.0	1.6×10^{-7} **50.4**	1.7×10^{-6} **4.8**	1.8×10^{-7} **43.4**	6.4×10^{-7} **12.6**	1.3×10^{-11} **6.1×10^5**

Comparison of the kinetic parameters in Table IV.3.2.1 reveals that both the spontaneous ($^{diss}k_1$) and OH⁻-assisted ($^{diss}k_2$) dissociation of [Bi(AAZTA)H$_{-1}$]$^{2-}$ are faster by about two times than the related dissociation processes of [Bi(DTPA)(OH)]$^{3-}$ species. However, the $^{diss}k_1$ and $^{diss}k_2$ values of [Bi(AAZTA-C4-COO⁻)(OH)]$^{3-}$ are about 2 – 4 and 14 – 32 times lower than the corresponding rate constants of [Bi(AAZTA)(OH)]$^{2-}$ and [Bi(DTPA)(OH)]$^{3-}$ species. Considering the stability constants of Bi(III) complexes, it can be assumed that the interaction of AAZTA-C4-COO⁻ with Bi(III) ion is higher than that of AAZTA ligand, which might explain the slower dissociation of [Bi(AAZTA-C4-COO⁻)]$^{2-}$ ([Bi(AAZTA)]⁻: log K_{BiL}=26.45, [Bi(AAZTA-C4-COO⁻)]$^{2-}$: log K_{BiL} = 28.75, from Table IV.2.3.1). Nevertheless, the Bi(III) affinity of the DTPA is similar to that of AAZTA-C4-COO⁻, whereas the OH⁻ catalysed dissociation of [Bi(DTPA)]$^{2-}$ is faster than that of [Bi(AAZTA-C4-COO⁻)]$^{2-}$ ([Bi(DTPA)]$^{2-}$: log K_{BiL} = 29.29)[142]. It is generally accepted that the spontaneous dissociation of the [Bi(L)(OH)] species likely occur by the simultaneous decoordination of the donor atoms followed by the release of the Bi(III) ion. It is reasonable to assume that the higher rigidity of semi-macrocyclic AAZTA-C4-COO⁻ results the slower dissociation of the [Bi(AAZTA-C4-COO⁻)(OH)]$^{2-}$ species than that of the [Bi(DTPA)(OH)] formed with the flexible DTPA ligand. This assumption has been further evidenced by the slower spontaneous dissociation of [Bi(DOTA)(OH)]$^{2-}$ in which the Bi(III) ion is tightly coordinated by the rigid DOTA ligand ([Bi(DOTA)]⁻: log K_{BiL}=30.86, 0.15 M NaClO$_4$, 25 °C).

Considering the k_d values of [Bi(AAZTA-C4-TATE)]⁻, [Bi(AAZTA-C4-COO⁻)]$^{2-}$, [Bi(AAZTA)]⁻ and [Bi(DTPA)]$^{2-}$ calculated at pH=9 indicates

that the kinetic inertness of [Bi(AAZTA-C4-TATE)]- is similar to that of [Bi(AAZTA-C4-COO-)]$^{2-}$ and higher by about 9 and 3.4 times than that of [Bi(AAZTA)]- and [Bi(DTPA)]$^{2-}$ complexes.

IV.3.3 NMR studies of [Bi(AAZTA)]- and [Bi(AAZTA-C4-COO-)]$^{2-}$ complexes

Variable temperature (VT) multinuclear 1D and 2D NMR studies of [Bi(AAZTA)]- and [Bi(AAZTA-C4-COO-)]$^{2-}$ have been performed to investigate the solution structure in D_2O. VT-^{1}H and VT-^{13}C spectra of [Bi(AAZTA)]- and [Bi(AAZTA-C4-COO-)]$^{2-}$ obtained in the temperature range 273 - 333 K are shown in Figures A.10, A.11, A.12 and A.13 respectively. ^{1}H and ^{13}C NMR resonances of [Bi(AAZTA)]- and [Bi(AAZTA-C4-COO-)]$^{2-}$ were assigned on the basis of COSY (Figures A.14 and A.17), HSQC and HMBC spectra (Figures A.15, A.16, A.18 and A.19) obtained at 273K.

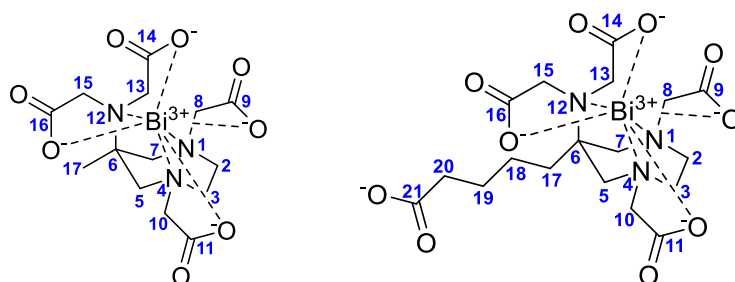**Figure IV.3.3.1** Structure and numbering of [Bi(AAZTA)]- and [Bi(AAZTA-C4-COO-)]$^{2-}$.

There is a single set of signals in the ^{1}H and ^{13}C NMR spectra of [Bi(AAZTA)]- and Bi(AAZTA-C4-COO-)]$^{2-}$ which is practically unchanged in the temperature range 273–333 K. The ^{13}C NMR spectra contain eight and twelve signals corresponding to 2:2:2 equally intense

methylene and carboxylate carbon atoms of pendant arms and the ring, and 1:1 methyl and quaternary C of [Bi(AAZTA)]$^-$ and 1:1:1:1:1:1 quaternary C, methylene and carboxylate of the n-valeric acid pendant of Bi(AAZTA-C4-COO$^-$)]$^{2-}$ confirming that Bi(III) complexes has C$_s$ symmetry in the investigated temperature range. Surprisingly, the ^{1}H NMR signals of the exocyclic carboxylate methylene protons in [Bi(AAZTA)]$^-$ and [Bi(AAZTA-C4-COO$^-$)]$^{2-}$ are singlet and AB system (13 and 15 in Figures A10 and A12), indicating a higher structural rigidity of [Bi(AAZTA-C4-COO$^-$)]$^{2-}$ in a respect to the parent [Bi(AAZTA)]$^-$.

IV.3.4 X-Ray Diffraction studies of the [Bi(HAAZTA)] and [Bi(AAZTA)]$^-$ complexes

The single crystals of the [Bi(AAZTA)] complex in two different protonation states, *i.e.*: [Bi(*H*AAZTA)(H$_2$O)]·3H$_2$O and {[C(NH$_2$)$_3$][Bi(AAZTA)]}·3.5H$_2$O, allowing a deeper insight into the structural properties of these systems. A simplified view of the protonated [Bi(*H*AAZTA)(H$_2$O)] and the nonprotonated [Bi(AAZTA)]$^-$ complexes found in the [Bi(*H*AAZTA)(H$_2$O)]·3H$_2$O and {[C(NH$_2$)$_3$][Bi(AAZTA)]}·3.5H$_2$O crystals is shown in Figures IV.3.4.1, A.21 and A.22. The bond distances of the Bi(III) coordination environment are summerized and compared with those of Sc(III) and Er(III) ions in [Sc(AAZTA)]$^-$ and [Er(AAZTA)]$^-$ complexes in Table A.22.

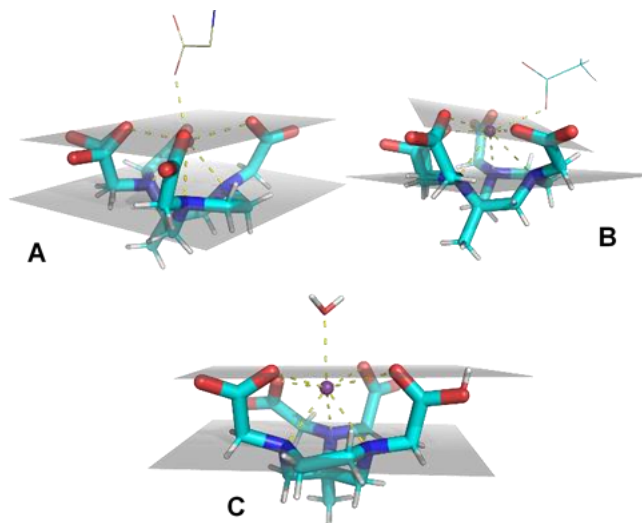**Figure IV.3.4.1** Stick representation of the Bi(III) coordination environment in [Bi(AAZTA)]⁻ (A and B) and [Bi(*H*AAZTA)(H₂O)] complexes found in the single crystals of [Bi(*H*AAZTA)(H₂O)]·3H₂O and {[C(NH₂)₃][Bi(AAZTA)]}·3.5H₂O.

Two crystallographically independent [Bi(AAZTA)]⁻ complexes are placed in the asymmetric unit of {[C(NH₂)₃][Bi(AAZTA)]}·3.5H₂O (Figure A.21 A). In both complexes of [Bi(AAZTA)]⁻, Bi(III) is octacoordinated by 7 donor atoms of the AAZTA ligand (four carboxylate O and three amino N donor atoms), whereas the eighth coordination site is occupied by a carboxylate bridging two neighbour metal centers, as previously reported for [Gd(AAZTA)]⁻. In the single crystals with the formula [Bi(*H*AAZTA)(H₂O)]}·3.H₂O [Bi(*H*AAZTA)] complex is placed in the crystallographic asymmetric unit (Figure.A.21 B). The [Bi(*H*AAZTA)] complex form dimers with units related to the crystallographic inversion centers and linked by hydrogen bonds between one protonated and one deprotonated carboxylate groups ($d_{OH\cdots O}$ = 2.508(5) Å, Figure.A.21 B). The structures of [Bi(AAZTA)]⁻ and [Bi(*H*AAZTA)(H₂O)] are comparable with those of [Er(AAZTA)(H₂O)]⁻ and of and [Sc(AAZTA)(H₂O)]⁻ [135],[136]. The coordination

110

polyhedrons around the Bi(III) ion can be described by an irregular dodecahedron defined by a 1:4:3 stack (top to bottom in Figure IV.3.4.1) of the apical ligand (H_2O molecule in [Bi(HAAZTA)(H_2O)] (Figure IV.3.4.1 C) or a carboxylate in [Bi(AAZTA)]⁻ (Figure IV.3.4.1 A)) and of two nearly parallel pseudo-planes (7.53(10)° offset in [Bi(HAAZTA)(H_2O)] (Figure IV.3.4.1 C) and 8.98(53)° in [Bi(AAZTA)]⁻ (Figure IV.3.4.1 A)): the first one involving O1, O3, O5, and O7 (mean deviation from planarity is 0.13(2) Å in [Bi(HAAZTA)(H_2O)]⁻ and 0.13(6) Å in [Bi(AAZTA)]⁻ and the second one by N1, N2, and N3 (Figures IV.3.4.1 A and C). In Figure IV.3.4.1 B, the Bi(III) ion has a somewhat different coordination environment with the apical group 0.633(1) Å far from the O1, O3, O5, and O7 average plane (while is ~2.1 Å in the other cases). Angle ofthe planes formed by the oxygen and nitrogen atoms remains similar (6.42(49)° - mean deviation from planarity is 0.34(25) Å; Figure IV.3.4.1 B). In the [Sc(AAZTA)(H_2O)]⁻ and [Er(AAZTA)(H_2O)]⁻ complexes, the angle betweenthe two nearly parallel planes formed by the carboxylate O and the amino N donor atoms are 8.0° and 8.3°,[144], [145] which is comparable with that of [Bi(*H*AAZTA)(H_2O)] (Figure IV.3.4.1 C) and [Bi(AAZTA)]⁻ (Figure IV.3.4.1 A). The distances between the Bi(III) ion and the coordinated N and O atoms of AAZTA fall within the range 2.25-2.75 Å and 2.21-2.72 Å, with nearly indentical average 2.515(4) Å and 2.501(6) Å values, respectively. The bond lengths of Er(III) and Sc(III) ions with the carboxylate O and amine N donor atoms of AAZTA ligand ([Er(AAZTA)]⁻: Er(III)-O=2.25-2.34 Å, Er(III)-N=2.47-2.57 Å; [Sc(AAZTA)]⁻: Sc(III)-O=2.12-2.25 Å, Sc(III)-N=2.41-2.47 Å) is comparable with that [Bi(AAZTA)]⁻ (Table A.22). Nevertheless, the distance of the innert sphere water molecule from the Bi(III) ion in

[Bi(HAAZTA)(H$_2$O)] is longer (Bi(III)-OH$_2$=2.605 Å, Table A.22) than in [Sc(AAZTA)(H$_2$O)]$^-$ and [Er(AAZTA)(H$_2$O)]$^-$ (Er(III)-OH$_2$=2.344 Å, Sc(III)-OH$_2$=2.247 Å, Table A.22), which is in line with the "softer" character or by the stereochemical activity of the $6s^2$ lone pair of the Bi(III) ion.[134]

IV.3.5 Labeling of AAZTA-C4-TATE and DOTA-TATE with $^{205/206}$Bi isotope, in vitro and *ex vivo* studies of [$^{205/206}$Bi][Bi(AAZTA-C4-TATE)]$^-$

To investigate the efficiency of [$^{212/213}$Bi][Bi(AAZTA-C4-TATE)]$^-$ as possible TAT agent, the effect of temperature, pH and ligand concentration on the labeling of AAZTA-C4-TATE and DOTA-TATE with $^{205/206}$Bi(III) isotope have been examined and compered. The labeling efficiency of AAZTA-C4-TATE and DOTA-TATE with $^{205/206}$Bi(III) has been studied by using 5 min reaction time at 25 and 95 °C in the presence of [AAZTA-C4-TATE] = [DOTA-TATE] 0.1 µM – 30 µM in the pH range 3 – 7 (Figure IV.3.5.1. and IV.3.5.2).
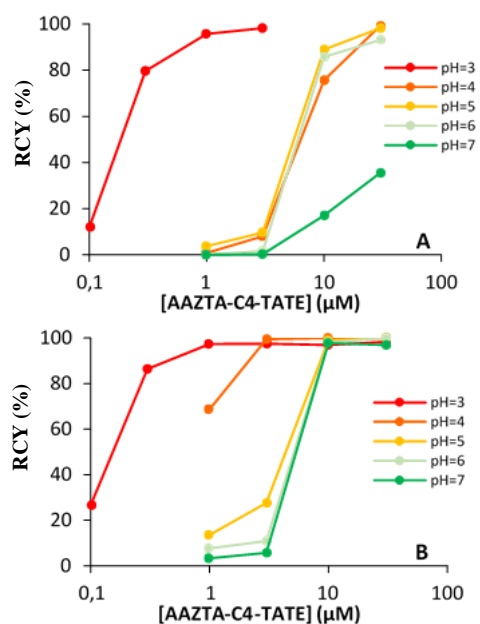
Figure IV.3.5.1 Labeling yield of AAZTA-C4-TATE with [205/206]Bi(III) as a function of [AAZTA-C4-TATE] at 25°C (**A**) and 95°C (**B**) in 5 min reaction time.
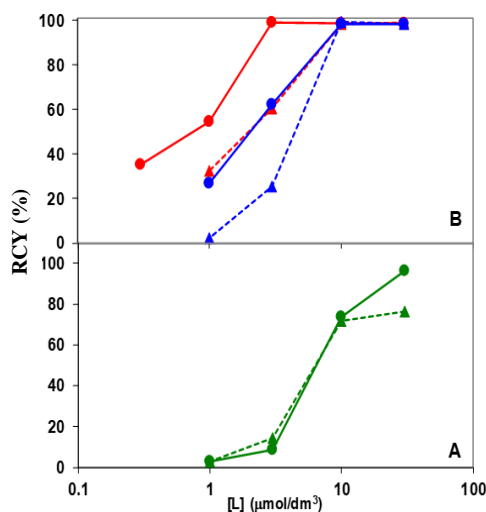
Figure IV.3.5.2 Labeling yield of AAZTA-C4-TATE (●, ●, ●) and DOTA-TATE (▲, ▲, ▲) with [205/206]Bi as a function of [AAZTA-C4-TATE] and [DOTA-TATE] at pH=**7** and 25°C (**A**), pH=**3** and **4**, 95°C (**B**) in 5 min reaction time.

HEPES and ammonium-acetate were applied as buffers at pH=3 and 7 and in the pH range of 4 - 6, respectively. The labeling efficiency has

been characterized by the radiochemical yield (RCY) defined as follows (equation IV.3.5.1):

$$RCY = \frac{ractivity\ of\ the\ indicated\ substance}{activity\ used\ for\ labeling} * 100 \qquad IV.3.5.1$$

The RCY values for both $^{205/206}$Bi(III) complexes increases with the decreasing pH. Temperature has practically no effect on the radiochemical yield at pH =3, 5 and 6 in the tempereature range of 298-368 K. However, the RCY values are siginificantly increased with the increase of the ligand concentration at pH= 4 and 7. On the other hand, the radiochemical yields of [$^{205/206}$Bi][Bi(DOTA-TATE)]⁻ increase at high temperatures. The comparison of the labeling efficiency of AAZTA-TATE and DOTA-TATE indicates that the incorporation of $^{205/206}$Bi takes place with higher yields at pH = 3 and 4 (95°C), and at pH = 7 at room temperature (Figure IV.3.5.2). The optimal labeling conditions of AAZTA-C4-TATE with $^{205/206}$Bi(III) isotopes by using 5 min reaction time (RCY>95 %) was found at pH=3, 25°C and 95°C in the presence of 1 µM of ligand. The highest labeling yield for DOTA-TATE with $^{205/206}$Bi(III) isotopes (RCY>95 %) was found at pH = 6 (95°C), [DOTA-TATE] = 30 mM, 0.1 M acetate buffer, 15 min reaction time.

The stability of [$^{205/206}$Bi][Bi(AAZTA-C4-TATE)]⁻ has been investigated in the presence of DTPA excess, in PBS and in human plasma. [$^{205/206}$Bi][Bi(AAZTA-C4-TATE)]⁻ was incubated up to 21 h at pH=7.4 and room temperature in 0.01 M DTPA solution and PBS buffer, as well as at 37°C in human plasma (Figure A.25). The unchanged radiochemical purity (RCP) values definited by the IV.3.5.2 equation confirm the stability of [$^{205/206}$Bi][Bi(AAZTA-C4-TATE)]⁻ in the examined period of time.

$$RCP = \frac{activity\ of\ the\ indicated\ substance}{total\ activity\ of\ the\ sample} * 100 \qquad IV.3.5.2$$

Outstanding results of the equilibrium, kinetic and labeling studies led us to assess the *in vitro* and *ex vivo* properties of $[^{205/206}Bi][Bi(AAZTA-C4-TATE)]^-$. The biodistribution of $[^{205/206}Bi][Bi(AAZTA-C4-TATE)]^-$ has been examined in healthy (control) and AR42J tumor-bearing mice. In the *ex vivo* biodistribution studies AR42J tumor-bearing SCID mice were sacrificed 15, 60 and 90 min (n=3 mice/time point) after intravenous injection of 1.18±0.2 MBq $[^{205/206}Bi][Bi(AAZTA-C4-TATE)]^-$ and the residual radioactivity of the organs and tissues were evaulated by gamma counter measurements after autopsy. Remarkable radiotracer accumulation was found in kidneys (approx. %ID/g: 8-16) and urine (approx. %ID/g: 160-300), and significantly lower uptake (p≤0.05) of the radiotracer was observed at each time point investigated in other healthy organs and tissues. The amount of the radiotracer (%ID/g) decreased monotnounusly from 15 to 90 minutes in each investigated organs (Figure IV.3.5.3).

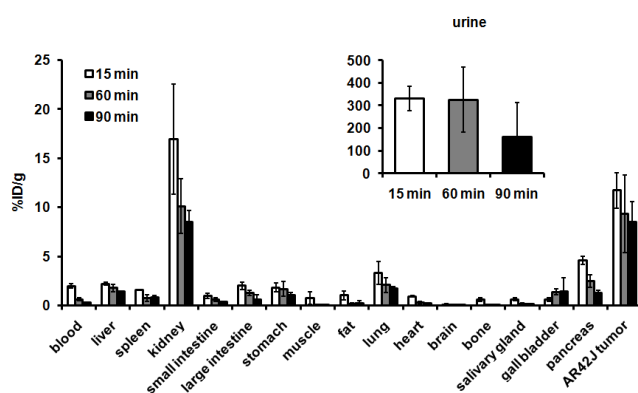**Figure IV.3.5.3** *Ex vivo* biodistribution of $[^{205/206}Bi][Bi(AAZTA-C4-TATE)^-$ in AR42J somatostatin receptor positive tumor-bearing CB17 SCID mice 15, 60 and 90 min after intravenous injection of the radiotracer. %ID/g values are presented as mean±SD.

The high %ID/g values (11.7±1.82 at 15 min, 9.32 ± 3.96 at 60 min, and 8.53 ± 2.02 at 90 min) of the AR42J tumour indicated a remarkable somatostatine receptor specificity of the [$^{205/206}$Bi][Bi(AAZTA-C4-TATE)]$^-$ radiotracer, which has been also confirmed by the accumulation of the [$^{205/206}$Bi][Bi(AAZTA-C4-TATE)]$^-$ in the somatostatin receptor positive AR42J cells (Figure A.26).

The cellular uptake of the two somatostatin specific radiotracers, indicates that the accumulation of [$^{205/206}$Bi][Bi(AAZTA-C4-TATE)]$^-$ in AR42J cells is somewhat higher (29.76±10.84 %ID/10^6 cells at 30 min; 22.99±3.16 %ID/10^6 cells at 60 min) than that of [$^{205/206}$Bi][Bi(DOTA-TATE)]$^-$ (22.25±3.78 %ID/10^6 cells at 30 min; 19.10±6.53 %ID/10^6 cells at 60 min) after 30 and 60 min incubation time (Figure A.26). The *in vitro* data supports that [$^{205/206}$Bi][Bi(AAZTA-C4-TATE)]$^-$ binds with higher affinity to somatostatin receptor positive cells than [$^{205/206}$Bi][Bi(DOTA-TATE)]$^-$ in 30 and 60 minute time points.

The *ex vivo* biodistribution of the free $^{205/206}$Bi(III) radiotracer (Figure IV.3.5.3), which might be present due to the demetallation of the $^{205/206}$Bi(III) complexes, shows high radioactivity in the liver, spleen, and kidneys, and moderate uptake by the lungs and gall bladder after 30 and 90 min incubation time. In contrary, the [$^{205/206}$Bi][Bi(AAZTA-C4-TATE)]$^-$ was accumulated only in the AR42J tumour and kidneys owing to its high stability and rapid excretion through the urinary system (Figure IV.3.5.4).
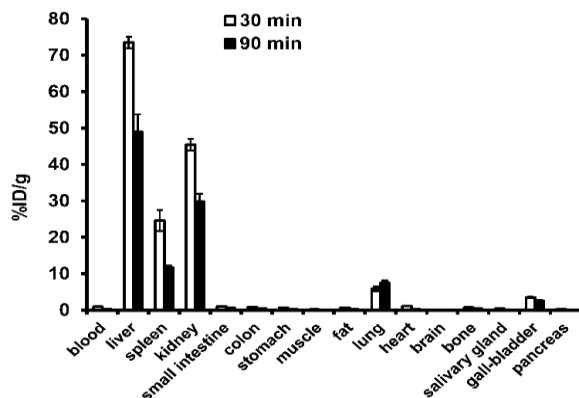
Figure IV.3.5.4 Assessment of *ex vivo* biodistribution studies of [205/206]Bi(III). Data values shown as means ± SD. ID%/g: Tracer accumulation in gram tissue as the percentage of the incubating dose.

In order to estimate the efficacy of [[213]Bi][Bi](AAZTA-C4-TATE)] as a possible TAT agent of neuroendocrine tumours, the relative accumulated dose (%ID/g) obtained at 15, 60 and 90 min for [[205/206]Bi][Bi(AAZTA-C4-TATE)] and 10 and 60 min for [[213]Bi][Bi(DOTA-TATE)] in rat pancreatic AR42J tumour-bearing Athymic male nu/nu mice[65] have been compared in Table IV.3.5.1. Such a biodistribution data allows for the comparison of the *in vivo* behaviour of the radiotracer (i.e. efficacy) even it has obtained with different isotopes of Bi(III) ion, since the decay of [205/206]Bi or [213]Bi isotopes has practically no effect on the relative distribution of the [Bi(AAZTA-C4-TATE)] and [Bi(DOTA-TATE)] complexes in different organs.

Table IV.3.5.1 Accumulated dose (%ID/g) obtained at 15, 60 and 90 min for $[^{205/206}Bi][Bi(AAZTA-C4-TATE)]^-$ and 10 and 60 min for $[^{213}Bi][Bi(DOTA-TATE)]^-$ in tumour and other organs.

	t (m)	Tumour	Pancreas	Stomach	Kidney	Liver	Blood
$[^{205/206}Bi][Bi(AAZTA-C4-TATE)]^-$	15	11.7	4.59	1.82	16.7	2.19	1.98
	60	**9.32**	**2.49**	**1.68**	**10.1**	**1.79**	**0.62**
	90	8.53	1.27	1.08	8.52	1.45	0.33
$[^{213}Bi][Bi(DOTA-TATE)]^{-[a]}$	10	5.3	4.0[b]	3.0[b]	18[b]	n.a.	9.0[b]
	60	**6.5**	**2.5[b]**	**2.0[b]**	**17.4**	**2.0[b]**	**1.5[b]**

[a]Ref. [65]; [b] Estimated values based on Fig. 2 in Ref. [65]

The comparison of the relative abundance (%ID/g) of $[^{205/206}Bi][Bi(AAZTA-C4-TATE)]^-$ and $[^{213}Bi][Bi(DOTA-TATE)]^-$ at 60 min after the administration of the radiotracers indicates that the relative tumour accumulation of $[^{205/206}Bi][Bi(AAZTA-C4-TATE)]^-$ is 1.5 times higher than that of $[^{213}Bi][Bi(DOTA-TATE)]^-$, which might be explained by the higher somatostatin receptor affinity of $[^{205/206}Bi][Bi(AAZTA-C4-TATE)]^-$ than that of $[^{213}Bi][Bi(DOTA-TATE)]^-$. Moreover, significantly lower %ID/g values of kidneys and blood suggest the faster clearance of $[^{205/206}Bi][Bi(AAZTA-C4-TATE)]^-$ as compared to that of $[^{213}Bi][Bi(DOTA-TATE)]^-$.

Based on the larger tumour accumulation of $[^{205/206}Bi][Bi(AAZTA-C4-TATE)]^-$ (Table IV.3.5.1), the expected tumour dose of $[^{213}Bi][Bi(AAZTA-C4-TATE)]^-$ is significantly higher than that of

118

[^{213}Bi][Bi(DOTA-TATE)]$^-$, predicting the higher efficacy of [^{213}Bi][Bi(AAZTA-C4-TATE)]$^-$ in a TAT of neuroendocrine tumours. Furthermore, the faster urinary excretion of [$^{205/206}$Bi][Bi(AAZTA-C4-TATE)]$^-$ indicates a reduced kidney toxicity of [^{213}Bi][Bi (AAZTA-C4-TATE)]$^-$ as compared to that of [^{213}Bi][Bi(DOTA-TATE)]$^-$.

V. Summary

In this work, we have investigated the equilibrium, formation and dissociation kinetics and structural characteristics of Bi(III) complexes formed with macrocyclic, cyclic and open-chain ligands. These studies are mainly related to the improvement of our knowledge in the coordination chemistry of the Bi(III) complexes. However, the results can also be useful for the development of $^{212/213}$Bi(III) based radiopharmaceuticals for Targeted Alpha Therapy (TAT). The new scientific achievements can be summarized as follows:

1. **We determined the stability constants of [Bi(DOTA)]⁻ (log K_{BiL} = 30.86 (7)) and [Bi(DOTP)]⁵⁻ (log K_{BiL} = 38.67(2))** using the competition method using NTA as a competitor ligand. Comparing the stability of [Bi(DOTA)]⁻ and [Bi(DOTP)]⁵⁻ complexes with those of the other trivalent metal ions (e.g.: In(III), Fe(III)) reveals that the stabilities of Bi(III) complexes are larger, which can be interpreted by the stronger interaction between the "soft" Bi(III) ion and N donor atoms of the ring.

2. The rate constants for the formation of [Bi(DOTA)]- and [Bi(DOTP)]⁵⁻ complexes were determined both in the presence and absence of citrate as an auxiliary ligand that prevents the hydrolysis of Bi(III) ion. In the case of **[Bi(DOTP)]⁵⁻, the rate of complex formation was found to be very fast** and the reaction can be followed by conventional photometry at 0°C only. The formation rate of [Bi(DOTP)]⁵⁻ is more than ten times higher that of [Bi(DOTA)]⁻ under identical conditions. In the case of both Bi(III) complexes, diprotonated intermediates *[Bi(H_2DOTA)]⁺ and *[Bi(H_2DOTP)]³⁻ are formed in a fast reaction, in which the Bi(III) ion is located outside of the coordination cavity and coordinated by the pendant arms, while the two opposite macrocyclic ring nitrogen atoms

remain protonated. The significant difference between the formation rates of the two Bi(III) complexes can be interpreted by the significantly higher stability of the diprotonated *[Bi(H_2DOTP)]$^{3-}$ intermediates ($\log K_{Bi(H2DOTA)}$) = 11.6 (3), $\log K_{Bi(H2DOTP)}$ = 21.8 (1)) resulted in the faster formation of [Bi(DOTP)]$^{5-}$. In the presence of the citrate ion, the formation rate of [Bi(DOTP)]$^{5-}$ decreases with the increase of the citrate concentration due to the formation of the [Bi(Cit)] and [Bi(Cit)$_2$]$^{3-}$ complexes, thereby lowering the concentration of kinetically active *[Bi(H_2DOTP)]$^{3-}$ intermediate. The presence of the citrate ion accelerated the formation of the [Bi(DOTA)]$^-$ almost ten times due to the formation of a *[Bi(H_2DOTA)(Cit)]$^{2-}$ intermediate.

3. The [Bi(DOTA)] and [Bi(DOTP)]$^{5-}$ complexes are characterized by high kinetic inertness in both acidic and alkaline media. **The half-lives of dissociation for [Bi(DOTA)]$^-$ at pH= 3 $t_{1/2}$ = 3.1 ×10^3 h while at pH= 11 $t_{1/2}$ = 2.5 ×10^5 h. For [Bi(DOTP)]$^{5-}$ at pH= 3 a half-life values of $t_{1/2}$ = 4.8 ×10^4 h was calculated. The dissociation of [Bi(DOTP)]$^{5-}$ can not be evidenced at pH= 11 even after weeks.**

4. The labeling efficiency of DOTA ligand with ^{213}Bi isotope have been examined in a collaboration with Prof. J. Notni in Technical University of Munich. **The labeling efficiency of DOTA ligand with ^{213}Bi isotope was found to improve by about** 3-4% **in the presence of** 100 μM DOTA and 0.1-10 μM **citrate at pH=5.0.** Interestingly, the presence of acetate buffer slowed down the labeling of the DOTA ligand with ^{213}Bi isotope under the same conditions.

5. Based on the results of the 1D and 2D multinuclear NMR studies, **the structure of the** [Bi(DOTP)]$^{5-}$ **complex in solution can be described by a twisted square antiprism (TSA). The activation parameters**

characterize the ring inversion of the $[Bi(DOTP)]^{5-}$ complex are $\Delta H^{\ddagger} = 64 \pm 1$ kJ·mol^{-1} , $\Delta S^{\ddagger} = -14 \pm 2$ J·mol^{-1}K^{-1} , $\Delta G^{\ddagger}_{298} = 68$ kJ·mol^{-1}. The obtained activation enthalpy and entropy values are higher than those of $[Bi(DOTA)]^{-}$, which **can be interpreted by the stronger interaction between the Bi(III) ion and the ring nitrogen atoms**.

6. **We have determined the stability and apparent stability constants of the $[Bi(AAZTA)]^{-}$, $[Bi(AAZTA-C4-COO^{-})]^{2-}$ and $[Bi(AAZTA-C4-TATE)]^{-}$ complexes** at pH=7.4 and 25°C in 0.15 M NaClO$_4$ solution (**log** $K_{[Bi(AAZTA)]^{-}}$ = **26.45(6); log** $K_{[Bi(AAZTA-C4-COO-)]2-}$ = **28.75(8); log** $K_{[Bi(AAZTA)]^{-}}$^{cond} = **23.5; log** $K_{[Bi(AAZTA-C4-COO-)]2-}$^{cond} = **25.6; log** $K_{[Bi(AAZTA-C4-TATE)]^{-}}$^{cond} = **24.3(2)).**

7. **$[Bi(AAZTA)]^{-}$, $[Bi(AAZTA-C4-COO-)]^{2-}$, $[Bi(AAZTA-C4-TATE)]^{-}$ and $[Bi(DTPA)]^{2-}$ complexes are characterized by high kinetic inertness. The dissociation half-lives of Bi(AAZTA)]$^{-}$, $[Bi(AAZTA-C4-COO-)]^{2-}$, $[Bi(AAZTA-C4-TATE)]^{-}$ and $[Bi(DTPA)]^{2-}$ are 115; 1210; 1042; 302 hours, respectively at pH=9.0 and 25°C.**

8. ^{1}H and ^{13}C NMR spectra of $[Bi(AAZTA)]^{-}$ and $[Bi(AAZTA-C4-COO^{-})]^{2-}$ contain a single set of signals those half with remain practically constant in the temperature range 273–333 K. **Bi(III) complexes are characterized by C$_s$ symmetry in the entire temperature range.** Interestingly, the ^{1}H NMR signal of the exocyclic carboxylate methylene protons in $[Bi(AAZTA)]^{-}$ is a siglet whereas in $[Bi(AAZTA-C4-COO^{-})]^{2-}$ an AB pattern was observed, revealing a higher structural rigidity of $[Bi(AAZTA-C4-COO^{-})]^{2-}$ with respect to the parent $[Bi(AAZTA)]^{-}$.

9. X-ray diffraction studies of the single crystals with formula **[Bi(HAAZTA)(H$_2$O)]·3H$_2$O and {[C(NH$_2$)$_3$][Bi(AAZTA)]}·3.5H$_2$O**

reveals that **the coordination polyhedron around the Bi(III) ion can be best described by an irregular dodecahedron defined by a 1:4:3 stack with the apical ligand (H_2O molecule in [Bi(HAAZTA)(H_2O)] and a carboxylate oxygen in [Bi(AAZTA)]⁻, respectively).**

10.   In cooperation with Scanomed Ltd. and Department of Nuclear Medicine, University of Debrecen we performed labeling of the AAZTA-C4-TATE and DOTA-TATE ligands with the [205/206]Bi isotope. **Optimal labeling conditions (RCY>95%) for AAZTA-C4-TATE are pH=3 at 25°C and 95°C and 1 µM ligand concentration and 5 min reaction time, while for DOTA-TATE pH=6 at 95° C 30 µM ligand concentration and 15 min reaction time.** Based on the given results, the AAZTA-C4-TATE conjugate can be considered as a better platform than DOTA-TATE as far as labeling with [205/206]Bi isotope is concerned. The [[205/206]Bi][Bi(AAZTAC4-TATE)] was stable for at least 21 hours at pH=7.4 at room temperature in the presence of 0.01M DTPA solution, PBS buffer and at 37°C in human serum.

11.   In collaboration with Scanomed Ltd. and Department of Nuclear Medicine, University of Debrecen, we investigated the *in vitro* and *ex vivo* properties of [[205/206]Bi][Bi(AAZTA-C4-TATE)]. Based on the results of the *ex vivo* studies, **the relative tumor uptake of [[205/206]Bi][Bi(AAZTA-C4-TATE)] is 1.5 times higher than that of [[213]Bi][Bi(DOTA-TATE)] as observed in** AR42J tumor-bearing mice**.** *In vitro* data reveal that **[[205/206]Bi][Bi(AAZTA-C4-TATE)]⁻ has a higher somatostatin receptor affinity than [[213]Bi][Bi(DOTA-TATE)]⁻. The significantly lower %ID/g values obtained in kidneys and blood indicate a faster clearance of [[205/206]Bi][Bi(AAZTA-C4-TATE)]⁻; than that of [[213]Bi][Bi(DOTA-TATE)]⁻.**

12. Owing to the higher tumor uptake, the expected tumor dose using[^{213}Bi][Bi(AAZTA-C4-TATE)]$^-$ is higher than with [^{213}Bi][Bi(DOTA-TATE)]$^-$ predicting a higher efficiency of [^{213}Bi][Bi(AAZTA-C4-TATE)]$^-$ in the TAT of neuroendocrine tumours.

VI. Összefoglalás

Munkánk során makrociklusos, makrociklusos valamint nyíltláncú tri- és tetraaza polikarboxilát ligandumok Bi(III)-komplexeinek egyensúlyi, képződés és disszociációs kinetikai, valamint szerkezeti sajátosságait vizsgáltuk. A vizsgálataink főleg alapkutatás jellegűek, de az eredményeink bővíthetik a Bi(III)-komplexekkel kapcsolatos koordinációs kémiai ismereteket, ill. hasznosak lehetnek a célzott alfa terápiában **(TAT)** alkalmazható [212/213]Bi(III)-alapú radiofarmakonok fejlesztésében. Az elért új tudományos eredmények az alábbiak szerint foglalhatók össze:

1. Meghatároztuk a [Bi(DOTA)]$^-$ (log K_{BiL} = 30.86(7)) valamint a [Bi(DOTP)]$^{5-}$ (log K_{BiL} = 38.67(2)) stabilitási állandóját kompetíciós módszerrel NTA ligandumot alkalmazva. A [Bi(DOTP)]$^{5-}$-komplex stabilitási állandója 8 nagyságrenddel nagyobb, mint a [Bi(DOTA)]$^-$-komplexszé, ami a DOTP ligandum lényegesen nagyobb bázicitásával értelmezhető. A DOTA és DOTP ligandumok háromértékű fémionnal (pl: In(III), Fe(III)) alkotott komplexeinek stabilitását összehasonlítva a [Bi(DOTP)]$^{5-}$- és [Bi(DOTA)]$^-$-komplexekével megállapítható, hogy a Bi(III)-komplexek stabilitása lényegesen nagyobb, amely a „soft" Bi(III)-ion és a gyűrű N-atomjai között fellépő erősebb kölcsönhatással értelmezhető.

2. Tanulmányoztuk a [Bi(DOTA)]$^-$ és [Bi(DOTP)]$^{5-}$-komplexek képződési sebességét citrát, mint a Bi(III)-ion hidrolízisét gátló segédligandum jelen és távollétében. A [Bi(DOTP)]$^{5-}$ képződése gyors folyamat, ami konvencionális spektrofotometriával csak kis hőmérsékleten (0°C) követhető a pH=3 – 6 tartományban. A [Bi(DOTP)]$^{5-}$ képződési sebessége egy nagyságrenddel nagyobb a [Bi(DOTA)]$^-$ ra jellemző értéknél azonos körülmények között. A

[Bi(DOTA)]⁻ és [Bi(DOTP)]$^{5-}$ esetében egy kétszeresen protonált köztitermék képződik (*[Bi(H_2L)]), melyben a Bi(III)-ion a koordinációs üregen kívül koordinálódik a funkcióscsoportokhoz, míg a makrociklus két szemközti gyűrű N-atomja protonálva van. A [Bi(DOTP)]$^{5-}$-komplex lényegesen nagyobb képződési sebessége *[Bi(H_2DOTP)]$^{3-}$ köztitermékek nagyobb stabilitásával értelmezhető (log $K_{\text{Bi}(H2DOTA)}$ = 11.6(3), log $K_{\text{Bi}(H2DOTP)}$ = 21.8(1)). Citrátion jelenlétében a [Bi(DOTP)]$^{5-}$ képződési sebessége csökken a citrátion koncentrációjának növekedésével, ami a [Bi(Cit)] és [Bi(Cit)$_2$]$^{3-}$ komplexek képződésével értelmezhető, amelyek csökkentik a katalitikusan aktív részecske koncentrációját. Ugyanakkor a [Bi(DOTA)]⁻ képződését a citrátion jelenléte közel tízszeresére gyorsította, ami a rendszerben képződő *[Bi(H_2DOTA)(Cit)]$^{2-}$ köztitermék képződésével és katalitikus szerepével értelmezhető.

3. A [Bi(DOTA)]⁻- és [Bi(DOTP)]$^{5-}$-komplexek disszociáció kinetikai vizsgálatai alapján mindkét Bi(III)-komplex kinetikailag rendkívül inert savas és lúgos közegben. A Bi(DOTA)]⁻ és [Bi(DOTP)]$^{5-}$-komplexek disszociációjára jellemző felezési idők rendre $t_{1/2}$ = 3.1 ×10^3 és 4.8 ×10^4 óra pH=3,0 és $t_{1/2}$ = 2.5 ×10^5 óra pH= 11,0, 25°C, 0,15 M NaClO$_4$ körülmények között. A [Bi(DOTP)]$^{5-}$ disszociációját lúgos közeben (pH = 11) hetek elteltével sem tudtuk kimutatni.

4. Prof. J. Notni-val (Müncheni Műszaki Egyetem) együttműködve elvégeztük a H$_4$DOTA ligandum ^{213}Bi izotóppal való jelzését citrát, acetát és MES puffer jelenlétében. MES puffer jelenlétében a citrátion koncentrációjának növekedése 0.1-10 µM tartományban 100 µM DOTA koncentráció mellet a jelzési hatásfok 3-4%-os javulását eredményezi.

5. Hőmérsékletfüggő 1D és 2D multinukleáris NMR méréseket alapján a [Bi(DOTP)]$^{5-}$-komplex torzult négyzetes antiprizmás szerkezettel jellemezhető oldatfázisban. A [Bi(DOTP)]$^{5-}$-komplex gyűrű inverzióját $\Delta H^{\ddagger}$= 64 ± 1 kJ·mol^{-1} , $\Delta S^{\ddagger}$= -14± 2 J·mol^{-1}K^{-1} és $\Delta G^{\ddagger}_{298}$=68 kJ·mol^{-1} aktiválási paraméterek jellemzik, amelyek lényegesen nagyobbak, mint a [Bi(DOTA)]$^{-}$-komplexszé a Bi(III)-ion és a gyűrű nitrogénatomok közötti erősebb kölcsönhatás eredményeként.

6. Meghatároztuk a [Bi(AAZTA)]$^{-}$, [Bi(AAZTA-C4-COO^{-})]$^{2-}$, valamint [Bi(AAZTA-C4-TATE)]$^{-}$-komplexek satabilitási és látszólagos stabilitási állandóit (log $K_{[Bi(AAZTA)]-}$= 26.45(6); log $K_{[Bi(AAZTA-C4-COO-)]2-}$ = 28.75(8); log $K_{[Bi(AAZTA)]-}$ ^{cond} = 23.5; log$K_{[Bi(AAZTA-C4-COO-)]2-}$^{cond} = 25.6; log$K_{[Bi(AAZTA-C4-TATE)]-}$^{cond} = 24.3(2), pH=7,4, 25°C, 0,15 M NaClO$_4$).

7. A [Bi(AAZTA)]$^{-}$, [Bi(AAZTA-C4-TATE)]$^{-}$, valamint a [Bi(DTPA)]$^{2-}$-komplexek ligandumcsere reakciói a Bi(III)-komplexek báziskatalizált disszociációjával játszódnak le nagyon lassan. A komplexek disszociációjára jellemző felezési idők rendre 115; 1210; 1042; 302 óránaknak adódtak (pH=9,0, 25°C, 0,15 M NaClO$_4$).

8. A [Bi(AAZTA)]$^{-}$ és [Bi(AAZTA-C4-COO^{-})]$^{2-}$-komplexek ^{1}H és ^{13}C NMR spektrzumában egy jelcsoport található, amelyek intenzitása, félértékszélessége és multiplicitása változatlan 273 – 333 K hőmérséklet tartományban. Mindkét Bi(III)-komplex C_s szimetriával jellemezhető oldatfázisban. A [Bi(AAZTA)]$^{-}$ esetében az exociklusos metiléncsoport protonjainak a ^{1}H NMR jele szingulet, míg és [Bi(AAZTA-C4-COO^{-})]$^{2-}$ esetében AB dublet, ami a [Bi(AAZTA-C4-COO^{-})]$^{2-}$ merevebb szerkezetével értlemzhető.

9. A [Bi(HAAZTA)(H$_2$O)]·3H$_2$O és {[C(NH$_2$)$_3$][Bi-(AAZTA)]}·3.5H$_2$O egykristályok röntgendiffrakciós szerkezetvizsgálatai alapján a Bi(III)-ion koordinációs környezete torzúlt dodekaéderes szerkezettel jellemezhető, amelyben az axiális pozíciót egy vízmolekula ([Bi(HAAZTA)]) vagy egy szomszédos Bi(III)-komplex hídhelyzetű karboxilát O$^-$ donoratomja ([Bi(AAZTA)]$^-$) foglalja el.

10. A Scanomed kft és a Debreceni Egyetem, Nukleáris Medicina tanszékének munkatársaival együttműködve sikeresen jeleztük az AAZTA-C4-TATE és DOTA-TATE ligandumokat $^{205/206}$Bi izotóppal. Az AAZTA-C4-TATE optimális jelzési körülménye (RCY>95%): pH=3, 25°C és 95°C, 1 μM ligandum koncentráció és 5 perces reakció idő. Ezzel szemben a DOTA-TATE esetében hasonló jelzési hatásfok pH=6, 95°C, 30 μM ligandum koncentráció és 15 perces reakcióidő alkalmazásával érhető el. Ennek megfelelően az AAZTA-C4-TATE lényegesen jobb hatásfokkal jelezhető $^{205/206}$Bi izotóppal, mint a DOTA-TATE. A [$^{205/206}$Bi][Bi(AAZTA-C4-TATE)]$^-$ disszociációját pH=7.4-en szobahőmérsékleten 0,01M DTPA oldatában, PBS pufferben, valamint 37°C-on humán szérumban 21 óra elteltével sem tudtuk kimutatni.

11. A Scanomed kft és a Debreceni Egyetem, Nukeláris Medicina tanszékének munkatársaival együttműködve tanulmányoztuk a [$^{205/206}$Bi][Bi(AAZTA-C4-TATE)]$^-$ *in vitro* és *ex vivo* sajátosságait AR42 J sejtvonalon állatmodellekben. Az AR42 J daganatot hordozó egerek esetében a [$^{205/206}$Bi][Bi(AAZTA-C4-TATE)]$^-$ relatív tumorfelvétele közel másfélszerese a [^{213}Bi][Bi(DOTA-TATE)]$^-$ kommplex esetében tapasztalt halmozásnak, ami a [$^{205/206}$Bi][Bi(AAZTA-C4-TATE)]$^-$ nagyobb szomatosztatin receptor

affinitásával értelmezhető. A vesében és a vérben mért lényegesen kissebb %ID/g értékei alapján [$^{205/206}$Bi][Bi(AAZTA-C4-TATE)]⁻ számottevően gyorsabb sebességgel ürül, mint a [^{213}Bi][Bi(DOTA-TATE)]⁻. A [^{213}Bi][Bi(AAZTA-C4-TATE)]⁻ nagyobb szomatosztatin receptor affinitása alapján lényegesen nagyobb tumordózis feltételezhető, mint a [^{213}Bi][Bi(DOTA-TATE)]⁻ esetében. Az *in vitro* és *ex vivo* vizsgálatok alapján a [^{213}Bi][Bi(AAZTA-C4-TATE)]⁻ lényegesen nagyobb hatékonysággal alkalmazható neuroendokrin tumorok célzott alfa terápiás kezelésében, mint a [^{213}Bi][Bi(DOTA-TATE)]⁻.

VII.   Appendix
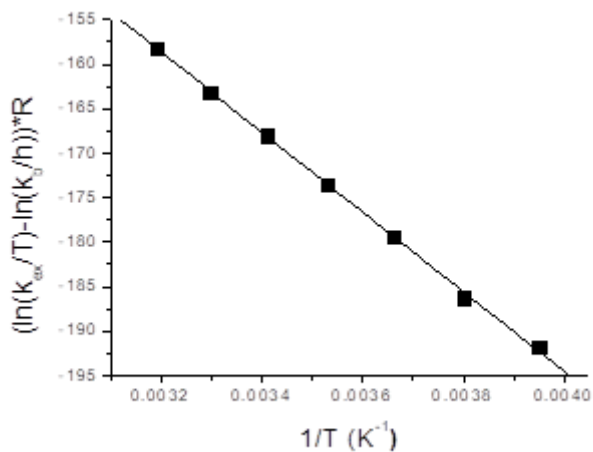
Figure.A.1. *Eyring* plot for determining the activation parameters of the isomerization processes of H_6DOTP species.
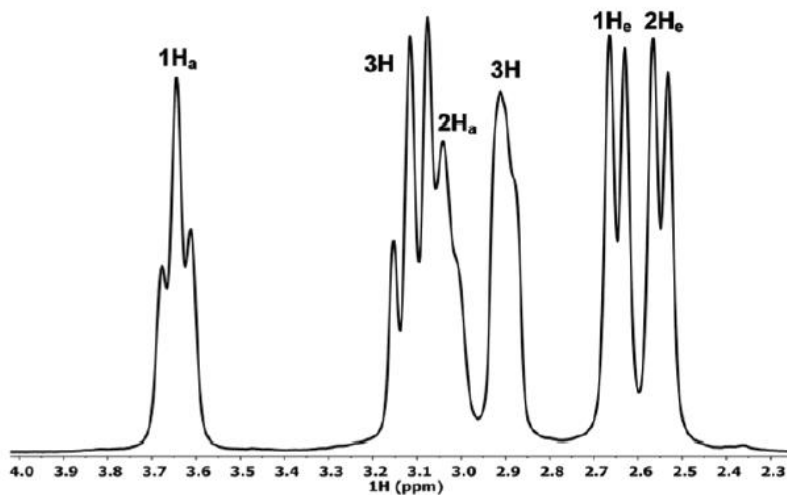
Figure.A.2 ^1H NMR spectra of $[Bi(DOTP)]^{5-}$ at pD=10.0 and 273K ($[BiL]_{tot}$=0.1 M, 400 MHz, D_2O).
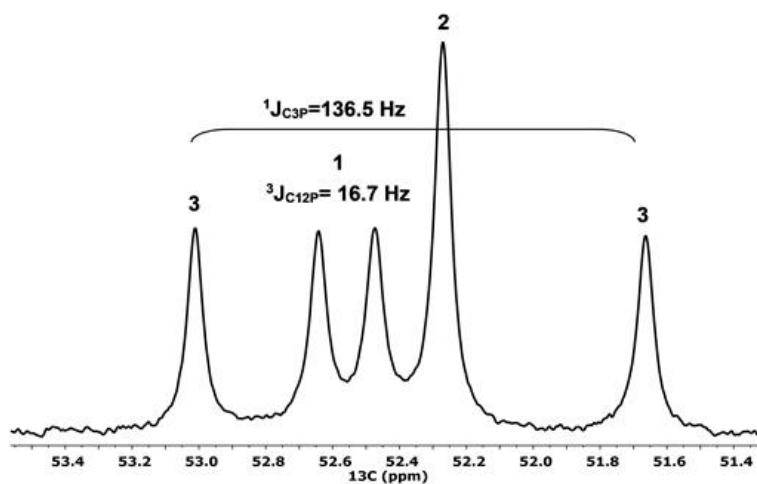
Figure.A.3 100 MHz ^{13}C NMR spectrum of [Bi(DOTP)]$^{5-}$ at pD=10.0 and 273 K ([BiL]$_{tot}$=0.1 M, D$_2$O).
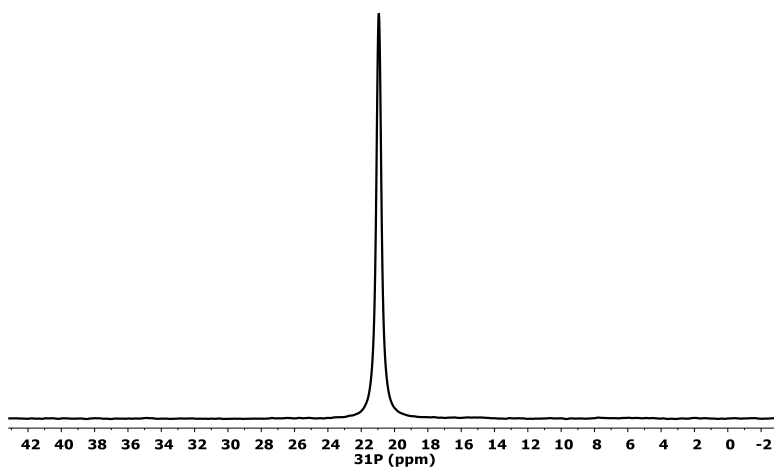
Figure.A.4 162 MHz ^{31}P NMR spectrum of [Bi(DOTP)] at pD=10.0 and 273K ([BiL]$_{tot}$=0.1 M, D$_2$O).
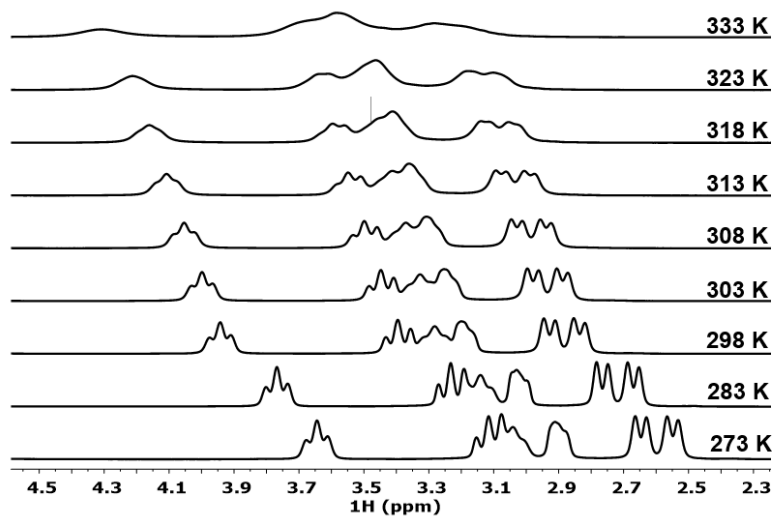
Figure.A.5 VT-^{1}H NMR spectra [Bi(DOTP)]$^{5-}$ in the temperature range 273-333 K ([BiL]$_{tot}$ = 0.1 M, 400 MHz, pD=10.0, D$_2$O).
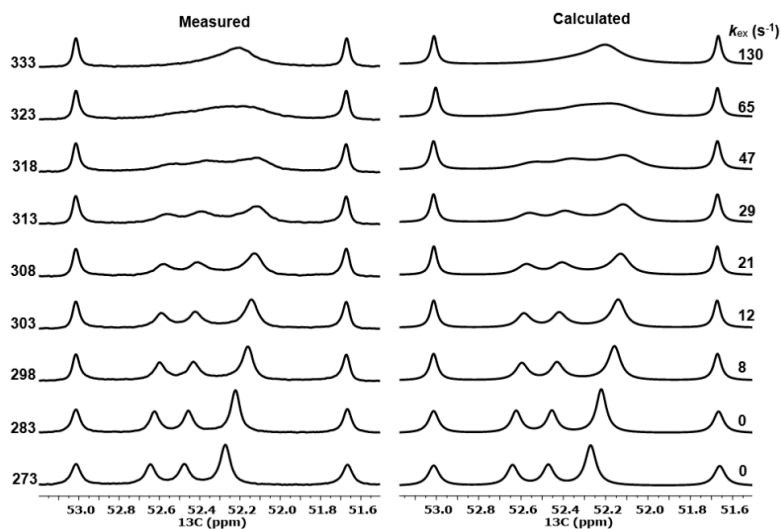
Figure.A.6 Measured and calculated VT-^{13}C NMR spectra of [Bi(DOTP)]$^{5-}$ in the temperature range 273-333 K ([BiL]$_{tot}$ = 0.1 M, 100 MHz, pD=10.0, D$_2$O).

132
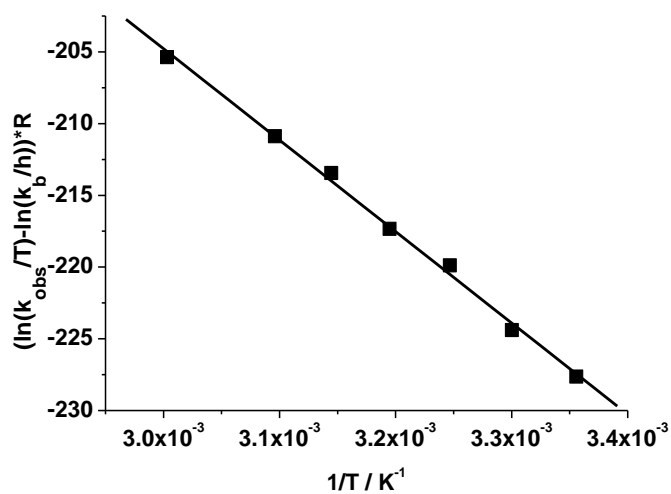
Figure.A.7 *Eyring* plot for determining the activation parameters of the ring inversion processes of [Bi(DOTP)]$^{5-}$.
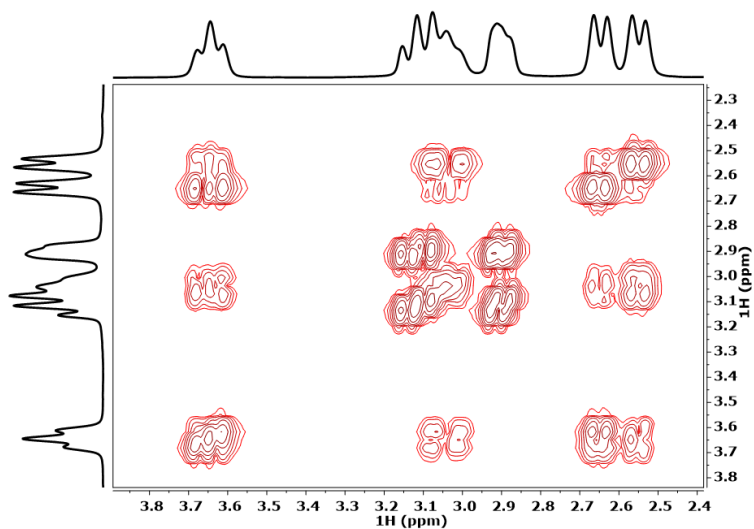
Figure.A.8 ^1H – ^1H COSY spectra of [Bi(DOTP)] at pD=10.0 and 273K ([BiL]$_{tot}$=0.1 M, D$_2$O).
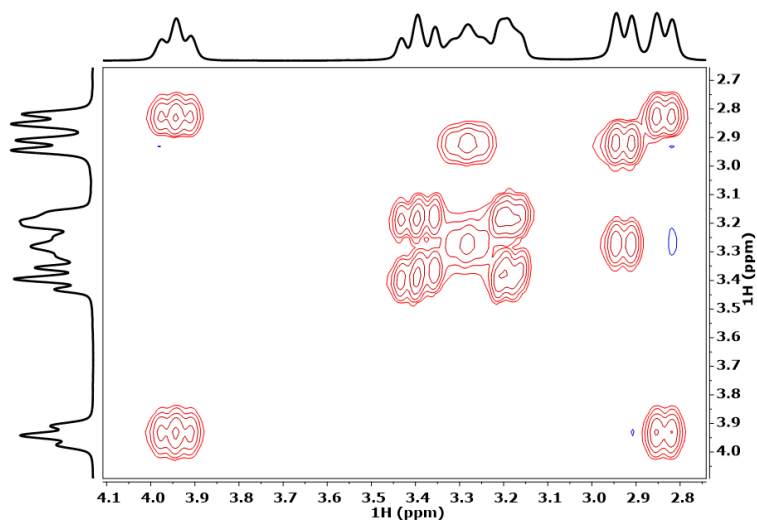
Figure.A.9 ^{1}H – ^{1}H EXSY spectra of [Bi(DOTP)]$^{5-}$ at pD=10.0 and 298 K ([BiL]$_{tot}$=0.1 M, mixing time D8=50 ms, D$_2$O).
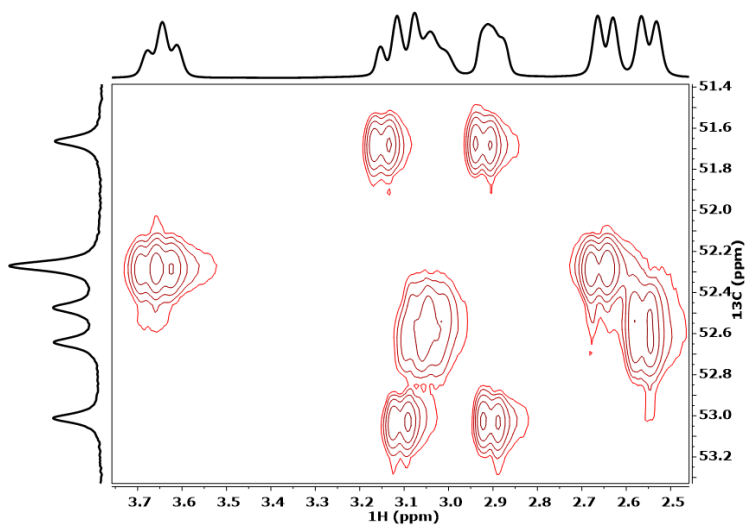
Figure.A.10 ^{1}H – ^{13}C HSQC of Bi(DOTP) at pH=10.0 and 273K ([BiL]$_{tot}$=0.1 M, D$_2$O)
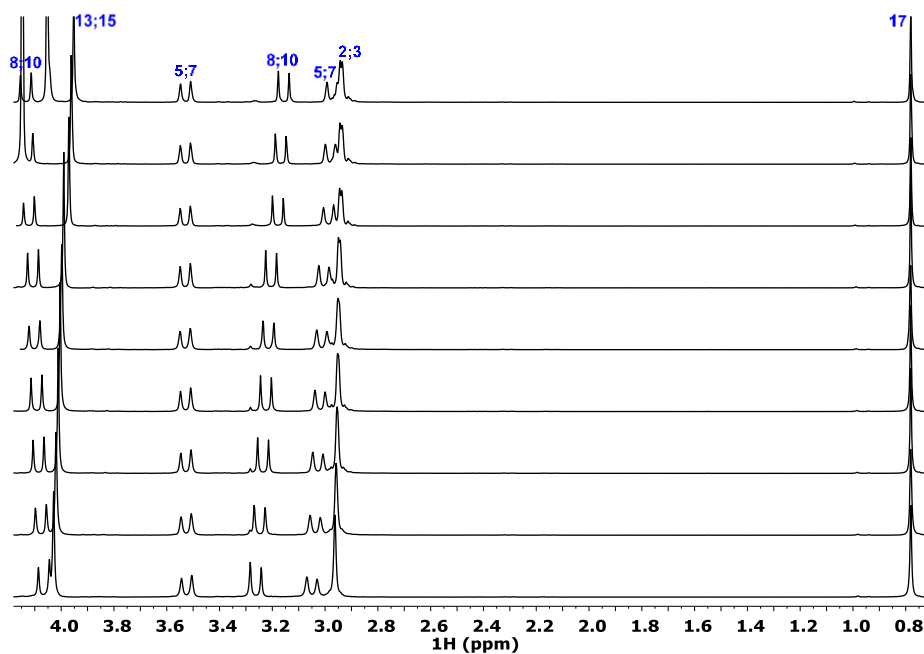
Figure.A.11 VT-^{1}H NMR spectra of [Bi(AAZTA)]$^-$ in the temperature range 273-333 K ([BiL] = 0.01 M, 400 MHz, pD=7.4, D$_2$O).
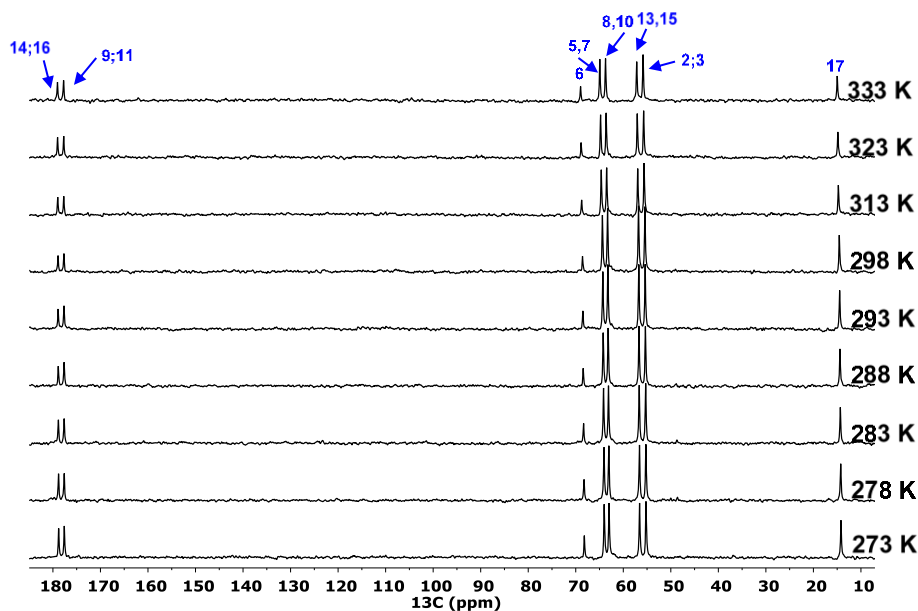
Figure.A.12. VT-^{13}C NMR spectra of [Bi(AAZTA)]$^-$ in the temperature range 273-333 K ([BiL] = 0.01 M, 400 MHz, pD=7.4, D$_2$O).
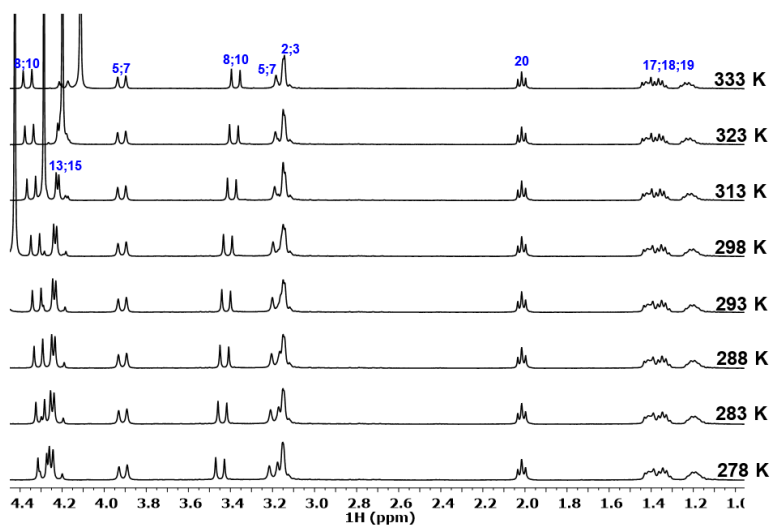
Figure.A.13. VT-^{1}H NMR spectra of [Bi(AAZTA-C4-COO$^-$)]$^{2-}$ in the temperature range 278-333 K ([BiL] = 0.02 M, 400 MHz, pD=7.4, D$_2$O).
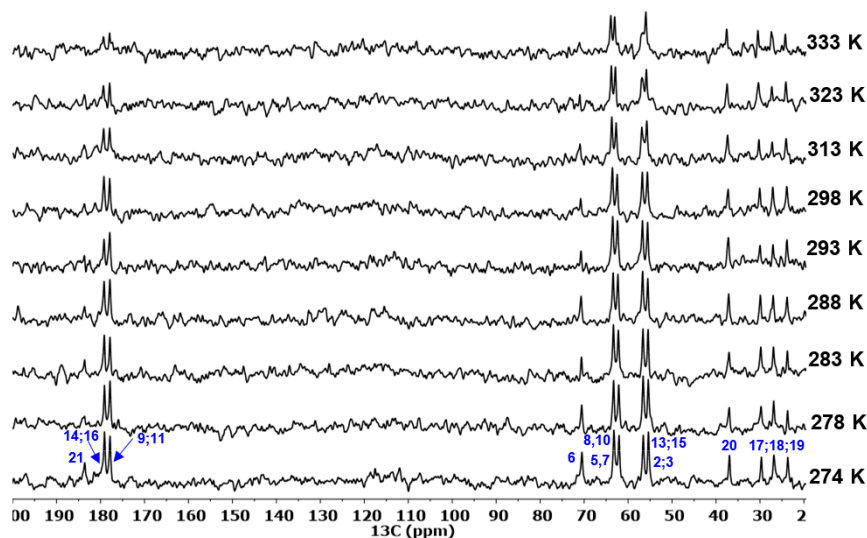
Figure.A.14 VT-^{13}C NMR spectra of [Bi(AAZTA-C4-COO$^-$)]$^{2-}$ in the temperature range 273-333 K ([BiL] = 0.02 M, 400 MHz, pD=7.4, D$_2$O).
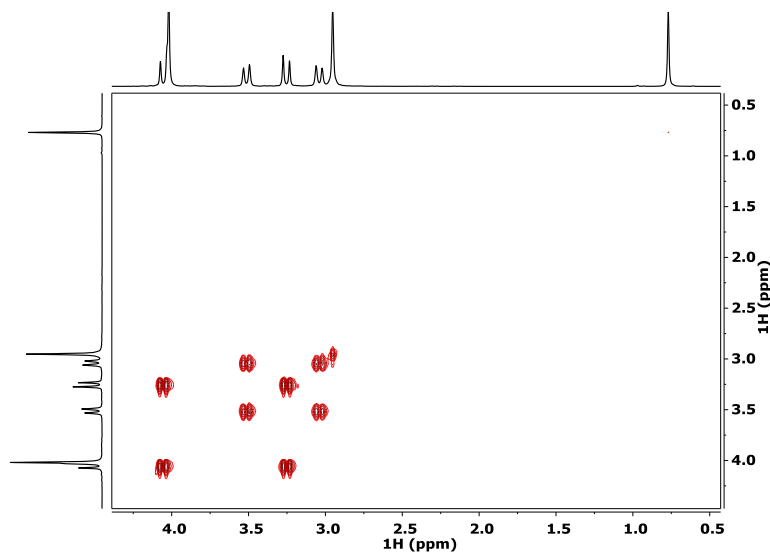
Figure.A.15 ^{1}H – ^{1}H COSY spectra of [Bi(AAZTA)]$^-$ at pD=7.4 and 273K ([BiL]=0.01 M, D$_2$O).
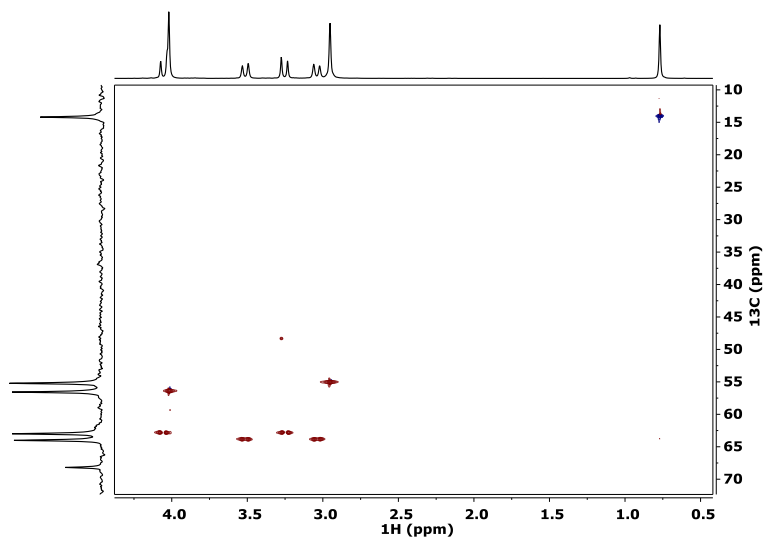
Figure.A.16 ^{1}H – ^{13}C HSQC spectra of [Bi(AAZTA)]$^-$ at pD=7.4 and 273K ([BiL]=0.01 M, D$_2$O).
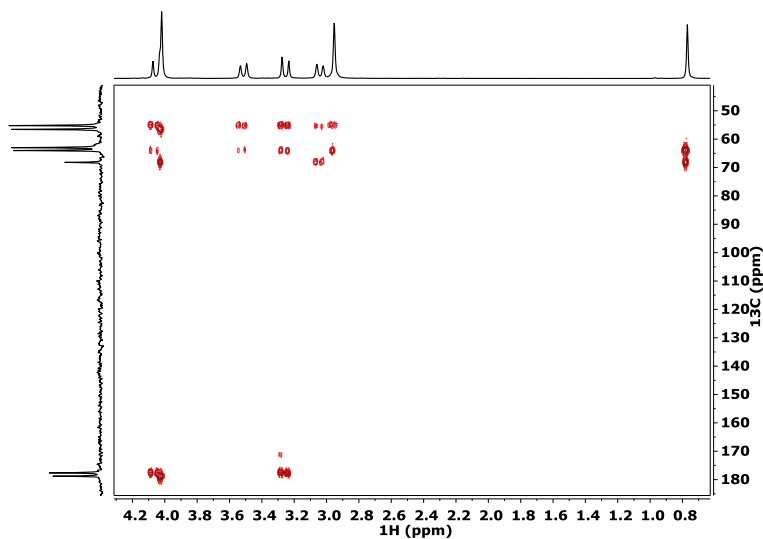
Figure.A.17 ^{1}H – ^{13}C HMBC spectra of [Bi(AAZTA)]$^-$ at pD=7.4 and 273K ([BiL]=0.01 M, D$_2$O).
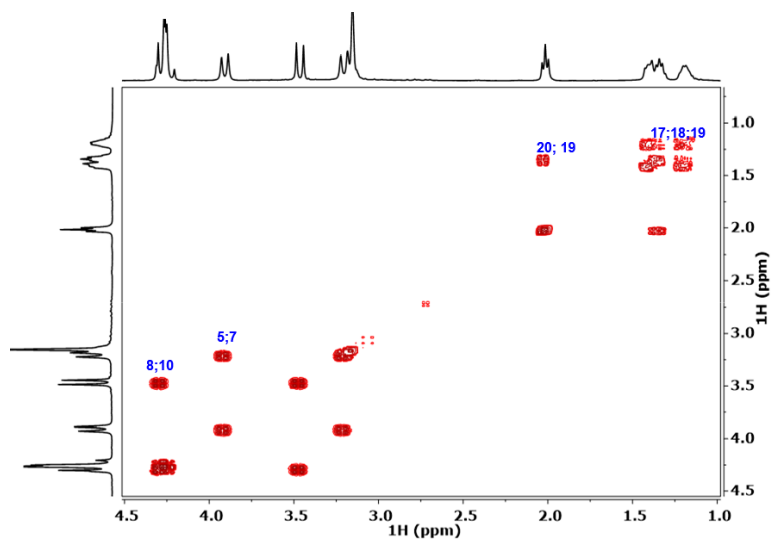
Figure.A.18 ^{1}H – ^{1}H COSY spectra of [Bi(AAZTA-C4-COO$^-$)]$^{2-}$ at pD=7.4 and 273K ([BiL]=0.02 M, D$_2$O).
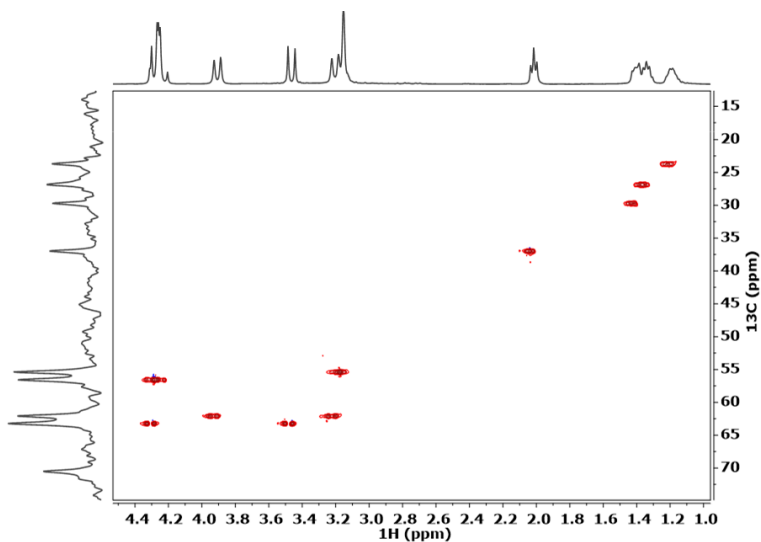
1. Figure.A.19 ^{1}H – ^{13}C HSQC spectra of [Bi(AAZTA-C4-COO$^-$)]$^{2-}$ at pD=7.4 and 273K ([BiL]=0.02 M, D$_2$O).
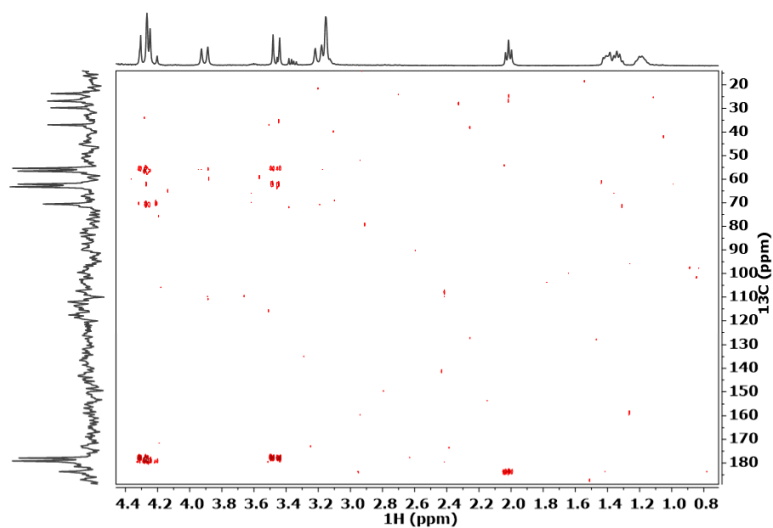
Figure.A.20 ^{1}H – ^{13}C HMBC spectra of [Bi(AAZTA-C4-COO^{-})]$^{2-}$ at pD=7.4 and 273K ([BiL]=0.02 M, D$_2$O).
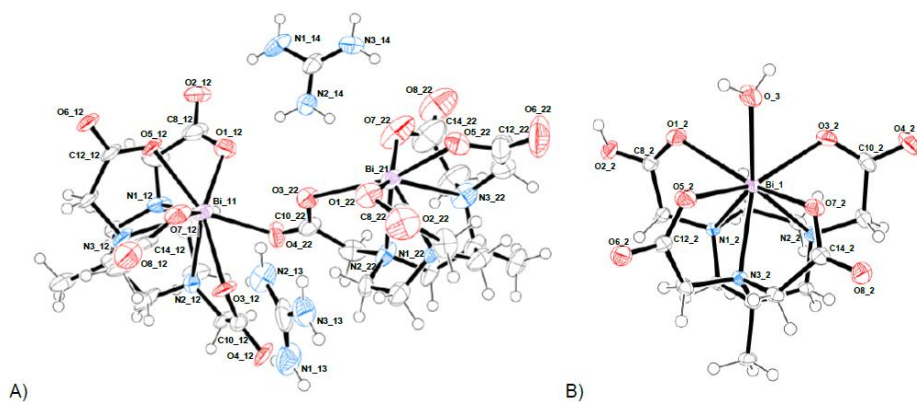
Figure.A.21 Ellipsoid representation of crystallographic asymmetric unit contents (ASU) for A) [Bi(AAZTA)]$^{-}$ and B) [Bi(HAAZTA)] (50% probability).
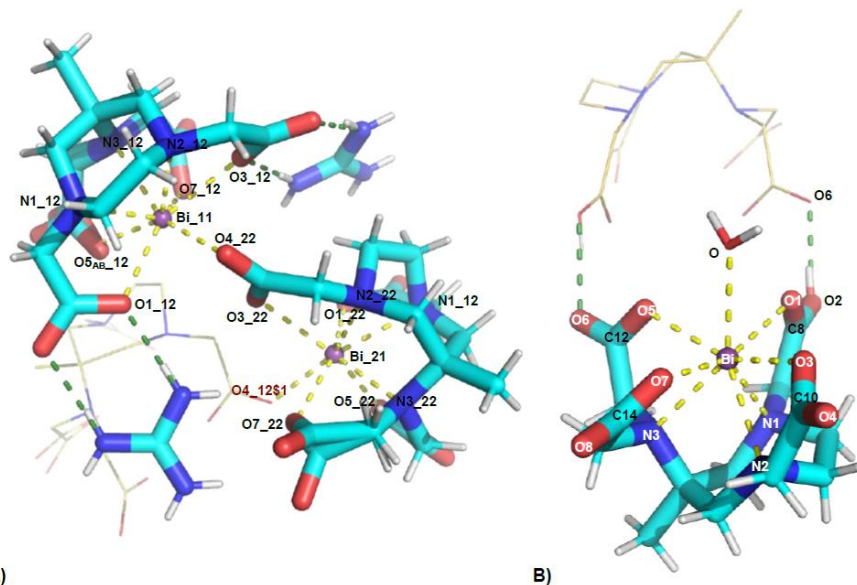
Figure.A.22 Stick representation of A) [Bi(AAZTA)]⁻.and B) [Bi(*H*AAZTA)].
Symmetry generated AAZTA molecules are shown with thin yellow sticks. Bismuth
coordination bonds are represented with yellow dashes, notable hydrogen bonds with
green ones.

Table A.23 Bond distances (Å) in [Bi(AAZTA)]⁻ (**A** and **B** crystallographically
independent molecules, Figure V.7.1), [Bi(*H*AAZTA)(H₂O)] (**C**, Figure V.7.1),
[Sc(AAZTA)(H₂O)]⁻ (**D**) and [Er(AAZTA)(H₂O)]⁻ (**E**) complexes.

	A	**B**	**C**	**D**[a]	**E**[b]
$M^{3+} - OH_2$	–	–	2.605(4)	2.247(1)	2.344 (9)
$M^{3+} - O1$	2.491(16)	2.588(16)	2.746(4)	2.202(1)	2.302 (8)
$M^{3+} - O3$	2.539(16)	2.723(12)	2.478(4)	2.152(1)	2.300 (8)
$M^{3+} - O5$	2.45(3) - 2.21(5)	2.302(13)	2.439(4)	2.119(1)	2.247 (8)
$M^{3+} - O7$	2.606(16)	2.344(19)	2.251(4)	2.158(1)	2.290 (8)

M^{3+} – N1	2.489(17)	2.505(16)	2.587(4)	2.412(2)	2.468 (9)
M^{3+} – N2	2.592(16)	2.551(15)	2.527(4)	2.443(2)	2.569 (10)
M^{3+} – N3	2.461(18)	2.525(19)	2.486(4)	2.476(2)	2.553 (9)

[a] Ref. [144]; [b] Ref. [145].

Table.A.24 Cristhallographic data and refinement details for [Bi(AAZTA)]$^-$ and [Bi(*HAAZTA*)(H$_2$O)].

	{[C(NH$_2$)$_3$][Bi(AAZTA)]}·3.5H$_2$O ([BiC$_{14}$H$_{19}$N$_3$O$_8$·CH$_6$N$_3$]·3.5H$_2$O)	[Bi(HAAZTA)(H$_2$O)]·3H$_2$O ([BiC$_{14}$H$_{20}$N$_3$O$_8$·H$_2$O]·3H$_2$O)
CCDC Number	2115291	2115292
Chemical Formula	C$_{15}$H$_{32}$BiN$_6$O$_{11.5}$	C$_{14}$H$_{28}$BiN$_3$O$_{12}$
Formula weight (g/mol)	689.44	639.37
Temperature (K)	100(2)	100(2)
Wavelength (Å)	0.700	0.700
Crystal system	Monoclinic	Monoclinic
Space Group	C 2/c	P 2$_1$/n
Unit cell dimensions	a = 35.085(7) Å	a = 9.427(2) Å
	b = 20.620(4) Å	b = 20.571(4) Å
	c = 14.962(3) Å	c = 10.701(2) Å
	α = 90°	α = 90°
	β = 113.90(3)°	β = 91.12(3)°
	γ = 90°	γ = 90°
Volume (Å^3)	9896(4)	2074.8(7)
Z	16	4
Density (calculated) (g·cm^{-3})	1.851	2.047
Absorption coefficient (mm^{-1})	6.874	8.186
F(000)	5424	1248
Crystal size (mm^3)	0.10 x 0.01 x 0.01	0.08 x 0.08 x 0.04
Crystal habit	Colorless thin needles	Colorless thin prisms
Theta range for data collection	1.16° to 24.01°	2.11° to 25.27°
Resolution (Å)	0.86	0.82
Index ranges	-40 ≤ h ≤ 40	-11 ≤ h ≤ 11
	-20 ≤ k ≤ 23	-25 ≤ k ≤ 25
	-17 ≤ l ≤ 16	-13 ≤ l ≤ 13
Reflections collected	24717	21017
Independent reflections (data with I>2σ(I))	7983 (4426)	3792 (3737)
Data multiplicity (max resltn)	2.99 (2.99)	5.26 (5.37)
I/σ(I) (max resltn)	4.44 (1.93)	22.43 (21.40)
R$_{merge}$ (max resltn)	0.1425 (0.4209)	0.0582 (0.0527)
Data completeness (max resltn)	97.6% (96.1%)	96.7% (95.0%)
Refinement method	Full-matrix least-squares on F^2	Full-matrix least-squares on F^2
Data / restraints / parameters	7983 / 116 / 639	3792 / 3 / 283
Goodness-of-fit on F^2	1.065	1.091
□/□$_{max}$	0.001	0.001
Final R indices [I>2σ(I)]^a	R$_1$ = 0.0779, wR$_2$ = 0.1753	R$_1$ = 0.0293, wR$_2$ = 0.0720
R indices (all data)^a	R$_1$ = 0.1463, wR$_2$ = 0.2039	R$_1$ = 0.0295, wR$_2$ = 0.0718
Largest diff. peak and hole (e·Å^{-3})	2.535 and -2.017	2.436 and -1.662
R.M.S. deviation from mean (e·Å^{-3})	0.250	0.148

^{a} R$_1$ = Σ ||Fo|–|Fc|| / Σ |Fo|, wR$_2$ = {Σ [w(Fo^2 – Fc^2)^2] / Σ [w(Fo^2)^2]}$^{1/2}$
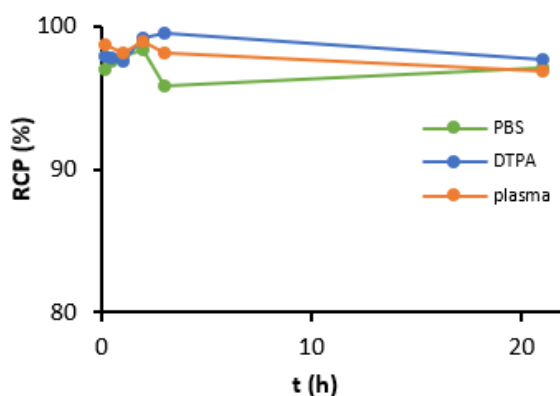
Figure A.25. Stability investigation of [$^{205/206}$Bi][Bi(AAZTA-C4-TATE)]$^-$ in PBS and 0.01 M DTPA solutions at room temperature, and in human plasma at 37°C.
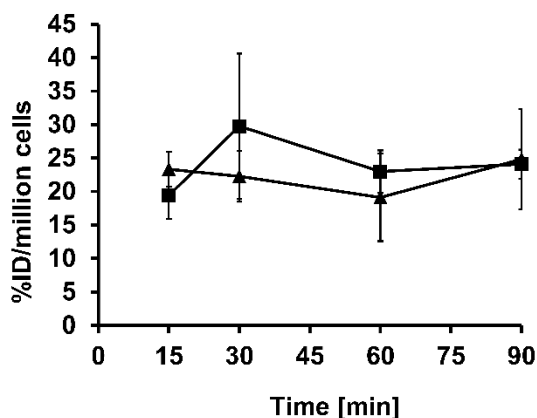
Figure A.26 Assessment of cellular uptake studies of [$^{205/206}$Bi][Bi(AAZTA-C4-TATE)]$^-$ (■) and [$^{205/206}$Bi][Bi(DOTA-TATE)]$^-$ (▲). The data values shown are means ± SD of the results of at least three independent experiments, each performed in triplicate. ID%: Tracer accumulation in 10^6 cells was expressed as the percentage of the incubating dose.

VIII. References

[1] N. N. Greenwood, A. Earnshaw, és Brücher Ernő, *Az elemek kémiája: felsőoktatási tankönyv*. Budapest: Nemzeti Tankönyvkiadó, **2004**.

[2] D. Keogan és D. Griffith, „Current and Potential Applications of Bismuth-Based Drugs", *Molecules*, köt. 19, sz. 9, o. 15258–15297, szept. **2014**, doi: 10.3390/molecules190915258.

[3] „Környei József: A nukleáris medicina fizikai, kémiai alapjai, Kossuth Egyetemi Kiadó, Debrecen, **1997**".

[4] G. Crişan, N. S. Moldovean-Cioroianu, D.-G. Timaru, G. Andrieş, C. Căinap, és V. Chiş, „Radiopharmaceuticals for PET and SPECT Imaging: A Literature Review over the Last Decade", *Int. J. Mol. Sci.*, köt. 23, sz. 9, o. 5023, ápr. **2022**, doi: 10.3390/ijms23095023.

[5] J. de Swart *és mtsai.*, „Utilizing High-Energy γ-Photons for High-Resolution [213] Bi SPECT in Mice", *J. Nucl. Med.*, köt. 57, sz. 3, o. 486–492, márc. **2016**, doi: 10.2967/jnumed.115.157685.

[6] S. Zidenberg-Cherr, N. J. Parks, és C. L. Keen, „Tissue and subcellular distribution of bismuth radiotracer in the rat: considerations of cytotoxicity and microdosimetry for bismuth radiopharmaceuticals", *Radiat. Res.*, köt. 111, sz. 1, o. 119–129, júl. **1987**.

[7] J. Fu *és mtsai.*, „Bismuth chelate as a contrast agent for X-ray computed tomography", *J. Nanobiotechnology*, köt. 18, sz. 1, o. 110, dec. **2020**, doi: 10.1186/s12951-020-00669-4.

[8] R. A. Revia és M. Zhang, „Magnetite nanoparticles for cancer diagnosis, treatment, and treatment monitoring: recent advances", *Mater. Today*, köt. 19, sz. 3, o. 157–168, ápr. **2016**, doi: 10.1016/j.mattod.2015.08.022.

[9] B. Wu *és mtsai.*, „Gadolinium-chelate functionalized bismuth nanotheranostic agent for in vivo MRI/CT/PAI imaging-guided photothermal cancer therapy", *Biomaterials*, köt. 159, o. 37–47, márc. **2018**, doi: 10.1016/j.biomaterials.2017.12.022.

[10] J. L. Lange *és mtsai.*, „An octadentate bis(semicarbazone) macrocycle: a potential chelator for lead and bismuth radiopharmaceuticals", *Dalton Trans.*, köt. 49, sz. 42, o. 14962–14974, **2020**, doi: 10.1039/D0DT02673E.

[11] W. Frank, G. J. Reiss, és J. Schneider, „The Nona aqua bismuth(III) Cation", *Angew. Chem. Int. Ed. Engl.*, köt. 34, sz. 21, o. 2416–2417, nov. **1995**, doi: 10.1002/anie.199524161.

[12] J. Emsley, *The elements*, 3rd ed. Oxford : New York: Clarendon Press ; Oxford University Press, **1998**.

[13] R. B. King, Szerk., *Encyclopedia of inorganic chemistry*, 2nd ed. Chichester, West Sussex, England ; Hoboken, NJ: Wiley, **2005**.

[14] J. Daintith, Szerk., *A dictionary of chemistry*, 6th ed. in Oxford paperback reference. New York: Oxford University Press, **2008**.

[15] C. F. Baes és R. E. Mesmer, *The hydrolysis of cations*. New York: Wiley, **1976**.

[16] É. Csajbók *és mtsai.*, „Equilibrium, ^{1}H and ^{13}C NMR Spectroscopy, and X-ray Diffraction Studies on the Complexes Bi(DOTA)[-] and Bi(DO3A-Bu)", *Inorg. Chem.*, köt. 42, sz. 7, o. 2342–2349, ápr. **2003**, doi: 10.1021/ic0261272.

[17] S. P. Summers, „Syntheses and Structures of Bismuth(II1) Complexes with Nitrilotriacetic Acid, Ethylenediaminetetraacetic Acid, and DiethylenetriaminepentaaceticAcid", o. 5.

[18] P. J. Sadler, H. Li, és H. Sun, „Coordination chemistry of metals in medicine: target sites for bismuth", *Coord. Chem. Rev.*, köt. 185–186, o. 689–709, máj. **1999**, doi: 10.1016/S0010-8545(99)00018-1.

[19] I. Grenthe és I. Toth, „Proton NMR studies of the bismuth(3+)-hydroxide system: stoichiometric composition of the hexanuclear complex and rate of proton exchange of coordinated water and hydroxide in mixed acetone/water solution", *Inorg. Chem.*, köt. 24, sz. 15, o. 2405–2407, júl. **1985**, doi: 10.1021/ic00209a018.

[20] B. Sundvall, „Crystal structure of tetraoxotetrahydroxohexabismuth (III) perchlorate heptahydrate, $Bi_6O_4(HO)_4(ClO_4)_6.7H_2O$: an x-ray and neutron diffraction study", *Inorg. Chem.*, köt. 22, sz. 13, o. 1906–1912, jún. **1983**, doi: 10.1021/ic00155a017.

[21] M. Graunar és F. Lazarini, „Di-µ-hydroxo-bis[aquasulfatobismuth(III)]", *Acta Crystallogr. B*, köt. 38, sz. 11, o. 2879–2881, nov. **1982**, doi: 10.1107/S0567740882010188.

[22] C. E. Housecroft és A. G. Sharpe, *Inorganic chemistry*, 3rd ed. Harlow, Essex: Pearson Prentice Hall, **2008**.

[23] S. A. Adonin, M. N. Sokolov, és V. P. Fedin, „Polynuclear halide complexes of Bi(III): From structural diversity to the new properties", *Coord. Chem. Rev.*, köt. 312, o. 1–21, ápr. **2016**, doi: 10.1016/j.ccr.2015.10.010.

[24] R. Floresca, M. Kurihara, D. S. Watt, és A. Demir, „Cleavage of unsaturated .alpha.-ketols to .omega.-oxo-.alpha.,.beta.-unsaturated acids", *J. Org. Chem.*, köt. 58, sz. 8, o. 2196–2200, ápr. **1993**, doi: 10.1021/jo00060a040.

[25]   H. Firouzabadi és I. Mohammadpour-Baltork, „Zinc Bismuthate $Zn(BiO_3)_2$. I. A Useful Oxidizing Agent for the Efficient Oxidation of Organic Compounds", *Bull. Chem. Soc. Jpn.*, köt. 65, sz. 4, o. 1131–1134, ápr. **1992**, doi: 10.1246/bcsj.65.1131.

[26]   J. Gehler, M. Cantz, J. F. O'Brien, M. Tolksdorf, és J. Spranger, „Mannosidosis: clinical and biochemical findings", *Birth Defects Orig. Artic. Ser.*, köt. 11, sz. 6, o. 269–272, **1975**.

[27]   N. Yang és H. Sun, „Biocoordination chemistry of bismuth: Recent advances", *Coord. Chem. Rev.*, köt. 251, sz. 17–20, o. 2354–2366, szept. **2007**, doi: 10.1016/j.ccr.2007.03.003.

[28]   R. Ge és H. Sun, „Bioinorganic Chemistry of Bismuth and Antimony: Target Sites of Metallodrugs", *Acc. Chem. Res.*, köt. 40, sz. 4, o. 267–274, ápr. **2007**, doi: 10.1021/ar600001b.

[29]   K. Robinson, R. H. Argent, és J. C. Atherton, „The inflammatory and immune response to Helicobacter pylori infection", *Best Pract. Res. Clin. Gastroenterol.*, köt. 21, sz. 2, o. 237–259, ápr. **2007**, doi: 10.1016/j.bpg.2007.01.001.

[30]   D. Cordier és A. Merlo, „Long-Term Results of Targeted Low-Grade Glioma Treatment with [213] Bi-DOTA-[Thi[8],Met(O$_2$)[11]]-Substance P", *Cancer Biother. Radiopharm.*, köt. 34, sz. 6, o. 413–416, aug. **2019**, doi: 10.1089/cbr.2018.2719.

[31]   C. Apostolidis, R. Molinet, G. Rasmussen, és A. Morgenstern, „Production of Ac-225 from Th-229 for Targeted α Therapy", *Anal. Chem.*, köt. 77, sz. 19, o. 6288–6291, okt. **2005**, doi: 10.1021/ac0580114.

[32]   R. Perron, P. Causey, és D. Gendron, „Development of a Research-Scale Thorium/Actinium Generator at the Canadian Nuclear Laboratories", *J. Med. Imaging Radiat. Sci.*, köt. 50, sz. 1, o. S42, márc. **2019**, doi: 10.1016/j.jmir.2019.03.127.

[33]   J. A. Lessa *és mtsai.*, „Coordination of Thiosemicarbazones and Bis(thiosemicarbazones) to Bismuth(III) as a Strategy for the Design of Metal-Based Antibacterial Agents", *Chem. Biodivers.*, köt. 9, sz. 9, o. 1955–1966, szept. **2012**, doi: 10.1002/cbdv.201100447.

[34]   K. S. O. Ferraz *és mtsai.*, „Investigation on the pharmacological profile of 2,6-diacetylpyridine bis(benzoylhydrazone) derivatives and their antimony(III) and bismuth(III) complexes", *Eur. J. Med. Chem.*, köt. 53, o. 98–106, júl. **2012**, doi: 10.1016/j.ejmech.2012.03.040.

[35]   I. Turel, „Crystal structure and characterization of the bismuth(III) compound with quinolone family member (ciprofloxacin).

Antibacterial study", *J. Inorg. Biochem.*, köt. 66, sz. 4, o. 241–245, jún. **1997**, doi: 10.1016/S0162-0134(96)00218-8.

[36] I. Turel, L. Golič, P. Bukovec, és M. Gubina, „Antibacterial tests of Bismuth(III)–Quinolone (Ciprofloxacin, cf) compounds against Helicobacter pylori and some other bacteria. Crystal structure of $(cfH_2)_2[Bi_2Cl_{10}]\cdot 4H_2O$", *J. Inorg. Biochem.*, köt. 71, sz. 1–2, o. 53–60, aug. **1998**, doi: 10.1016/S0162-0134(98)10032-6.

[37] C. Gösweiner *és mtsai.*, „Tuning Nuclear Quadrupole Resonance: A Novel Approach for the Design of Frequency-Selective MRI Contrast Agents", *Phys. Rev. X*, köt. 8, sz. 2, o. 021076, jún. **2018**, doi: 10.1103/PhysRevX.8.021076.

[38] D. Kruk *és mtsai.*, „[209]Bi quadrupole relaxation enhancement in solids as a step towards new contrast mechanisms in magnetic resonance imaging", *Phys. Chem. Chem. Phys.*, köt. 20, sz. 18, o. 12710–12718, **2018**, doi: 10.1039/C8CP00993G.

[39] D. Kruk, E. Umut, E. Masiewicz, P. Hermann, és H. Scharfetter, „[1]H spin–lattice relaxation in water solution of [209]Bi counterparts of Gd^{3+} contrast agents", *Mol. Phys.*, köt. 117, sz. 7–8, o. 927–934, ápr. **2019**, doi: 10.1080/00268976.2018.1517907.

[40] M. A. Walicka, G. Vaidyanathan, M. R. Zalutsky, S. J. Adelstein, és A. I. Kassis, „Survival and DNA Damage in Chinese Hamster V79 Cells Exposed to Alpha Particles Emitted by DNA-Incorporated Astatine-211", *Radiat. Res.*, köt. 150, sz. 3, o. 263, szept. **1998**, doi: 10.2307/3579974.

[41] A. K. Claesson, B. Stenerlöw, L. Jacobsson, és K. Elmroth, „Relative Biological Effectiveness of the α-Particle Emitter [211]At for Double-Strand Break Induction in Human Fibroblasts", *Radiat. Res.*, köt. 167, sz. 3, o. 312–318, márc. **2007**, doi: 10.1667/RR0668.1.

[42] F. Lacoeuille, N. Arlicot, és A. Faivre-Chauvet, „Targeted alpha and beta radiotherapy: An overview of radiopharmaceutical and clinical aspects", *Médecine Nucl.*, köt. 42, sz. 1, o. 32–44, jan. **2018**, doi: 10.1016/j.mednuc.2017.12.002.

[43] H. Jadvar és D. I. Quinn, „Targeted α-Particle Therapy of Bone Metastases in Prostate Cancer", *Clin. Nucl. Med.*, köt. 38, sz. 12, o. 966–971, dec. **2013**, doi: 10.1097/RLU.0000000000000290.

[44] F. D. C. Guerra Liberal, J. M. O'Sullivan, S. J. McMahon, és K. M. Prise, „Targeted Alpha Therapy: Current Clinical Applications", *Cancer Biother. Radiopharm.*, köt. 35, sz. 6, o. 404–417, aug. **2020**, doi: 10.1089/cbr.2020.3576.

[45]   R. A. Boll, D. Malkemus, és S. Mirzadeh, „Production of actinium-225 for alpha particle mediated radioimmunotherapy", *Appl. Radiat. Isot.*, köt. 62, sz. 5, o. 667–679, máj. **2005**, doi: 10.1016/j.apradiso.2004.12.003.

[46]   A. Morgenstern, C. Apostolidis, és F. Bruchertseifer, „Supply and Clinical Application of Actinium-225 and Bismuth-213", *Semin. Nucl. Med.*, köt. 50, sz. 2, o. 119–123, márc. **2020**, doi: 10.1053/j.semnuclmed.2020.02.003.

[47]   A. Morgenstern, K. Abbas, F. Bruchertseifer, és C. Apostolidis, „Production of Alpha Emitters for Targeted Alpha Therapy", *Curr. Radiopharm.*, köt. 1, sz. 3, o. 135–143, szept. **2008**, doi: 10.2174/1874471010801030135.

[48]   F. F. Knapp és T. A. Butler, Szerk., *Radionuclide Generators: New Systems for Nuclear Medicine Applications*, köt. 241. in ACS Symposium Series, vol. 241. Washington, D.C.: American Chemical Society, **1984**. doi: 10.1021/bk-1984-0241.

[49]   V. Radchenko *és mtsai.*, „Production and Supply of α-Particle–Emitting Radionuclides for Targeted α-Therapy", *J. Nucl. Med.*, köt. 62, sz. 11, o. 1495–1503, nov. **2021**, doi: 10.2967/jnumed.120.261016.

[50]   R. W. Atcher, A. M. Friedman, és J. J. Hines, „An improved generator for the production of ^{212}Pb and ^{212}Bi from ^{224}Ra", *Int. J. Rad. Appl. Instrum. [A]*, köt. 39, sz. 4, o. 283–286, jan. **1988**, doi: 10.1016/0883-2889(88)90016-0.

[51]   F.-M. Su, P. Beaumier, D. Axworthy, R. Atcher, és A. Fritzberg, „Pretargeted radioimmunotherapy in tumored mice using an in vivo ^{212}Pb/^{212}Bi generator", *Nucl. Med. Biol.*, köt. 32, sz. 7, o. 741–747, okt. **2005**, doi: 10.1016/j.nucmedbio.2005.06.009.

[52]   J. Rotmensch, R. W. Atcher, J. Hines, M. Toohill, és A. L. Herbst, „Comparison of short-lived high-LET α-emitting radionuclides lead-212 and bismuth-212 to low-LET X-rays on ovarian carcinoma", *Gynecol. Oncol.*, köt. 35, sz. 3, o. 297–300, dec. **1989**, doi: 10.1016/0090-8258(89)90067-X.

[53]   S. Westrøm, R. Generalov, T. B. Bønsdorff, és R. H. Larsen, „Preparation of 212 Pb-labeled monoclonal antibody using a novel 224 Ra-based generator solution", *Nucl. Med. Biol.*, köt. 51, o. 1–9, aug. **2017**, doi: 10.1016/j.nucmedbio.2017.04.005.

[54]   R. W. Atcher, A. M. Friedman, P. Forest, J. Hines, és G. Ellyn, „(54) ISOTOPIC GENERATOR FOR BISMUTH-212", o. 10.

[55]   H. Sun, Szerk., *Biological chemistry of arsenic, antimony and bismuth*. Chichester, West Sussex: Wiley, **2011**.

[56] P. P. Boldyrev *és mtsai.*, „^{212}Pb/^{212}Bi Generator for nuclear medicine", *At. Energy*, köt. 111, sz. 6, o. 422–427, ápr. **2012**, doi: 10.1007/s10512-012-9513-x.

[57] T. I. Kostelnik és C. Orvig, „Radioactive Main Group and Rare Earth Metals for Imaging and Therapy", *Chem. Rev.*, köt. 119, sz. 2, o. 902–956, jan. **2019**, doi: 10.1021/acs.chemrev.8b00294.

[58] E. W. Price és C. Orvig, „Matching chelators to radiometals for radiopharmaceuticals", *Chem Soc Rev*, köt. 43, sz. 1, o. 260–290, **2014**, doi: 10.1039/C3CS60304K.

[59] D. E. Milenic *és mtsai.*, „*In Vivo* Evaluation of Bismuth-Labeled Monoclonal Antibody Comparing DTPA-Derived Bifunctional Chelates", *Cancer Biother. Radiopharm.*, köt. 16, sz. 2, o. 133–146, ápr. **2001**, doi: 10.1089/108497801300189227.

[60] M. W. Brechbiel és O. A. Gansow, „Synthesis of C-functionalized trans-cyclohexyldiethylenetriaminepenta-acetic acids for labelling of monoclonal antibodies with the bismuth-212 α-particle emitter", *J Chem Soc Perkin Trans 1*, sz. 9, o. 1173–1178, **1992**, doi: 10.1039/P19920001173.

[61] H. S. Chan *és mtsai.*, „Improved safety and efficacy of ^{213}Bi-DOTATATE-targeted alpha therapy of somatostatin receptor-expressing neuroendocrine tumors in mice pre-treated with l-lysine", *EJNMMI Res.*, köt. 6, sz. 1, o. 83, dec. **2016**, doi: 10.1186/s13550-016-0240-5.

[62] H. S. Chan *és mtsai.*, „In Vitro comparison of ^{213}Bi- and ^{177}Lu-radiation for peptide receptor radionuclide therapy", *PLOS ONE*, köt. 12, sz. 7, o. e0181473, júl. **2017**, doi: 10.1371/journal.pone.0181473.

[63] G. Montavon, A. Le Du, J. Champion, T. Rabung, és A. Morgenstern, „DTPA complexation of bismuth in human blood serum", *Dalton Trans.*, köt. 41, sz. 28, o. 8615, **2012**, doi: 10.1039/c2dt30230f.

[64] J. P. Norenberg *és mtsai.*, „^{213}Bi-[DOTA0, Tyr3]Octreotide Peptide Receptor Radionuclide Therapy of Pancreatic Tumors in a Preclinical Animal Model", *Clin. Cancer Res.*, köt. 12, sz. 3, o. 897–903, febr. **2006**, doi: 10.1158/1078-0432.CCR-05-1264.

[65] H. S. Chan *és mtsai.*, „Improved safety and efficacy of ^{213}Bi-DOTATATE-targeted alpha therapy of somatostatin receptor-expressing neuroendocrine tumors in mice pre-treated with l-lysine", *EJNMMI Res.*, köt. 6, sz. 1, o. 83, nov. **2016**, doi: 10.1186/s13550-016-0240-5.

[66] H. S. Chan *és mtsai.*, „Influence of tumour size on the efficacy of targeted alpha therapy with [213]Bi-[DOTA0,Tyr3]-octreotate", *EJNMMI Res.*, köt. 6, sz. 1, o. 6, dec. **2016**, doi: 10.1186/s13550-016-0162-2.

[67] Ho Sze Chan *és mtsai.*, „Optimizing labeling conditions of [213]Bi-somatostatin analogs for receptor-mediated processes in preclinical models", *J. Nucl. Med.*, köt. 55, sz. supplement 1, o. 1179, máj. **2014**.

[68] M. Sathekge, O. Knoesen, M. Meckel, M. Modiselle, M. Vorster, és S. Marx, „[213]Bi-PSMA-617 targeted alpha-radionuclide therapy in metastatic castration-resistant prostate cancer", *Eur. J. Nucl. Med. Mol. Imaging*, köt. 44, sz. 6, o. 1099–1100, jún. 2017, doi: 10.1007/s00259-017-3657-9.

[69] K. Garmestani *és mtsai.*, „Synthesis and evaluation of a macrocyclic bifunctional chelating agent for use with bismuth radionuclides", *Nucl. Med. Biol.*, köt. 28, sz. 4, o. 409–418, máj. **2001**, doi: 10.1016/S0969-8051(00)00203-1.

[70] L. M. P. Lima, M. Beyler, R. Delgado, C. Platas-Iglesias, és R. Tripier, „Investigating the Complexation of the Pb $^{2+}$/Bi $^{3+}$ Pair with Dipicolinate Cyclen Ligands", *Inorg. Chem.*, köt. 54, sz. 14, o. 7045–7057, júl. **2015**, doi: 10.1021/acs.inorgchem.5b01079.

[71] H.-S. Chong, H. A. Song, N. Birch, T. Le, S. Lim, és X. Ma, „Efficient synthesis and evaluation of bimodal ligand NETA", *Bioorg. Med. Chem. Lett.*, köt. 18, sz. 11, o. 3436–3439, jún. **2008**, doi: 10.1016/j.bmcl.2008.03.084.

[72] H. A. Song *és mtsai.*, „Efficient Bifunctional Decadentate Ligand 3p- *C* -DEPA for Targeted α-Radioimmunotherapy Applications", *Bioconjug. Chem.*, köt. 22, sz. 6, o. 1128–1135, jún. **2011**, doi: 10.1021/bc100586y.

[73] H.-S. Chong *és mtsai.*, „Novel Bimodal Bifunctional Ligands for Radioimmunotherapy and Targeted MRI", *Bioconjug. Chem.*, köt. 19, sz. 7, o. 1439–1447, júl. **2008**, doi: 10.1021/bc800050x.

[74] C. S. Kang, H. A. Song, D. E. Milenic, K. E. Baidoo, M. W. Brechbiel, és H.-S. Chong, „Preclinical evaluation of NETA-based bifunctional ligand for radioimmunotherapy applications using 212Bi and 213Bi: Radiolabeling, serum stability, and biodistribution and tumor uptake studies", *Nucl. Med. Biol.*, köt. 40, sz. 5, o. 600–605, júl. **2013**, doi: 10.1016/j.nucmedbio.2013.01.012.

[75] M. Dadwal *és mtsai.*, „Synthesis and evaluation of a bifunctional chelate for development of Bi(III)-labeled

radioimmunoconjugates", *Bioorg. Med. Chem. Lett.*, köt. 21, sz. 24, o. 7513–7515, dec. **2011**, doi: 10.1016/j.bmcl.2011.06.107.

[76] I. Lazar, D. C. Hrncir, W. D. Kim, G. E. Kiefer, és A. D. Sherry, „Optimized synthesis, structure, and solution dynamics of 1,4,7,10-tetraazacyclododecane-1,4,7,10-tetrakis(methylenephosphonic acid) (H_8DOTP)", *Inorg. Chem.*, köt. 31, sz. 21, o. 4422–4424, okt. **1992**, doi: 10.1021/ic00047a034.

[77] S. Aime *és mtsai.*, „[Gd-AAZTA]⁻: a new structural entry for an improved generation of MRI contrast agents", *Inorg Chem.*, köt. 43, sz. 24, o. 7588–90, 0 **2004**, doi: 10.1021/ic0489692.

[78] „Synthesis of Gd and ^{68}Ga Complexes in Conjugation with a Conformationally Optimized RGD Sequence as Potential MRI and PET Tumor-Imaging Probes - Manzoni - 2012 - ChemMedChem - Wiley Online Library". Elérés: **2022**. április 13. [Online]. Elérhető: https://chemistry-europe.onlinelibrary.wiley.com/doi/abs/10.1002/cmdc.201200043

[79] H. M. Irving, M. G. Miles, és L. D. Pettit, „A study of some problems in determining the stoicheiometric proton dissociation constants of complexes by potentiometric titrations using a glass electrode", *Anal. Chim. Acta*, köt. 38, o. 475–488, 0 **1967**, doi: 10.1016/S0003-2670(01)80616-4.

[80] J. L. Submeier és C. N. Reilley, „Nuclear Magnetic Resonance Studies of Protonation of Polyamine and Aminocarboxylate Compounds in Aqueous Solution", *Anal. Chem.*, köt. 36, sz. 9, o. 1698–1706, 0 **1964**, doi: 10.1021/ac60215a006.

[81] A. Lausi *és mtsai.*, „Status of the crystallography beamlines at Elettra", *Eur. Phys. J. Plus*, köt. 130, sz. 3, o. 43, márc. **2015**, doi: 10.1140/epjp/i2015-15043-3.

[82] W. Kabsch, „XDS", *Acta Crystallogr. D Biol. Crystallogr.*, köt. 66, sz. 2, Art. sz. 2, febr. **2010**, doi: 10.1107/S0907444909047337.

[83] „G. M. Sheldrick, SADABS, University Of Göttingen, Germany, 2012."

[84] G. M. Sheldrick, „SHELXT – Integrated space-group and crystal-structure determination", *Acta Crystallogr. Sect. Found. Adv.*, köt. 71, sz. 1, Art. sz. 1, jan. **2015**, doi: 10.1107/S2053273314026370.

[85] G. M. Sheldrick, „Crystal structure refinement with SHELXL", *Acta Crystallogr. Sect. C Struct. Chem.*, köt. 71, sz. 1, Art. sz. 1, jan. **2015**, doi: 10.1107/S2053229614024218.

[86] P. Emsley, B. Lohkamp, W. G. Scott, és K. Cowtan, „Features and development of Coot", *Acta Crystallogr. D Biol. Crystallogr.*, köt. 66, sz. 4, Art. sz. 4, ápr. **2010**, doi: 10.1107/S0907444910007493.

[87]   L. J. Farrugia, „WinGX and ORTEP for Windows: an update", *J. Appl. Crystallogr.*, köt. 45, sz. 4, Art. sz. 4, aug. **2012**, doi: 10.1107/S0021889812029111.

[88]   C. F. Macrae *és mtsai.*, „Mercury CSD 2.0 – new features for the visualization and investigation of crystal structures", *J. Appl. Crystallogr.*, köt. 41, sz. 2, Art. sz. 2, ápr. **2008**, doi: 10.1107/S0021889807067908.

[89]   „L. Schrodinger, The PyMOL Molecular Graphics System, Schrodinger, LLC, **2015**."

[90]   Z. Baranyai, F. Uggeri, G. B. Giovenzana, A. Bényei, E. Brücher, és S. Aime, „Equilibrium and Kinetic Properties of the Lanthanoids(III) and Various Divalent Metal Complexes of the Heptadentate Ligand AAZTA", *Chem. - Eur. J.*, köt. 15, sz. 7, Art. sz. 7, febr. **2009**, doi: 10.1002/chem.200801803.

[91]   L. Barcza és K. Mihályi, „Dimerization of Lower Fatty Acids in Aqueous Solutions", *Z. Für Phys. Chem.*, köt. 104, sz. 4–6, o. 199–212, ápr. **1977**, doi: 10.1524/zpch.1977.104.4-6.199.

[92]   S. Chaves, R. Delgado, és J. J. Da Silva, „The stability of the metal complexes of cyclic tetra-aza tetra-acetic acids", *Talanta*, köt. 39, sz. 3, o. 249–254, márc. **1992**.

[93]   R. Delgado, L. C. Siegfried, és T. A. Kaden, „Metal Complexes with Macrocyclic Ligands. Part XXXI. Protonation studies and complexation properties of tetraazamacrocyclic methylenephosphonates with earth-alkali ions", *Helv. Chim. Acta*, köt. 73, sz. 1, o. 140–148, **1990**, doi: https://doi.org/10.1002/hlca.19900730115.

[94]   Z. Baranyai *és mtsai.*, „Equilibrium, Kinetic and Structural Studies of AAZTA Complexes with Ga^{3+}, In^{3+} and Cu^{2+}", *Eur. J. Inorg. Chem.*, köt. 2013, sz. 1, o. 147–162, **2013**, doi: 10.1002/ejic.201201108.

[95]   F. V. C. Kock *és mtsai.*, „[Gd(AAZTA)]⁻ Derivatives with *n*-Alkyl Acid Side Chains Show Improved Properties for Their Application as MRI Contrast Agents**", *Chem. – Eur. J.*, köt. 27, sz. 5, o. 1849–1859, jan. **2021**, doi: 10.1002/chem.202004479.

[96]   P. Caravan, C. Comuzzi, W. Crooks, T. J. McMurry, G. R. Choppin, és S. R. Woulfe, „Thermodynamic Stability and Kinetic Inertness of MS-325, a New Blood Pool Agent for Magnetic Resonance Imaging", *Inorg. Chem.*, köt. 40, sz. 9, o. 2170–2176, ápr. **2001**, doi: 10.1021/ic001117r.

[97]   J. F. Desreux, E. Merciny, és M. F. Loncin, „Nuclear Magnetic-Resonance and Potentiometric Studies of the Protonation Scheme of

2 Tetraaza Tetraacetic Macrocycles", *Inorg Chem*, köt. 20, sz. 4, o. 987–991, **1981**, doi: 10.1021/Ic50218a008.

[98] A. Takacs *és mtsai.*, „Solution structures, stabilities, kinetics, and dynamics of DO3A and DO3A-sulphonamide complexes", *Inorg. Chem.*, köt. 53, sz. 6, o. 2858–72, márc. **2014**, doi: 10.1021/ic4025958.

[99] A. Bianchi *és mtsai.*, „Thermodynamic and structural properties of Gd^{3+} complexes with functionalized macrocyclic ligands based upon 1,4,7,10-tetraazacyclododecane", *J Chem Soc Dalton Trans*, sz. 5, o. 697–705, **2000**, doi: 10.1039/A909098c.

[100] R. Delgado és J. J. da Silva, „Metal complexes of cyclic tetra-azatetra-acetic acids", *Talanta*, köt. 29, sz. 10, o. 815–22, okt. **1982**.

[101] B. P. Karadakov és D. I. Venkova, „The complexes of bismuth(III) and nitrilotriacetic acid", *Talanta*, köt. 17, sz. 9, o. 878–883, szept. **1970**, doi: 10.1016/0039-9140(70)80184-9.

[102] G. Anderegg, „The stability of iron(III) complexes formed below pH=3 with glycinate, iminodiacetate, β-hydroxyethyliminodiacetate, N,N-Di-(hydroxyethyl)-glycinate, nitrilotriacetate and triethanolamine", *Inorganica Chim. Acta*, köt. 121, sz. 2, o. 229–231, nov. **1986**, doi: 10.1016/S0020-1693(00)84525-9.

[103] W. R. Harris, Y. Chen, és K. Wein, „Equilibrium Constants for the Binding of Indium(III) to Human Serum Transferrin", *Inorg. Chem.*, köt. 33, sz. 22, o. 4991–4998, okt. **1994**, doi: 10.1021/ic00100a024.

[104] T. F. Gritmon, M. P. Goedken, és G. R. Choppin, „The complexation of lanthanides by aminocarboxylate ligands—I: Stability constants", *J. Inorg. Nucl. Chem.*, köt. 39, sz. 11, o. 2021–2023, jan. **1977**, doi: 10.1016/0022-1902(77)80538-1.

[105] E. T. Clarke és A. E. Martell, „Stabilities of the alkaline earth and divalent transition metal complexes of the tetraazamacrocyclic tetraacetic acid ligands", *Inorganica Chim. Acta*, köt. 190, sz. 1, o. 27–36, dec. **1991**, doi: 10.1016/S0020-1693(00)80228-5.

[106] R. Garcia *és mtsai.*, „Synthesis, characterization and biological evaluation of In(III) complexes anchored by DOTA-like chelators bearing a quinazoline moiety", *Metallomics*, köt. 2, sz. 8, o. 571–580, aug. **2010**, doi: 10.1039/C004797J.

[107] W. P. Cacheris, S. K. Nickle, és A. D. Sherry, „Thermodynamic study of lanthanide complexes of 1,4,7-triazacyclononane-N,N',N"-triacetic acid and 1,4,7,10-tetraazacyclododecane-N,N',N",N'''-tetraacetic acid", *Inorg. Chem.*, köt. 26, sz. 6, o. 958–960, márc. **1987**, doi: 10.1021/ic00253a038.

[108] A. Bianchi *és mtsai.*, „Thermodynamic and structural properties of Gd^{3+} complexes with functionalized macrocyclic ligands based upon 1,4,7,10-tetraazacyclododecane", *J. Chem. Soc. Dalton Trans.*, sz. 5, Art. sz. 5, **2000**, doi: 10.1039/a909098c.

[109] J. Moreau, E. Guillon, J.-C. Pierrard, J. Rimbault, M. Port, és M. Aplincourt, „Complexing Mechanism of the Lanthanide Cations Eu^{3+}, Gd^{3+}, and Tb^{3+} with 1,4,7,10-Tetrakis(carboxymethyl)-1,4,7,10-tetraazacyclododecane (dota)—Characterization of Three Successive Complexing Phases: Study of the Thermodynamic and Structural Properties of the Complexes by Potentiometry, Luminescence Spectroscopy, and EXAFS", *Chem. – Eur. J.*, köt. 10, sz. 20, o. 5218–5232, **2004**, doi: https://doi.org/10.1002/chem.200400006.

[110] A. D. Sherry *és mtsai.*, „Characterization of Lanthanide(III) DOTP Complexes: Thermodynamics, Protonation, and Coordination to Alkali Metal Ions", *Inorg. Chem.*, köt. 35, sz. 16, o. 4604–4612, jan. **1996**, doi: 10.1021/ic9600590.

[111] E. Toth, E. Brucher, I. Lazar, és I. Toth, „Kinetics of Formation and Dissociation of Lanthanide(III)-Dota Complexes", *Inorg. Chem.*, köt. 33, sz. 18, o. 4070–4076, 0 **1994**, doi: 10.1021/Ic00096a036.

[112] L. Burai, I. Fábián, R. Király, E. Szilágyi, és E. Brücher, „Equilibrium and kinetic studies on the formation of the lanthanide(III) complexes, [Ce(dota)]⁻ and [Yb(dota)]⁻ (H4dota = 1,4,7,10-tetraazacyclododecane-1,4,7,10-tetraacetic acid)", *J. Chem. Soc. Dalton Trans.*, sz. 2, o. 243–248, **1998**, doi: 10.1039/a705158a.

[113] L. Burai, R. Kiraly, I. Lazar, és E. Brucher, „Formation and dissociation kinetics of the complexes Gd(DOTP)⁵⁻ and Gd(DOTPMB)⁻", *Eur. J. Inorg. Chem.*, sz. 3, o. 813–820, márc. **2001**.

[114] M. Perez-Malo *és mtsai.*, „Improved Efficacy of Synthesizing *M(III)-Labeled DOTA Complexes in Binary Mixtures of Water and Organic Solvents. A Combined Radio- and Physicochemical Study", *Inorg. Chem.*, köt. 57, sz. 10, o. 6107–6117, máj. **2018**, doi: 10.1021/acs.inorgchem.8b00669.

[115] S. L. Wu és W. DeW. Horrocks, „Kinetics of Complex Formation by Macrocyclic Polyaza Polycarboxylate Ligands: Detection and Characterization of an Intermediate in the Eu^{3+}-dota System by Laser-Excited Luminescence", *Inorg. Chem.*, köt. 34, sz. 14, o. 3724–3732, júl. **1995**, doi: 10.1021/ic00118a020.

[116] C. F. Baes és R. E. Mesmer, *The Hydrolysis of Cations*. New York, London, Sydney, Toronto: John Wiley & Son, **1976**.

[117] L. Burai, I. Fábián, R. Király, E. Szilágyi, és E. Brücher, „Equilibrium and kinetic studies on the formation of the lanthanide(III) complexes, [Ce(dota)]$^-$ and [Yb(dota)]$^-$ (H4dota = 1,4,7,10-tetraazacyclododecane-1,4,7,10-tetraacetic acid)", *J. Chem. Soc. Dalton Trans.*, sz. 2, o. 243–248, jan. **1998**, doi: 10.1039/A705158A.

[118] E. Toth, E. Brucher, I. Lazar, és I. Toth, „Kinetics of Formation and Dissociation of Lanthanide(III)-DOTA Complexes", *Inorg. Chem.*, köt. 33, sz. 18, o. 4070–4076, aug. **1994**, doi: 10.1021/ic00096a036.

[119] L. Burai, R. Király, I. Lázár, és E. Brücher, „Formation and Dissociation Kinetics of the Complexes Gd(DOTP)$^{5-}$ and Gd(DOTPMB)$^-$", *Eur. J. Inorg. Chem.*, köt. 2001, sz. 3, o. 813–820, **2001**, doi: https://doi.org/10.1002/1099-0682(200103)2001:3<813::AID-EJIC813>3.0.CO;2-6.

[120] P. M. May, D. R. Williams, P. W. Linder, és R. G. Torrington, „The use of glass electrodes for the determination of formation constants—I A definitive method for calibration", *Talanta*, köt. 29, sz. 4, o. 249–256, ápr. **1982**, doi: 10.1016/0039-9140(82)80108-2.

[121] W. A. Herrmann, Eberhardt. Herdtweck, és Liba. Pajdla, „»Colloidal bismuth subcitrate« (CBS): isolation and structural characterization of the active substance against Helicobacter pylori, a causal factor of gastric diseases", *Inorg. Chem.*, köt. 30, sz. 12, o. 2579–2581, jún. **1991**, doi: 10.1021/ic00012a001.

[122] Eiji. Asato, W. L. Driessen, R. A. G. De Graaff, F. B. Hulsbergen, és Jan. Reedijk, „Synthesis, structure, and spectroscopic properties of bismuth citrate compounds. 1. Crystal structures of K$_{5-x}$(NH$_4$)$_x$[Bi$_2$(cit)$_2$(Hcit)](H$_2$O)$_y$ (x = 0.25, y = 13) and (NH$_4$)$_8$[Bi$_2$(cit)$_2$(Hcit)$_2$(H$_2$O)$_4$](H$_2$O)$_2$", *Inorg. Chem.*, köt. 30, sz. 22, o. 4210–4218, okt. **1991**, doi: 10.1021/ic00022a023.

[123] E. Asato, K. Katsura, M. Mikuriya, T. Fujii, és J. Reedijk, „Synthesis, structure, and spectroscopic characterization of bismuth citrate compounds and bismuth-containing ulcer healing agent colloidal bismuth subcitrate (CBS). 3. Crystal and solution structures of K(NH$_4$)[Bi$_2$(cit)$_2$(H$_2$O)$_2$](H$_2$O)$_x$ (x = 2, 4)", *Inorg. Chem.*, köt. 32, sz. 23, o. 5322–5329, nov. **1993**, doi: 10.1021/ic00075a060.

[124] E. Asato, K. Katsura, M. Mikuriya, U. Turpeinen, I. Mutikainen, és J. Reedijk, „Synthesis, Structure, and Spectroscopic Properties of Bismuth Citrate Compounds and the Bismuth-Containing Ulcer-

Healing Agent Colloidal Bismuth Subcitrate (CBS). 4. Crystal Structure and Solution Behavior of a Unique Dodecanuclear Cluster $(NH_4)_{12}[Bi_{12}O_8(cit)_8](H_2O)_{10}$", *Inorg. Chem.*, köt. 34, sz. 9, o. 2447–2454, ápr. **1995**, doi: 10.1021/ic00113a028.

[125] P. J. Barrie *és mtsai.*, „Solid-state carbon-13 nuclear magnetic resonance investigations of bismuth citrate complexes and crystal structure of $Na_2[Bi_2(cit)_2]·7H_2O$", *J. Chem. Soc. Dalton Trans.*, sz. 12, o. 2417–2422, jan. **1996**, doi: 10.1039/DT9960002417.

[126] D. R. Williams, „Analytical and computer simulation studies of a colloidal bismuth citrate system used as an ulcer treatment", *J. Inorg. Nucl. Chem.*, köt. 39, sz. 4, o. 711–714, 0 **1977**, doi: 10.1016/0022-1902(77)80600-3.

[127] J. F. Morfin és E. Toth, „Kinetics of Ga(NOTA) formation from weak Ga-citrate complexes", *Inorg Chem*, köt. 50, sz. 20, o. 10371–8, okt. **2011**, doi: 10.1021/ic201445e.

[128] J. Simecek *és mtsai.*, „Efficient formation of inert Bi-213 chelates by tetraphosphorus acid analogues of DOTA: towards improved alpha-therapeutics", *EJNMMI Res*, köt. 8, sz. 1, o. 78, 0 **2018**, doi: 10.1186/s13550-018-0431-3.

[129] A. E. Martell és R. M. Smith, *Critical stability constants*, köt. 1–5. New York: Plenum Press, **1974**.

[130] Z. Baranyai, Z. Palinkas, F. Uggeri, A. Maiocchi, S. Aime, és E. Brucher, „Dissociation Kinetics of Open-Chain and Macrocyclic Gadolinium(III)-Aminopolycarboxylate Complexes Related to Magnetic Resonance Imaging: Catalytic Effect of Endogenous Ligands", *Chem Eur J*, köt. 18, sz. 51, o. 16426–16435, dec. **2012**, doi: 10.1002/chem.201202930.

[131] É. Tóth, R. Király, J. Platzek, B. Radüchel, és E. Brücher, „Equilibrium and kinetic studies on complexes of 10-[2,3-dihydroxy-(1-hydroxymethyl)-propyl]-1,4,7,10-tetraazacyclododecane-1,4,7-triacetate", *Inorg Chim Acta*, köt. 249, sz. 2, o. 191–199, 0 **1996**, doi: 10.1016/0020-1693(96)05094-3.

[132] K. Kumar, T. Jin, X. Wang, J. F. Desreux, és M. F. Tweedle, „Effect of Ligand Basicity on the Formation and Dissociation Equilibria and Kinetics of Gd^{3+} Complexes of Macrocyclic Polyamino Carboxylates", *Inorg Chem*, köt. 33, sz. 17, o. 3823–3829, 0 **1994**, doi: 10.1021/ic00095a028.

[133] L. M. P. Lima, M. Beyler, R. Delgado, C. Platas-Iglesias, és R. Tripier, „Investigating the Complexation of the Pb^{2+}/Bi^{3+} Pair with Dipicolinate Cyclen Ligands", *Inorg. Chem.*, köt. 54, sz. 14, o. 7045–7057, júl. **2015**, doi: 10.1021/acs.inorgchem.5b01079.

[134] R. Pujales-Paradela *és mtsai.*, „On the consequences of the stereochemical activity of the Bi(III) $6s^2$ lone pair in cyclen-based complexes. The [Bi(DO3A)] case", *Dalton Trans.*, köt. 47, sz. 39, o. 13830–13842, okt. **2018**, doi: 10.1039/C8DT02602E.

[135] S. Hassfjell, K. O. Kongshaug, és C. Rømming, „Synthesis, crystal structure and chemical stability of bismuth(III) complexed with 1,4,7,10-tetraazacyclododecane-1,4,7,10-tetramethylene phosphonic acid (H8DOTMP)", *Dalton Trans.*, sz. 7, o. 1433–1437, márc. **2003**, doi: 10.1039/B300282A.

[136] C. F. G. C. Geraldes, A. D. Sherry, és G. E. Kiefer, „The solution structure of Ln (DOTP)$^{5-}$ complexxes. A comparison of lanthanide-induced paramagnetic shifts with the MMX energy-minimized structure", *J. Magn. Reson. 1969*, köt. 97, sz. 2, o. 290–304, ápr. **1992**, doi: 10.1016/0022-2364(92)90314-W.

[137] S. Aime, M. Botta, és G. Ermondi, „NMR study of solution structures and dynamics of lanthanide(III) complexes of DOTA", *Inorg. Chem.*, köt. 31, sz. 21, o. 4291–4299, 0 **1992**, doi: 10.1021/ic00047a016.

[138] L. D. Quin, M. J. Gallagher, G. T. Cunkle, és D. B. Chesnut, „Phosphorus-31 and carbon-13 NMR spectra of 2-norbornyl phosphorus compounds. Karplus equations for 3JPC in several phosphorus(III) and phosphorus(IV) derivatives", *J. Am. Chem. Soc.*, köt. 102, sz. 9, o. 3136–3143, ápr. **1980**, doi: 10.1021/ja00529a042.

[139] S. P. Hassfjell, Ø. S. Bruland, és P. Hoff, „212Bi-DOTMP: An alpha particle emitting bone-seeking agent for targeted radiotherapy", *Nucl. Med. Biol.*, köt. 24, sz. 3, o. 231–237, ápr. **1997**, doi: 10.1016/S0969-8051(97)00059-0.

[140] F. Travagin, L. Lattuada, és G. B. Giovenzana, „AAZTA: The rise of mesocyclic chelating agents for metal coordination in medicine", *Coord. Chem. Rev.*, köt. 438, o. 213908, júl. **2021**, doi: 10.1016/j.ccr.2021.213908.

[141] J.-P. Sinnes, J. Nagel, és F. Rösch, „AAZTA5/AAZTA5-TOC: synthesis and radiochemical evaluation with ^{68}Ga, [44]Sc and [177]Lu", *EJNMMI Radiopharm. Chem.*, köt. 4, sz. 1, o. 18, dec. **2019**, doi: 10.1186/s41181-019-0068-1.

[142] V. I. Kornev és A. V. Trubachev, „The Stability of Bi(III) Complexonates in Aqueous Solution", *Russ J. Inorg. Chem.*, köt. 32, sz. 10, o. 2433–2437, **1987**.

[143] M. W. Brechbiel, O. A. Gansow, C. G. Pippin, R. D. Rogers, és R. P. Planalp, „Preparation of the Novel Chelating Agent N-(2-

Aminoethyl)-trans-1,2-diaminocyclohexane- N,N',N''-pentaacetic Acid (H$_5$CyDTPA), a Preorganized Analogue of Diethylenetriaminepentaacetic Acid (H$_5$DTPA), and the Structures of Bi^{III}(CyDTPA)$^{2-}$ and Bi^{III}(H$_2$DTPA) Complexes", *Inorg. Chem.*, köt. 35, sz. 21, o. 6343–6348, **1996**, doi: 10.1021/ic951326p.

[144] G. Nagy *és mtsai.*, „AAZTA: An Ideal Chelating Agent for the Development of (44) Sc PET Imaging Agents", *Angew Chem Int Ed Engl*, köt. 56, sz. 8, o. 2118–2122, 0 **2017**, doi: 10.1002/anie.201611207.

[145] Z. Baranyai *és mtsai.*, „Combined NMR, DFT and X-ray studies highlight structural and hydration changes of [Ln(AAZTA)]⁻ complexes across the series", *Inorg. Chem. Front.*, köt. 7, sz. 3, o. 795–803, 0 **2020**, doi: 10.1039/C9QI01442J.

Köszönetnyilvánítás

Ezúton szeretném kifejezni köszönetemet két témavezetőimnek Dr. Baranyai Zsoltnak és Dr. Tircsó Gyulának, szakmai tanácsaikért, egész munkámra kiterjedő segítségükért, valamint türelmükért.

Szeretnék köszönetet mondani Prof. Dr. Tóth Imre Tanár Úrnak szakmai támogatásáért.

Köszönettel tartozom Takács Katalin tanszéki mérnöknek a kísérleti munkában nyújtott segítségért, valamint a kellemes légkörét és tanácsaiért.

Köszönöm Dr. Garda Zoltánnak szakmai tanácsait, valamint, hogy bármikor fordulhattam hozzá segítségért és tanácsért. Köszönöm a baráti légkört és a mindennapi szakmázást.

Szeretném hálámat kifejezni családomnak, akik mindvégig támogattak tanulmányaim során.

Szeretném megköszönni Józsa Rékának, feleségemnek, támogatását, türelmét és segítségét, ami nélkülözhetetlen volt munkám során.

Szeretnék külön köszönetet mondani Nicol Guidolinnak, Dr. Mariangela Boccalonnak és a trieszti csapatnak kintlétem során gyújtott rengeteg segítségüket, baráti légkört és a kedves szavakat.

Szeretnék köszönetet mondani Dr. Federica Bounsantinak, a kémiai osztály vezetőjének, hogy doktori munkám a Bracco Imaging S.p.A-nél végezhettem.

Köszönöm a jó beszélgetéseket, baráti légkört és támogatásukat mind a magánéletben mind a szakmában Csupász Tibornak, Szolnoki Csengének, Hámori Csabának és Udvardy Antalnak.

Végül de nem utolsó sorban szeretném megköszönni a Fizikai Kémiai Tanszék és a Ritka(föld)fém Kutatócsoport összes dolgozójának, aki valamilyen formában hozzájárult dologatom elkészüléséhez.

Acknowledgement

I would like to express my gratitude to my two supervisors, Dr. Zsolt Baranyai and Dr. Gyula Tircsó, for their professional advice, their help covering my entire work, and their patience.

I would like to thank Prof. Dr. Imre Tóth for his professional support.

I am grateful to departmental engineer Katalin Takács for the help she provided during the experimental work, as well as for her pleasant atmosphere and advices.

I would like to thank Dr. Zoltán Garda for his professional advice and for the fact that I could turn to him for help and advice at any time. Thank you for the friendly atmosphere and everyday professionalism.

I would like to express my gratitude to my family, who supported me throughout my studies.

I would like to thank Réka Józsa, my wife, for her support, patience and help, which was indispensable during my work.

I would like to especially thank Nicol Guidolin, Dr. Mariangela Boccalon and the team in Trieste for their great help, friendly atmosphere and kind words during my stay.

I would like to thank Federica Bounsanti, Manager of the Chemistry Department, that I could do my doctoral work at Bracco Imaging S.p.A.

I thank Tibor Csupász, Csenge Szolnoki, Csaba Hámori and Antal Udvardy for the good conversations, friendly atmosphere and support both in life in the profession.

Last but not least, I would like to thank all the employees of the Department of Physical Chemistry and the Rare Earth Metals research group, who helped me prepare my thesis.